The Dissertation Committee for Carlos Alfredo Rios Perez Certifies that this is the approved version of the following dissertation:

Analysis of Gas Differential Diffusion Through Porous Media Using Prompt Gamma Activation Analysis

Committee:

Mark Deinert, Supervisor

Carlos Hidrovo

Steven Biegalski

John Howell

David DiCarlo

Analysis of Gas Differential Diffusion Through Porous Media Using Prompt Gamma Activation Analysis

by

Carlos Alfredo Rios Perez, B.S.; M.S.E.

Dissertation

Presented to the Faculty of the Graduate School of

The University of Texas at Austin

in Partial Fulfillment

of the Requirements

for the Degree of

Doctor of Philosophy

The University of Texas at Austin

December, 2013

Dedication

To God. To my family: Gloria, Jorge, Coqui, Javi, Cris, Dieguito, and Brooke. To all the wonderful people I met in La Oroya, Lima, Munali, Lusaka, and Austin. With love

Acknowledgements

I would like to thank God, for always being with me. He makes everything possible. I would like to thank my advisor Dr. Mark Deinert for giving me the opportunity to work on his research group. Thanks for his support, guidance and teaching during this entire project. I also would like to thank his research group (Dr. Andy Osborne, Dr. Geoff Recktenwald, Jeong-Heon Shin, Brady Stoll, and Tim Silverman), the staff and students at NETL (especially to Dana Judson, Tracy Tipping, Larry Welch, Hunter Fuentes, Nick Mohammed, and Elan Herrera) for all their help during the last three years. Thanks to Dr. David DiCarlo for being part of my Doctoral Committee. Thanks to Dr. Steven Biegalski and Dr. John Howell for their teaching and advice in both, academic and personal matters. Thanks to Dr. Carlos Hidrovo for his teaching, counsel, and support in many difficult times in Austin, and for letting me work and guide a group of undergraduate research assistants in his lab. Thanks to Mara Sweeney, Rebecca Clifton, Rachel Naylor, Ellen Wilkes, Onur Demirer, Dr. Brian Carrol, Dr. Tae-Jin Kim, Collier Miers, and the MTFL lab for their teachings, help, and hard work. Thanks to my friends Karla Montestruque, Javier Davila, Gonzalo Sevillano, Laurene Dobrowolski, Andres Jaramillo, Colin Beal, and Philip Kokel for always truly care and help me. Thanks to my mom, dad, brothers, Diego Rios, and Brooke Rios for their infinite love and support that make me smile everyday and help me go through the toughest days, you are my favorite people. Thanks to Rachel and Silvia Kokel, Felipe Lopez, Gloriana Arrieta, Julio and Eliana Carrillo, Sonia Hernandez, Bonie Canion, Franziska Klingberg, Alex Fay, Alan Watts, Patrick Jurney, and every wonderful person I met at Austin. I will always keep you y'all in my heart.

Analysis of Gas Differential Diffusion Through Porous Media Using Prompt Gamma Activation Analysis

Carlos Alfredo Rios Perez, PhD

The University of Texas at Austin, 2013

Supervisor: Mark Deinert

Accurate estimates for the molecular transport coefficients are critical to predicting the movement of gases in geological media. Here I present a novel methodology for using prompt gamma activation analysis to measure the effective diffusivity of noble gases in a porous medium. I also present a model to estimate the connectivity parameter of a soil from measurements of its saturated conductivity, macro porosity, and pore volume and pore surface fractal dimensions. Experiments with argon or xenon diffusing through a nitrogen saturated geological media were conducted. The noble gas concentration variations at its source were measured using prompt gamma activation analysis and later compared to a numerical diffusion model to estimate the effective diffusion coefficient. Numerical simulations using the estimated diffusivity and the experimental argon data produced results with a correlation parameter $R^2 = 0.98$. However, neglecting transport mechanisms other than diffusion largely under-predicted the xenon depletion rates observed during the first hours of experiment. To explain these results, a second model was developed which included the effect of pressure gradients and bulk convection that might arise from the faster molecular migration of the light species in a non-equimolar system and gravitational currents. Finally, the fractal model

developed for this dissertation was used to estimate the connectivity parameters and walking fractal dimension of a group of geological samples that were previously characterized. This model successfully predicted positive connectivity factors and walking fractal dimensions between two and three for every sample analyzed.

Table of Contents

List of Tables

List of Figures

INTRODUCTION

MOTIVATION

The movement of subsurface gases affects the aeration of soils, transport of volatile pollutants and radon [1, 2]. The ratios of noble gas isotopes are used to screen for underground nuclear tests and the subsurface movement of these anthropogenic radionuclides is important for the detection of belowground nuclear tests [3-8]. The detection of anthropogenic noble gas isotopes at ground surface can also be used as an indicator of contamination from buried radioactive materials [9]. Modeling the movement of gases in the subsurface requires information on the gas diffusion coefficients for the system and these must typically be determined experimentally.

The International Monitoring System of the Comprehensive Nuclear Test Ban Treaty is charged with determining whether or not clandestine nuclear tests have taken place [8]. This monitoring network combines four different technologies: infrasound (60 stations total), seismic (170 stations total), hydro acoustic (11 stations total), and radionuclide (80 stations total) facilities [7, 8, 10]. Among these four technologies, detection of anthropogenic radionuclides provides the only definite method to screen the nuclear nature of a surface or underground weapon test [3, 4, 8]. Figure 1 shows the location of radionuclide stations (radionuclide particle and noble gas).

Figure 1 Location of CTBT International Monitoring System's radionuclide facilities. Position of the radionuclide particle (purple) and particle and noble gas (red) monitoring stations [10].

Detection of noble gas radioisotopes from air sampling, or during on-site inspection, is essential for uncovering of an anthropogenic radionuclide source [11, 12]. Isotopes of radioxenon and radioargon are most commonly used to help establish whether or not a nuclear test has taken place, and monitoring stations that can analyze for these gases are crucial. Unfortunately, the mere detection of radioactive isotopes is not sufficient for the monitoring of a nuclear detonation. Nuclear power plants and medical facilities also produce radioactive noble gas isotopes [5, 6, 13, 14]. Recent research on characterization of ^{37}Ar sources [14-16] and detection systems of this radionuclide [17], aim to use radioactive argon for on site inspections within a CTBT frame. However, currently ratios ^{135}Xe/^{133}Xe and ^{133m}Xe/^{131m}Xe are used to screen for nuclear weapons tests [5, 18].

In the event of a suspected nuclear weapon test, the International Monitoring System will assay for radioxenon and use the $^{135}Xe/^{133}Xe$ and $^{133m}Xe/^{131m}Xe$ ratios to help determine whether or not it came from a nuclear detonation. On a Multi-Isotope Ratio Concentration (MIRC) plot, the evolution $^{135}Xe/^{133}Xe$ and $^{133m}Xe/^{131m}Xe$ ratios can be used to determine whether or not the xenon signal sits in the region that is commonly assumed to correspond to that of a nuclear weapon (between the fully fractionated and non-fractionated curves), Figure 2. Construction of these bounding curves comes from the assumption that radioxenon isotopic ratios are affected only by their direct fission yield and their production by the decay of radioxenon precursors. This assumption ignores the potential isotopic fractionation of the xenon gas during its migration to the surface after an underground explosion.

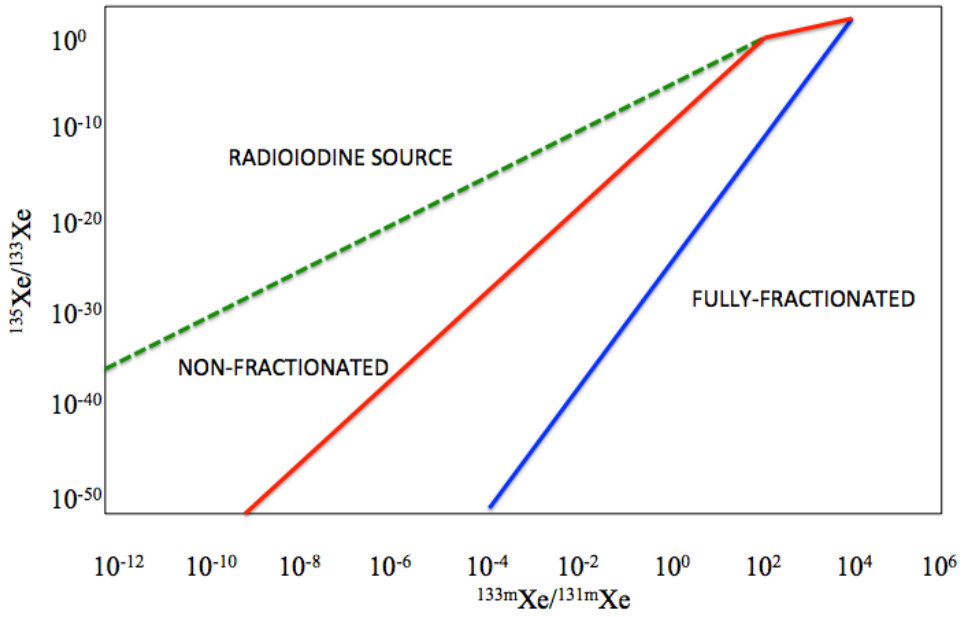

Figure 2 Multiple Isotope Ratio Concentration (MIRC) plot for a ^{235}U weapon. Evolution of radioxenon isotope signals from fully-fractionated, non-fractionated and radioiodine sources [19]. The signal of a weapon is assumed to sit between the fully and non-fractionated lines.

Recent numerical studies of radio xenon diffusion within a geological medium, combined with barometric pumping advection through underground fractures, has shown that isotopic fractionation can lead to variations in the expected radioisotope ratios after a nuclear weapon explosion [19, 20]. In fact, the work of Lowrey *et al*. has shown that the xenon signal of a nuclear test is better bounded by the region between the radioiodine and fully fractionated curves (Figure 2) [19]. This work showed that diffusion coefficients are essential to modeling the expected signal. As a result, more accurate estimation of the radionuclide transport coefficients within porous media, and better understanding on the effect of the porous media structure, could narrow the discrimination region in a MIRC plot.

TRANSPORT OF GASES THROUGH A GEOLOGICAL POROUS MEDIA

In general, the time rate change in concentration of an isotope within any control volume is a function of its molecular diffusion, bulk advection of this species crossing the control volume boundaries, and its net rate of production [21, 22]. Frequently, when the migration of species takes place within a geological media, molecular diffusion dominates bulk advection [22-24]. Consequently, an adequate model for mass transport through a porous media must rely on a strong understanding of the molecular migration mechanism and how it is affected by variations in pressure, temperature, media structure, gas composition, and external (or body) forces. The two most popular models employed by geological and environmental researchers are the Dusty Gas Model and the classical Advection Diffusion Model [25, 26].

It is commonly assumed that the bulk transport of a species and its migration by molecular diffusion can be linearly superimposed. In general, the molecular migration of inert gases within a porous media is affected by the interaction of gas molecules with each other, and with the matrix surfaces. In both cases (molecule-molecule and molecule-wall interactions), the transport rate is inversely proportional to the square root of the mass of the molecules migrating as shown by the Chapman-Enskog Kinetic gas theory and various empirical correlations [21, 22, 27]. Consequently, isotopes of the same chemical element could transport at dissimilar rates due to their different molecular weights. Indeed, it is well established that isotopic fractionation occurs during diffusion of relatively light elements such as helium, oxygen, lithium, carbon, and this is due to differences in their molecular mass [28-32]. However, the effects of mass dependent diffusion have never been investigated for heavier isotopes, *e.g.* xenon, moving through a geological structure.

Another parameter that strongly influences the rate at which a gas migrates through a porous medium is the structure of the pore space [21, 33, 34]. Because of the complexity and large variability of the media's topology, diffusion coefficients are usually estimated using empirical correlations to experimental observations often with little or no physical insight [35], or using powerful computational approaches such as Monte Carlo simulations or Lattice Boltzmann techniques [36-38]. However, work over the past two decades have shown fractal characteristics in many porous media, and have exploited this mathematical concept to model the transport coefficients for fluids and gasses in porous systems [39-41]. In this regard, most of the work published in the literature has been aimed to study the soil water retention [42, 43], permeability [44, 45], and capillary condensation [46]. Less attention has been driven towards the fractal

analysis of the medium tortuosity, which is a key factor in determining diffusion coefficients for gases in porous systems [21, 22, 47]. However, work to date has correlated the tortuosity of a medium to the 'tortuous fractal dimension' (which is hard to measure and poorly understood for natural porous media) and not to the pore space, or mass fractal, dimensions (which are relatively easy to measure and well parameterized for natural media) [48, 49].

MEASUREMENT OF TRANSPORT COEFFICIENTS

Measurement of the diffusion coefficient of a gas through a porous media requires the ability to determine the time dependent concentration of the species of interest [50-56]. To evaluate the separation of isotopes caused by differential diffusion, the analytical technique must be able to differentiate one isotope from another. To do so, the proposed method should aim at measuring nuclear and not chemical properties. The most common techniques for doing this are mass spectrometry (sometimes combined with gas chromatography analysis) [57-59], and nuclear magnetic resonance [60, 61]. The selection of one or another method is mostly based on its availability, precision, type of gas under study and other aspects such as the invasiveness of the proposed technique [62]. Of the above list, mass spectrometry is probably the best-known technique used with noble gases. The principal advantages of this technique (in an inductively coupled plasma mass spectrometer) are the small detection limits (parts per trillion), and high sensitivity [57-59]. However, this technique is not only time consuming in its sample preparation, but it is also considered invasive and destructive as a sample needs to be extracted from the system and then destroyed during its analysis [57, 58].

Two nuclear analytical techniques commonly used in the examination of geological samples are neutron activation analysis and prompt gamma activation analysis. Unlike neutron activation analysis, prompt gammas can be used to analyze non-radioactive isotopes of the same chemical species [63, 64]. This method is based on the detection of the prompt gamma photons emitted by the sample nuclides after their interaction with an incident neutron beam. These gamma particles are registered by a gamma radiation detector combined with a signal amplifier and a multichannel analyzer [65]. The detection system registers the energy and intensity of the emitted prompt photons. The energy spectrum of the prompt gamma rays emitted by every non-radioactive isotope is unique and can be used to differentiate between them [66]. The intensities (or number of photons detected) at specific energies are proportional to the concentration of a detected isotope in the sample [67].

AIMS OF THIS DISSERTATION

Currently, the use of radio xenon signatures as a means to determine whether or not a clandestine nuclear test has taken place fails in considering how isotopic mass affects gas transport in the subsurface. Relationships that are used to model gas diffusion coefficients in geological systems themselves are often based on semi-empirical relationships that would be difficult to apply to natural systems that have not been directly characterized (such as the locations of suspect nuclear weapons tests in foreign countries). The main objective of the proposed work is to develop a non-invasive method for measuring gas diffusion coefficients for a porous medium. The second objective is to present a relationship for the mass dependent binary diffusion coefficient, based on a

fractal description of pore topology. In this context this dissertation looks at the following specific aims:

Aim 1. Development of an experimental technique for using prompt gamma activation analysis to measure the variation of xenon isotope concentration caused by the diffusion of this noble gas within a porous media. The variation of a noble gas concentration after diffusing through a porous media will be quantified using prompt gamma activation analysis and compared to numerical models to obtain the transport parameters of the system designed.

Aim 2. Use prompt gamma activation analysis to determine the mass dependent diffusion coefficients for xenon isotopes in a porous medium. Prompt gamma activation analysis will be used to detect variations in the isotopic composition of a natural xenon gas sample before and after it diffuses through nitrogen within a uniform porous media.

Aim 3. Use fractal geometry to model the correlation between transport parameters such as tortuosity of a porous media to the pore volume, and pore surface fractal dimensions of the system. Methods established by Gimenez et. al. [68], and Coleman and Vassilicos [69] were followed to develop a model for the tortuosity of a porous medium that can be used to model diffusion through geological structures.

The rest of this dissertation is organized as follows: the next three main sections (one for every specific aim), will present the theory, methodology, results and discussion of each of the above aims as separate chapters. Each chapter corresponds to work that has either been published or that is in preparation for submission. The final chapter is a

discussion that summarizes the results and conclusions of each chapter under the main objective of this dissertation.

Chapter 1: Methodology to measure variations on noble gas concentrations using prompt gamma activation analysis to analyze noble gas diffusion through a porous media

Experimental analysis of gas diffusion through porous media requires the use of methods capable of measuring the concentrations of the species involved with appropriate spatial and temporal resolutions. Mass spectroscopy (complemented by gas chromatography sometimes) is the most popular technique used to measure the gas diffusivity of a system. However, the invasive and destructive nature of this technique limits its spatial and temporal resolution, which affects its suitability for use with transient experiments. Other popular methods for measuring gas concentrations are: gas chromatography, mass spectroscopy [51, 70, 71], photo-thermal deflection [72], and nuclear magnetic resonance [60, 61].

Nuclear analytical methods using neutron beams have proven to be an attractive option to study the transport of liquid fluids, charged particles, and specific nuclides within different type of systems noninvasively. Neutron radiography, for example, has been used to determine the transport coefficients for fluids within porous media [73, 74] as well as ionic diffusion coefficients in solid state materials [75]. Likewise, petroleum contamination and moisture profiles in a geological medium have been described in situ using neutron backscatter [e.g. 76]. Another technique, neutron depth profiling, has been used to quantify the transport of specific nuclides into the near surface region of solids [77].

This chapter presents a novel method developed to measure the variation in concentration of a noble gas caused by its diffusion within a geological medium using prompt gamma activation analysis.

1. THEORETICAL BACKGROUND

Prompt gamma activation analysis

The selection of prompt gamma activation analysis (PGAA) over other nuclear techniques for this research project was based on its non-intrusive and non-destructive characteristics, as well as availability of facilities at the Nuclear Engineering Teaching Laboratory at The University of Texas at Austin [67], Figure 3. The ability of this analytical technique to measure a wide energy range of decay photons from excited isotopes [78, 79] was also important for this project.

Table 1 compares the advantages and disadvantages of measuring the isotopic composition of a gas sample by mass spectroscopy [57-59], neutron activation analysis, and prompt gamma activation analysis [67].

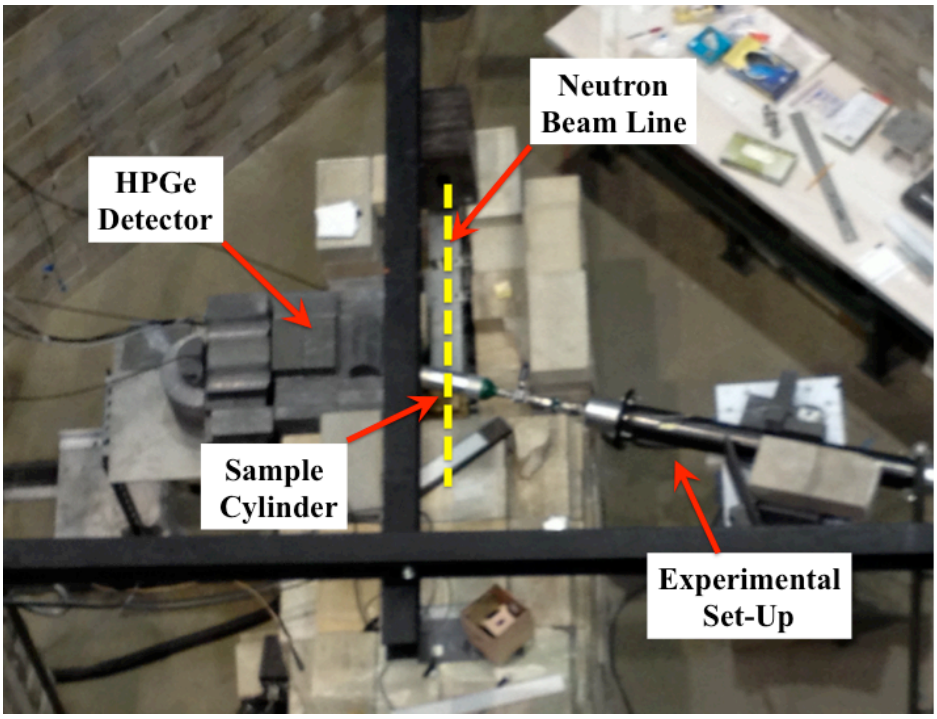

Figure 3 Overview of the prompt gamma activation analysis facility at the Nuclear Engineering Teaching Lab. Location of the High Purity Germanium detector, sample (sample cylinder), and neutron beam.

Technique	***Pros***	***Cons***
Prompt gamma activation analysis	Non-invasive Can analyze stable isotopes	Relatively large detection limits
Neutron activation analysis	Non-invasive	Requires radioactive isotopes
Mass spectrometry	Small detection limits Can analyze stable isotopes	Invasive Long time required for sample preparation (extraction, purification, separation) Destructive

Table 1 Comparison of concentration measurement techniques. Advantages and disadvantages of alternative methods to estimate the isotopic composition of a noble gas.

Nuclear physics of the prompt gamma decay

During the irradiation of a sample with a neutron beam, the probability of an incident neutron being absorbed or scattered (nuclear cross section) depends on the target nuclide, and the neutron's energy [65, 80]. When a neutron is absorbed, a compound nucleus is formed that exists in an excited state [67]. From here, the excited nucleus often decays to a stable energy level by emitting gamma photons and/or other nuclear particles [66]. The photons emitted during the first 10^{-9} to 10^{-12} seconds after the neutron absorption are called prompt gamma rays [65, 67, 80] and are specific to every nuclide. For example, Figure 4 shows the energy of the prompt gamma photons emitted by ^{9}Be and ^{131}Xe, and the probability (or cross section) of these nuclides to emit each of these gamma rays after interacting with a neutron. Since nucleus energy levels are discrete, so are the energies of the emitted photons.

Prompt gamma energy spectrum

Proper examination of a prompt gamma activation analysis requires understanding the interaction mechanisms of the emitted gamma photons with the detector and its surroundings. The major interaction mechanisms of gamma rays with matter are: Photoelectric adsorption, Compton scattering, and pair production. The probability of each of these interactions to take place varies with the energy of the incident gamma ray [65, 66].

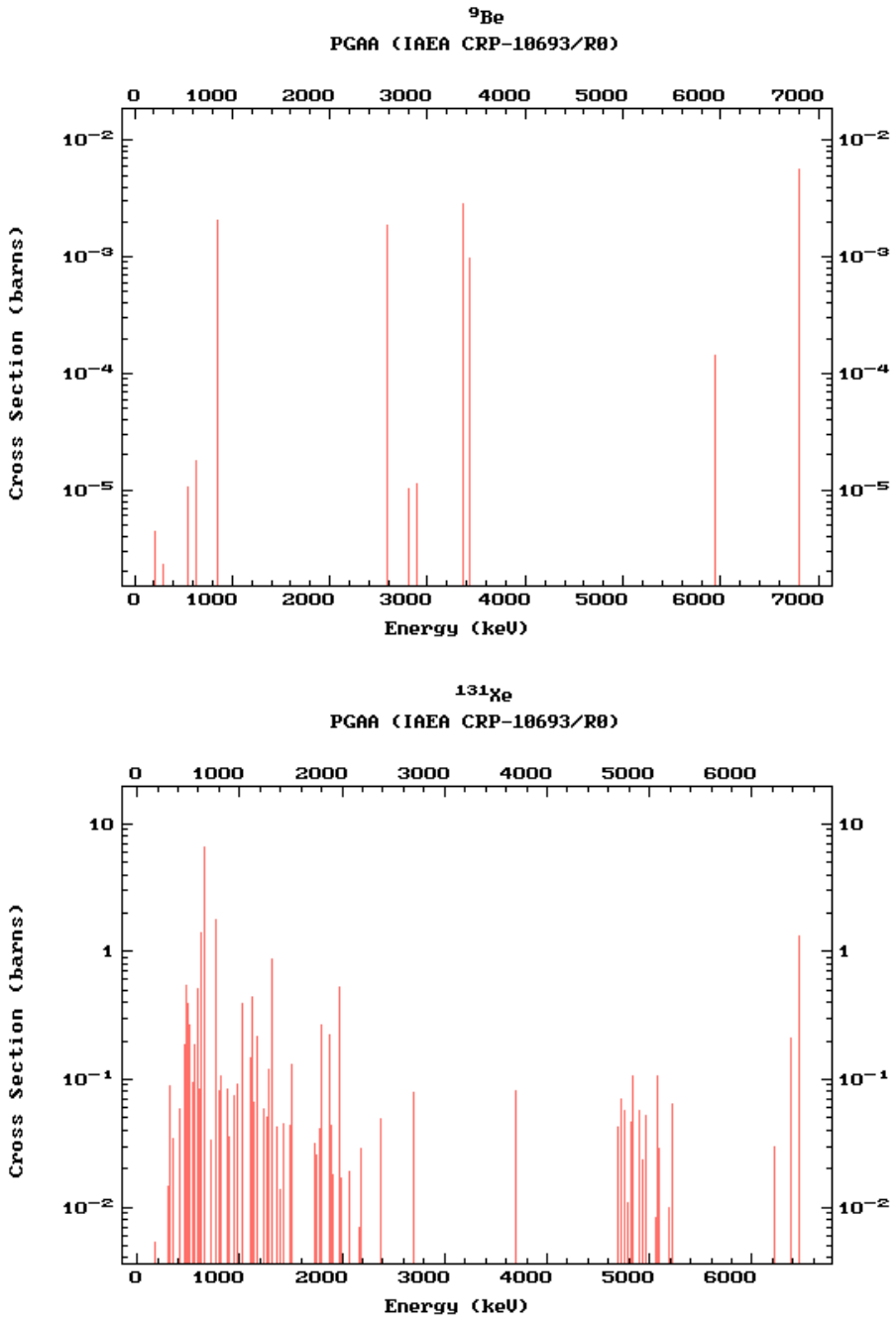

Figure 4 Energies of the prompt gamma rays emitted by ^{9}Be and ^{131}Xe (horizontal axis) and their respective neutron-gamma cross sections (vertical axis) [81].

During photoelectric absorption, a detector atom absorbs the sample's gamma photon and emits a photoelectron. The energy of the emitted photoelectron is the difference between the incident photon energy (*hv* in Figure 5) and the binding energy of the electron. After the emission of this photoelectron, electrons from the target atom (or from its immediate surroundings) are rearranged to fill the vacancy left. In this process, characteristic X-rays or Auger electrons are emitted. These X-rays might also interact with the detector through a photoelectric absorption. When all the cascade of secondary X-rays (emitted almost-instantaneously after the interaction of the original photon) are re-absorbed in the detector, a delta function would appear in the spectrum at the incident photon energy value. This energy peak is called the photon full-energy peak.

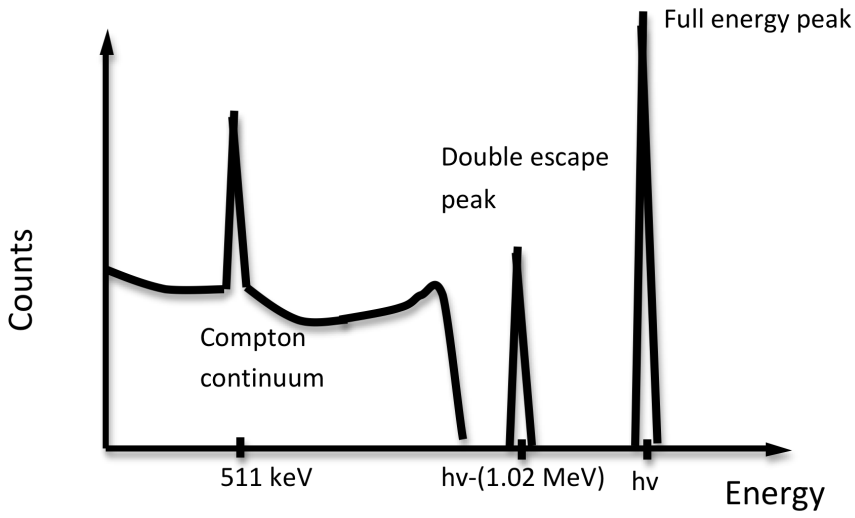

Figure 5 Schematic of a gamma spectrum of a mono-energetic photon showing the principal features of this type of analysis.

When the striking gamma photon does not fully transfer all its energy to the detector, it could be recoiled and leave with a fraction of its original energy. Since the

scattering angle can vary in all directions, the kinetic energy of the electron can also vary and this produces the 'Compton continuum' in the prompt gamma spectrum shown in Figure 5. This continuum region lowers the accuracy of the detection of low energy photons and could eventually hide a full energy peak. Various techniques have been developed to reduce the Compton continuum, such as coincidence and anticoincidence event analysis [65, 82-84]. Other methods to reduce the Compton are the sum-coincidence mode, and the pair spectrometer [80]. Last, an energy gap between the photoelectric absorption peak and the Compton distribution appears because an elastically scattered photon cannot deposit more energy that in a 180° scatter event.

In the third interaction mechanism, called pair production, the photon disappears in a region of large electric fields near the protons producing a positron-electron pair. This reaction can take place only if the energy of the incident photon is larger than 1.02 MeV (large enough to create a positron-electron pair). Any excess of energy in the photon above this value would be transformed into kinetic energy of the two new charged particles and lost in the near surroundings of the absorbing medium. The signal of the two charged particles kinetic energies would appear in the spectrum as a peak with energy 1.02 MeV lower than the incident photon energy, Figure 5. After the unstable positron loses its kinetic energy, it combines with an electron in the medium and disappears emitting two annihilation photons of 511 keV each. These 511 keV photons give origin to the annihilation peak that shows up in every gamma spectrum, Figure 5.

Another aspect that influences the prompt gamma energy spectrum is the type and geometry of the detector employed. The two most common types are the inorganic scintillators such as the NaI(T1), and the solid state ionization detectors such as the high-purity germanium detector. The selection of one over the other would require a trade off between efficiency and energy resolution. The superior energy resolution of the

germanium detector allows this instrument to differentiate between different photons with very similar energies. On the other hand, the NaI(T1) detector presents a larger detection efficiency because of the large atomic number of iodine.

The physical size of the detector utilized for gamma spectroscopy and its shielding, also influence the spectrum of the sample. If the detector is small compared to the mean free path of the scattered gamma and annihilation photons, the probability of these two reactions decreases. Since commercial detectors are relatively small, and usually do not enclose the sample, their surroundings will also affect the shape of the gamma energy spectrum. The scattering of gamma rays and production of annihilation photons in the elements around the detector will make these materials act as sources of gamma radiation. This secondary gamma radiation effect on the spectrum could for example produce an energy peak around 250 keV from backscattered photons, and increase the intensity of the 511 keV peak after the interaction of secondary annihilation photons with the detector by a photo-electron absorption process. Appropriate shielding of the detector will reduce the influence of secondary radiation.

Calibration and detection limits of the PGAA facility

Before noble gas concentrations can be measured using a prompt gamma activation analysis facility, efficiency and energy calibrations must be performed and the detection limits for the gases of interest need to be established. Both calibrations (the total counting efficiency and energy calibration) of the system located at the Nuclear Engineering Teaching Laboratory were performed using a ^{152}Eu source from the National Institute of Standards and Technology. Equation (1) relates the channel number, *X*,

where the signal from the detector is sorted, and the energy of the gamma photon sensed, E {keV}. Equation (2) is the relationship between the counting efficiency, e, and the energy of the gamma rays, E {keV} [64].

$$E = 0.6813X + 8.4788 \quad (1),$$

$$\ln(e) = -0.0827\ln(E)^3 + 1.5323\ln(E)^2 - 9.6935\ln(E) + 14.565 \quad (2).$$

Both, Equation (1) and Equation (2), were obtained by fitting the counting efficiency measured for the photons emitted by the ^{152}Eu source at different energies using an analog system. This type of signal processing system was used for the analysis of argon diffusion. An advance digital signal processing system (Lynx® from Canberra) was used during the analysis of xenon. Equations (3, 4) show the energy and counting efficiency calibration of the digital processing system, respectively.

$$E = 0.3098X + 0.1185 \quad (3),$$

$$\ln(e) = 0.0099\ln(E)^3 - 0.327\ln(E)^2 + 2.384\ln(E) - 10.606 \quad (4).$$

The minimum number of counts required to detect a trace of a noble gas or counting detection limit, L_D(counts), was determined at different energies from the critical limit, L_C, following Currie's statistical method [85-87] presented in Equations (5, 6). In both expressions, the minimum number of counts needed to discriminate a net signal from the Compton background (L_C) is a function of the statistical variable k corresponding to a wanted error probability, and the number of background counts at the

channels where the peak of interest would be located, μ_C. For a probability of 5% for a false positive/negative, k equals 1.624 assuming a normal distribution. The number of counts in the background Compton are determined from a vacuumed sample cylinder with all the other test parameters (reactor power and counting time for example) equal to those that will be used for a sample analysis.

$$L_C = k\sqrt{2\mu_C} \quad (5),$$

$$L_{D(counts)} = k^2 + 2L_C \quad (6).$$

Once the counting limits are estimated, the pressure and concentration detection limits ($L_{D(pressure)}$ {kPa} and $L_{D(concentration)}$ {moles·cm^{-3}} respectively) can be approximated using Equations (7, 8) which assume that the sample behaves as an Ideal Gas. In both equations R is the ideal gas constant (8.31446 J·mol^{-1}·K^{-1}), and $netcounts_{sample}$ is the net area of a peak obtained during the analysis of a noble gas sample at pressure p {Pa} and temperature T {K}.

$$L_{D(pressure)} = \frac{L_{C(counts)} \cdot p}{1000 \cdot netcounts_{sample}} \quad (7),$$

$$L_{D(concentration)} = \frac{L_{D(pressure)} \cdot 10^{-9}}{R \cdot T} \quad (8).$$

Estimation of noble gas concentration's variation using PGAA

The concentration of a noble gas within a sample, C {moles·cm^{-3}}, can be determined from the number of counts in a peak within a region of interest, the total energy efficiency, e, the incident thermal neutron flux, ϕ {cm^{-2}s^{-1}}, the neutron-gamma cross section, σ_γ {barns}, the analysis live-time, t {seconds}, and the effective sample volume, V_{eff} {cm^3} [88]:

$$C = \frac{counts}{0.6023 \cdot e \cdot \phi \cdot \sigma_\gamma \cdot t \cdot V_{eff}} \qquad (9).$$

2. EXPERIMENTAL METHODOLOGY

Diffusion experiments were carried out using natural argon and xenon diffusing through a uniform porous medium. The variations on noble gas concentrations were measured at the Beam Port 3 in the Nuclear Engineering Teaching Laboratory at The University of Texas at Austin. *Appendix A* lists the steps followed in this procedure with more detail

Experimental set-up

The experimental set-up consists of a 10.3 cm diameter and 1 meter long steel pipe (4 in. diameter ANSI Schedule 40) packed with 20/30 sieve Ottawa sand. One 10 cm. long by 10 cm. inner diameter aluminum chamber was added on each end. The purpose of these chambers is to allow for a uniform diffusion front during the

experiments and provide a location for its potential non-invasive analysis. To guarantee a process dominated by diffusion, two differential pressure transducers (OMEGA PX653-05D5V) were employed to: regulate the pressure within the system and the gas sample cylinder (source of the noble gas to diffuse), and measure pressure differentials between the two ends of the experimental set-up during the experiments. A schematic of the experimental set-up is shown in Figure 6.

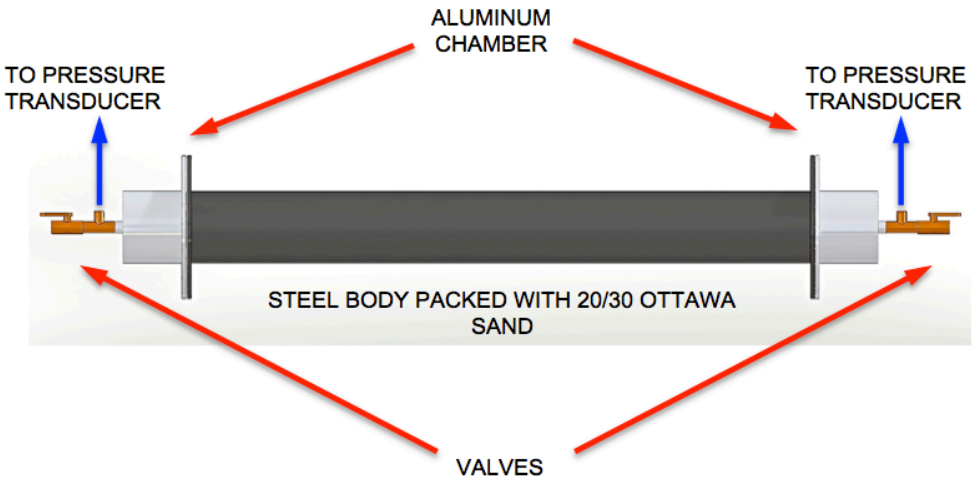

Figure 6 Schematic of the diffusion experimental set-up at the Nuclear Engineering Teaching Lab [89].

The prompt gamma activation analysis facility at the Nuclear Engineering Teaching Laboratory uses a 1.1 MW TRIGA Mark II nuclear research reactor as a neutron source. A parabolic focusing element located at the end of the neutron guide increases the equivalent thermal neutron flux at the sample location up to 5.3×10^{6} $cm^{-2}s^{-1}$ when the reactor operates at 950 kW [90, 91]. The photon detector used is a p-type ORTEC high purity germanium detector with a resolution of 1.95 keV at 1332 keV and a 65% relative efficiency. This semiconductor radiation detector is shielded with various

materials from lead bricks to a borated foam and cadmium sheets to reduce the signal from the background elements [91]. A Tennelec TC 702 amplifier and a 16k Canberra 8713 analog to digital convertor with a Multiport II Canberra multichannel analyzer were first located in this facility and used on the argon transport experiments. During the analysis of xenon migration, a digital signal processing system, Lynx® from Canberra was used. Genie 2000 software was used to analyze the energy spectrum obtained fro argon and xenon samples.

Experimental procedure

The background continuum to estimate the counting detection limit was obtained from a four hours live-time analysis of the aluminum sample cylinder vacuum up to 0.667 kPa (abs) with the TRIGA Mark II reactor operating at 950 kW. The noble gas samples used to estimate the pressure detection limits were obtained from the analysis of noble gas samples from PRAXAIR (99.9999% high purity argon and natural xenon research grade 6.0) at 106.92 kPa(abs) and 298 K. Similar to the background analysis, these samples were irradiated during 4 hours live time with the reactor running at 950 kW. The spectra obtained for the argon and xenon samples (and shown in Figure 7) were evaluated using the 2nd Difference Peak Locator and the Peak Area Analysis tools from the Genie2000 software. The estimated detection limits at different energies are tabulated in Table 2.

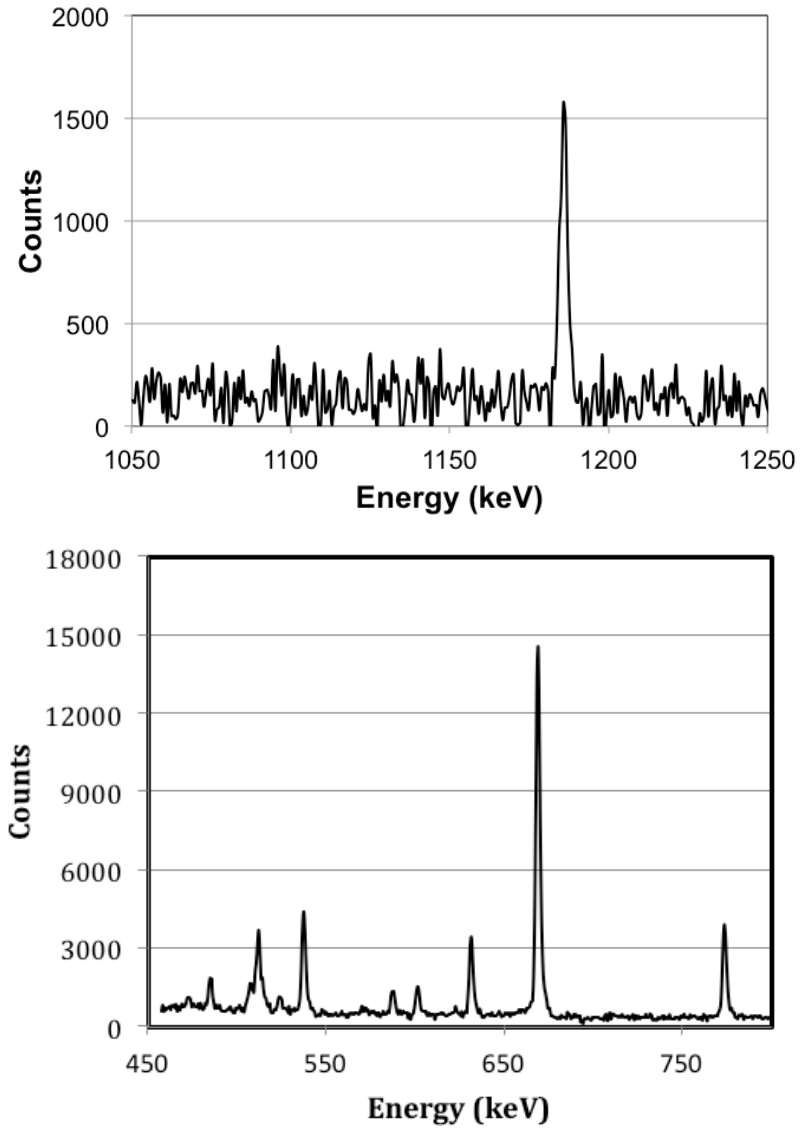

Figure 7 Argon and xenon prompt gamma energy spectra. Top: PGAA spectrum and counts of the 1186.8(3) keV peak from a pure argon sample at 106.9 kPa (abs) and 298 K. Bottom: PGAA spectrum of a natural xenon sample at 107.1 kPa (abs) and 296 K [67, 88].

The argon cross sections used for this analysis, and listed in Table 2, are lower than those available in the literature [67]. The listed cross sections were experimentally estimated from a prompt gamma analysis of a pure argon sample at a known pressure.

The published argon cross section had to be reduced by a factor of 0.417 to match the argon concentration, ρ_{Ar} {g·cm^{-3}}, estimated from the sample pressure and Equation (10) with the prompt gamma results and Equation (11) [88].

$$\rho_{Ar} = \frac{p \cdot M_{Ar} \cdot 10^{-6}}{R \cdot T} \quad (10).$$

$$\rho_{Ar} = \frac{netcounts_{sample} \cdot M_{Ar}}{0.6023 \cdot e \cdot \phi \cdot \sigma_{\gamma} \cdot V_{eff} \cdot t} \quad (11).$$

Isotope	***Energy {keV}***	***σ_{γ}{b}***	***Efficiency (4.02% error)***	***Detection Limit x10^{6} {mol·cm^{-3}}***	***Detection Limit {kPa}***
^{40}Ar	166.3	0.22	0.002494	3.681±0.22	8.87±0.07
	1185.8	0.14	0.001353	6.367±0.38	15.36±0.20
^{129}Xe	536.17	1.71	0.001724	0.436±0.03	1.05±0.01
	586.17	0.48	0.001688	1.708±0.10	4.12±0.03
	1482.06	0.112	0.001215	10.889±0.66	26.25±0.42
^{131}Xe	630.29	1.41	0.001658	0.607±0.04	1.45±0.01
	667.79*	6.7	0.001635	0.113±0.01	0.28±0.01
	772.72	1.78	0.001572	0.476±0.03	1.15±0.01

Table 2 Prompt gamma detection limits Detection limits of ^{129}Xe and ^{131}Xe using the analog analysis system. (^{*131}Xe and ^{129}Xe also present peaks at 670.02 keV and 668.59 keV with neutron-gamma cross sections of 0.22 and 0.17 barn respectively) [67, 89].

The procedure followed during the noble gas diffusion experiments includes three major steps: venting of the porous column, preparation of the noble gas sample, and diffusion through the porous media. The experimental set-up is vented by flowing a

minimum of 120 dm^3 (liters), *i.e*. 12 times the empty set-up volume of nitrogen at two flow-rates 0.025 $dm^3 \cdot s^{-1}$ (1.5 $liter \cdot min^{-1}$) during 1 hour, and at 0.0883 $dm^3 \cdot s^{-1}$ (0.5 $liter \cdot min^{-1}$) during at least another 60 minutes to remove any remnant of argon or xenon from previous diffusion experiments. Then, the purge valve is closed and the experimental set-up pressure was raised to 1120±125 Pa (4.5±0.5 in H_2O).

Preparation of the noble gas sample consists of a series of vacuum and fill cycles for the aluminum gas sample cylinder. Argon or natural xenon *Research Grade 6.0* from PRAXAIR are used to safeguard that more than 99.95% of the gas molecules in the sample correspond to the noble gas of interest. The aluminum cylinder is then pressurized up to 105 kPa (abs) in a different room than where the media column is located. The gas sample cylinder is taken to the prompt gamma facility and its pressure is lowered to match the one of the experimental set-up with pressure surplus lower than 70 Pa using a ¼ in *SS Low-Flow Metering Valve* from Swagelok®, and a PX653-05D5V differential pressure transducer from OMEGA®. Then, the noble gas concentration within the cylinder is measured using prompt gamma activation analysis with the reactor operating at 950 kW.

The sample cylinder is connected to the experimental set-up through a full-flow quick connector from Swagelok® and the argon is allow to diffuse within the porous media for a desired amount of time. Finally, the noble gas concentration left within the sample cylinder is quantified using prompt gamma and a neutron flux of about 5.3×10^6 $cm^{-2}s^{-1}$.

The standard deviation in gas concentration was determined following Knoll [65]:

$$\left(\frac{S_C}{C}\right)^2 = \left(\frac{S_{counts}}{counts}\right)^2 + \left(\frac{S_e}{e}\right)^2 + \left(\frac{S_\phi}{\phi}\right)^2 + \left(\frac{S_{\sigma_\gamma}}{\sigma_\gamma}\right)^2 + \left(\frac{S_{V_{eff}}}{V_{eff}}\right)^2 \quad (12),$$

where S_i is the standard deviation or error of every variable i that appears in Equation (12). The standard deviation for the detection efficiency is estimated by a least-squares regression analysis [92] of the energy and efficiency calibration measurements. The total efficiency error obtained was 4.02%. The variance of the net number of counts was obtained from the Genie™ 2000 *Peak Area Analysis* tool after fitting a Gaussian distribution to the peak of interest in the gamma spectrum. For the neutron-gamma cross sections, the relative standard deviations employed were equal to those reported by Molnar [67]. The variance for the neutron flux was assumed to be equal to its own value presuming a single measurement was conducted to determine this value. The error for the effective sample volume was assumed to equal 5% (0.8 cm^3). The standard deviation of the analysis time was neglected as the computer internal clock was used to control this variable.

3. RESULTS AND DISCUSSION

For each of these experiments, the concentration of argon or xenon was measured using prompt gamma activation analysis at the sample cylinder before and after every diffusion test. The results are shown in Table 3, Table 4, Figure 8, and Figure 9. The amount of noble gas remaining within the cylinder after each test is compared to the initial one to estimate the reduction of the initial concentration. The amount of noble gas within the sample is proportional to the net peak areas in the gamma photon energy spectrum (at 1186.6 keV for argon, and 772.72 keV for xenon). The decision to analyze

argon concentration at its second largest and not its largest neutron-gamma cross section (166.3 keV) was due to the smaller Compton continuum and smaller errors at 1186.6 keV. For xenon, the analysis was conducted also at the energy of the second largest cross section due to the superposition of photons from ^{129}Xe and ^{131}Xe around the largest cross section energy (667.79 keV).

The relatively small detection limits, and the significant reduction in the amount of gas within the sample after few hours of diffusion, prove the suitability of using PGAA to evaluate the variation of noble gas concentration after varying diffusion times. Two absolute errors are given in Table 3 and Table 4 for every experiment. *Error1* was estimated considering only the variance of the number of counts, Equation (13). *Error 2* includes all other sources included in the determination of the detection limits, Equation (14). The significant larger *Error 2* is due to the the neutron-gamma cross section errors (8.8% for ^{40}Ar at 1186.6 keV and 7.9% for ^{131}Xe at 772.72 keV)

$$Error1 = ratio \cdot \sqrt{\left(\frac{S_{counts\_aft}}{counts\_aft}\right)^2 + \left(\frac{S_{counts\_bef}}{counts\_bef}\right)^2} \qquad (13),$$

$$Error2 = ratio \cdot \sqrt{\left(\frac{S_{counts\_aft}}{counts\_aft}\right)^2 + \left(\frac{S_{counts\_bef}}{counts\_bef}\right)^2 + 2 \cdot \left[\left(\frac{S_e}{e}\right)^2 + \left(\frac{S_\phi}{\phi}\right)^2 + \left(\frac{S_{\sigma_\gamma}}{\sigma_\gamma}\right)^2 + \left(\frac{S_{V_{eff}}}{V_{eff}}\right)^2\right]} \qquad (14),$$

where

$$ratio = C / Co$$

Diffusion time (hours)	*Prompt gamma counting live-time (hours)*	*C/CO (%)*	*Error 1 (%)*	*Error 2 (%)*
4.0	4.4	94.3	4.5	15.2
6.0	5.0	95.5	4.8	15.5
8.0	4.0	81.7	4.1	13.2
16.0	3.0	71.5	4.4	11.9
20.0	4.0	67.9	4.2	11.3
23.5	4.0	63.2	4.3	10.7
42.5	4.0	48.4	3.4	8.2
66.0	5.0	34.6	2.7	6.0
89.5	5.0	27.0	2.8	5.0

Table 3 Argon concentration variations. Change on the argon concentration at the sample cylinder after various diffusion experiments measured with prompt gamma activation analysis (1186.6 keV).

Diffusion time (hours)	*C/CO (%)*	*Error 1 (%)*	*Error 2 (%)*
1.0	78.6	0.7	11.3
3.0	73.3	0.9	10.6
4.0	61.5	0.6	8.9
16.7	44.0	0.6	6.3
17.0	41.1	0.6	5.9
20.0	38.0	0.5	5.5
30.0	35.0	0.3	5.0
42.0	30.1	0.5	4.3
48.0	28.1	0.5	4.1
69.0	27.1	0.5	3.9
111.0	21.6	0.5	3.1

Table 4 Xenon concentration variations. Change on the xenon concentration at the sample cylinder after various diffusion experiments measured with prompt gamma activation analysis (772.72 keV).

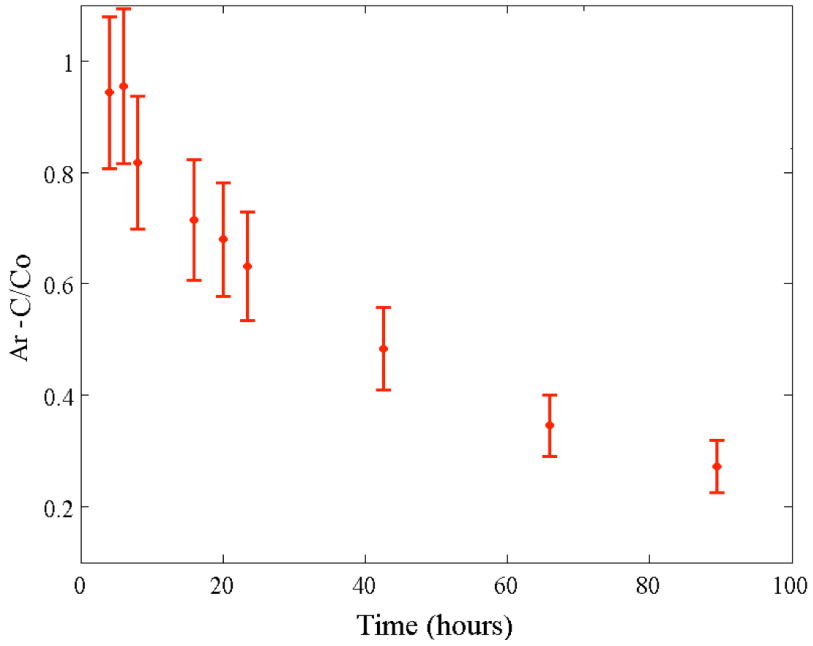

Figure 8 Variation of ^{40}Ar concentration (1186 keV) in the sample cylinder for various diffusion times. Error bars correspond to *Error 2* in Table 3.

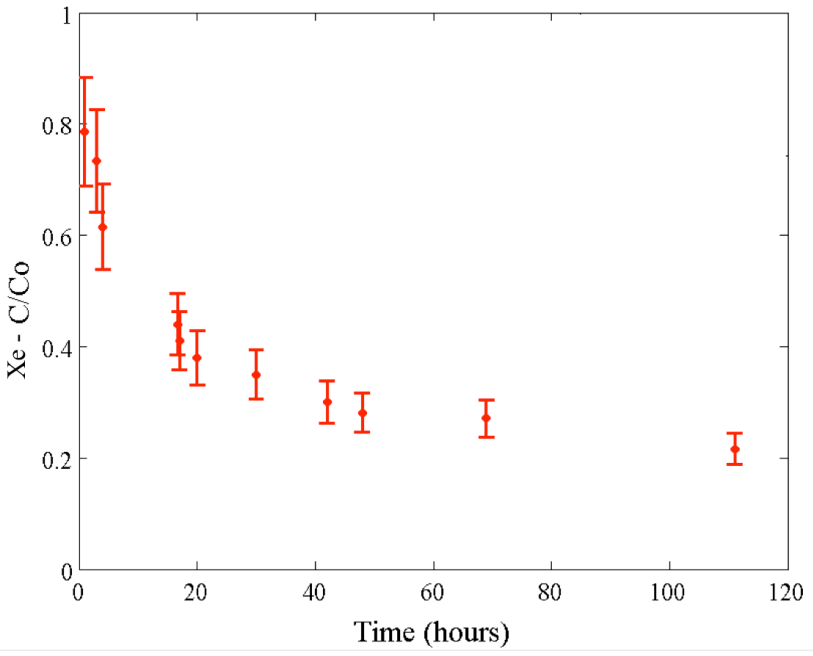

Figure 9 Variation of ^{131}Xe (772.72 keV) concentration in the sample cylinder for various diffusion times. Error bars correspond to *Error 2* in Table 4.

Chapter 2: Using prompt gamma activation analysis to determine the mass dependent diffusion coefficients of a noble gas within a porous media.

Modeling subsurface gas diffusion can be challenging because of its dependence on media structure, the composition and thermodynamic properties of the gases, and the interaction between molecules. The Chapman-Enskog kinetic theory considers all these variables and is often used for estimating gas diffusion coefficients [21, 22, 93]. This theoretical model, as well as several empirical correlations to estimate gas binary diffusivities, shows that light molecules migrate faster than heavy ones within the same medium [22, 23, 26].

Experimental evidence for the variation in the isotopic composition of light-gases suggests that differences in isotopic mass cause corresponding differences in diffusion rates [28, 29, 94]. It is also known that such mass driven differences in diffusion rates can lead to bulk convection in the direction of the heavier molecule diffusion [95, 96]. However, there has been little experimental work to analyze how mass driven differential diffusion rates can lead to convection in heavy noble gases that are moving through porous systems. This situation is important to the Comprehensive Nuclear Test Ban Treaty where radioactive argon and xenon isotopes that migrate to the surface test can be used as a marker for nuclear tests [16, 19].

The diffusion experiments described in the previous chapter show a markedly different behavior for the argon and xenon gases, with the concentration of xenon dropping much more quickly than does that of argon.

1. THEORETICAL BACKGROUND

The effects of mass-dependent species migration in diffusive processes have been well documented in the literature [23, 26, 96]. Convectively driven flow raised by the inter-diffusion of two gases with different molecular weights has been observed in steady and isobaric systems [95, 97]. Likewise, assorted articles have commented on the possibility of growing transient pressure gradients in closed systems when the molecular weights of the species diffusing are very different [96, 98].

In general, the flux of a particular species into or out of a control volume is a function of both molecular diffusion and bulk advection [21]. When the migration of species takes place within geological media, the effects of the porosity and tortuosity of the media also affect the transport. The two most popular models used to describe gas transport through porous systems are the Dusty Gas Model and the Advection Diffusion Model [23, 25, 26]. The main difference between these models is that as the Dusty Gas Model directly accounts for the interaction of the gas molecules with the porous medium in the equations it solves, the Advection Diffusion model takes these interactions into consideration in the boundary conditions. In this work, I have used the Advection Diffusion approach to model the movement of argon and xenon through the experimental system described in chapter 1.

In the absence of reactions, the Advection Diffusion Model for a binary system can be written as:

$$\frac{\partial C_A}{\partial t} = \nabla \cdot \left(D_{AB} C \nabla x_A - V^* C_A \right)$$

$$\frac{\partial C_B}{\partial t} = \nabla \cdot \left(D_{BA} C \nabla x_B - V^* C_B \right) \qquad (15).$$

Here C_A, C_B, x_A, and x_B are the molar concentration {mol·m^{-3}} and molar fraction of species A and B, respectively, D_{AB} and D_{BA} are the effective binary diffusion coefficients of the corresponding species {m^2·s^{-1}}, and V^* is the molar averaged bulk velocity {m·s^{-1}} [21, 22].

For a binary system $x_A + x_B = 1$, and Equation (15) can be modified to:

$$\frac{\partial C_A}{\partial t} = \nabla \cdot \left(D_{AB} C \frac{M_B \nabla x_A}{x_A M_A + x_B M_B} - V C_A \right)$$

$$\frac{\partial C_B}{\partial t} = \nabla \cdot \left(D_{BA} C \frac{M_A \nabla x_B}{x_A M_A + x_B M_B} - V C_B \right) \qquad (16).$$

Here V is the bulk mass averaged velocity {m·s^{-1}} and M_A and M_B are the molecular weights of species A and B, accordingly. The above expression can be further simplified to:

$$\frac{\partial C_A}{\partial t} = \nabla \cdot \left(D_A \nabla C_A - U_A C_A \right)$$

$$\frac{\partial C_B}{\partial t} = \nabla \cdot \left(D_B \nabla C_B - U_B C_B \right) \qquad (17),$$

where:

$$D_A = D_{AB}\frac{M_B}{x_A M_A + x_B M_B}$$
$$D_B = D_{BA}\frac{M_A}{x_A M_A + x_B M_B} \qquad (18).$$

Assuming Ideal Gas behavior, U_A and U_B can be written as:

$$U_A = V + \frac{D_A}{p}\nabla p$$
$$U_B = V + \frac{D_B}{p}\nabla p \qquad (19),$$

where p is the pressure of the mixture at a particular location {Pa}. Equations similar to (17, 18) were also developed by McCarty and Mason [96] for a Stefan-tube set-up assuming a frictionless plug. Such restrictions/assumption were not necessary here.

The mass averaged bulk velocity, V, in Equation (19) is estimated from the conservation of linear momentum [21]:

$$\rho_{TOT}\frac{\partial \vec{V}}{\partial t} = -\rho_{TOT}\vec{V}\cdot\nabla\vec{V} + \vec{f} \qquad (20),$$

where ρ_{TOT} is the mass density of the gas mixture {kg·m^{-3}}, f groups the effect of surface and body forces acting on the control volume {kg·m^{-2}s^{-2}}, and the arrows indicate the

vector nature of these variables. As a first approximation, the fluid-wall friction was neglected and only pressure forces were considered in *f, i.e.* $f = -\nabla p + \rho_{TOT}\vec{g}$, which allowed for a estimate of the maximum effect that diffusively driven convection can have in a one-dimensional model.

With the appropriate boundary conditions, Equations (17, 20) constitute a set of coupled differential equations with which to model the transport of a noble gas through a porous system in the absence of externally pressure gradients or reactions.

Because the experimental set-up used here has varying cross section areas and porosities, a direct discretization of partial differential equations is not possible. Assuming a one-dimensional approximation and using a control volume analysis, Equations (17, 20) can be rewritten as:

$$\forall_{gas}\frac{\partial C_A}{\partial t} = \oint\left(-D_A\nabla C_A + U_A C_A\right)\cdot dA_S$$

$$\forall_{gas}\frac{\partial C_B}{\partial t} = \oint\left(-D_B\nabla C_B + U_B C_B\right)\cdot dA_S \qquad (21),$$

$$\forall_{gas}\rho_{TOT}\frac{\partial \vec{V}}{\partial t} = \oint\left(\overrightarrow{-V_z}\rho_{TOT}\vec{V_z}\cdot\vec{n} + \vec{p}\right)dA \qquad (22).$$

Here $\forall_{gas}$ {m^3} is the gas volume within a particular volume element of the experimental system, A_S {m^2} is the cross sectional surface area of the control volume where the mass transfer takes place, and p {Pa} is the pressure at the control volume interface. This pressure is equal to the sum of the pressure developed by the different diffusion rates of species *A* and *B*, p_o {Pa}, and a pressure equivalent to the average hydrostatic pressure within a giving section of the experimental system, p_g {Pa}.

Inclusion of the gravitational pressure term, p_g, aims to approximate the effect of potential gravity currents that rise when two gases of different composition (and density) are put in contact [99]. Assuming an ideal gas behavior, p_g is:

$$p_g = \frac{\int_{A_S} p_o \exp\left(-\frac{g\ M_{mix} y}{RT}\right) dA}{\int_{A_S} dA} \qquad (23),$$

where g is the gravitational constant (9.81 $m \cdot s^{-2}$), A_S {m^2} is the cross sectional area of the experimental set-up region under analysis, and M_{mix} is the molar averaged gas mixture molecular weight {$kg \cdot mol^{-1}$} and is estimated by:

$$M_{mix} = \sum_{i=1,N} x_i M_i \qquad (24).$$

The diffusion coefficients in Equation (21) depend on temperature, molecular mass, the relative concentration of the species as shown in Equation (18). The free space binary diffusivity, D_{XeN2}, used in Equation (18) can be determined using the correlation given by Bird *et al*. [21]:

$$D_{AB} = 2.745 \times 10^{-4} \cdot \frac{T^{1.823}}{\left(T_{cA} T_{cB}\right)^{0.4948}} \cdot \frac{\left(p_{cA} p_{cB}\right)^{1/3}}{p} \cdot \left(\frac{1}{M_A} + \frac{1}{M_B}\right)^{1/2} \qquad (25).$$

Here T_{ci}, p_{ci}, and M_i are the critical temperature, critical pressure, and molecular weight of gas *i* respectively.

Within the section of the experimental set-up filled with SiO_2 Ottawa sand, the effects of the porous media structure are taken into consideration by scaling the diffusivities D_A and D_B by ϕ/τ, where ϕ is the media porosity and τ is the tortuosity [100, 101]. As a first approximation ϕ was taken to be 0.3, with $\tau = 1\text{-}k\ ln(\phi)$, where k is an empirical parameter (= 0.5 for a hard sphere approximation) [37].

2. METHODS.

Equations (21, 22) are discretized using a finite difference implementation in both MATLAB and Fortran 90 and simulation results are compared with experimental data presented previously. Because of the similarity in molecular weight between argon and nitrogen, the migration of argon in the experimental set-up was modeled under the assumption of a fully isobaric process. For xenon however, this assumption was relaxed and the full Equations (21, 22) were solved together.

a) Numerical methods.

Time and space discretization

For this work, the direction of a positive flux is defined from the xenon cylinder to the porous media (left to right), Figure 10. Assuming a one-dimensional system, for a general species B, Equation (21) is discretized as:

$$\forall_{gas}\frac{C_B^{t+\Delta t}-C_B^t}{\Delta t}=\left[-\frac{D_{B\_L}}{2}\left[\left(\frac{\partial C_B}{\partial x}\right)_L^{t+\Delta t}+\left(\frac{\partial C_B}{\partial x}\right)_L^{t}\right]+\frac{U_L}{2}\left(C_{B\_L}^{t+\Delta t}+C_{B\_L}^{t}\right)\right]A_L- \tag{26}$$

$$\left[-\frac{D_{B\_R}}{2}\left[\left(\frac{\partial C_B}{\partial x}\right)_R^{t+\Delta t}+\left(\frac{\partial C_B}{\partial x}\right)_R^{t}\right]+\frac{U_L}{2}\left(C_{B\_R}^{t+\Delta t}+C_{B\_R}^{t}\right)\right]A_R$$

Here Δt is the time step {s}, the super scripts t and $t+\Delta t$ indicate the time step at which the concentration is evaluated. The right hand side of Equation (26) is the net flux at the boundary of the specific control volume. Accordingly, A_L and A_R are the left and right areas {m^2} through which species migration takes place, Figure 10. The sub scripts L and R on areas, diffusivities, concentration, and concentration gradients explicitly indicate that these variables are estimated at the left and right ***boundaries*** of the control volume under analysis, *e.g.* i, and should not be taken as i-*1* and i+*1*.

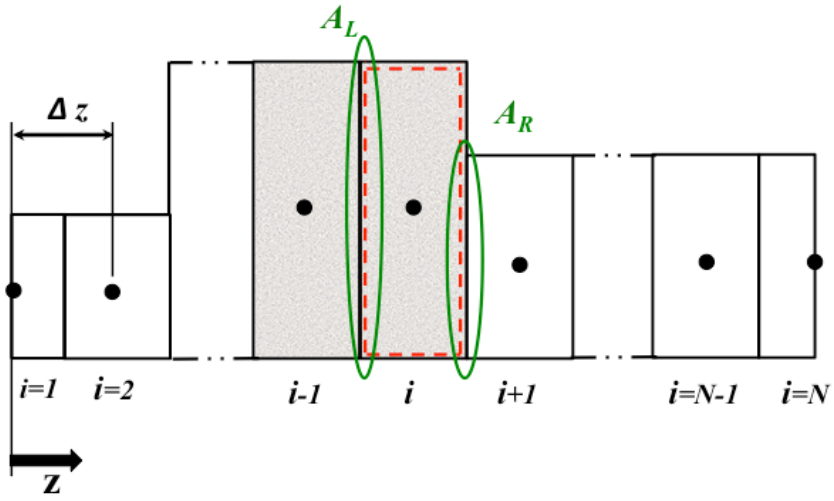

Figure 10 Schematic of the discretized experimental set-up. Schematic showing the principal grid and the control volume of the general element i. Note the difference between the left, A_L, and right area, A_R, of this element.

From here subscripts indicate the spatial location of the control volume we are interested on, and superscripts the time point. The experimental set-up is uniformly discretized in N elements of length Δz {m^2}. From Equation (26), the control volume analysis of every element of this main grid is:

$$A_i \Delta z \phi_i \frac{C_i^{t+1} - C_i^t}{\Delta t} = \left[-D_L^* \left(\frac{C_i^{t+1} - C_{i-1}^{t+1} + C_i^t - C_{i-1}^t}{2\Delta z} \right) + U_L^* \left(\frac{C_i^{t+1} + C_{i-1}^{t+1} + C_i^t + C_{i-1}^t}{4} \right) \right] A_L -$$

$$\left[-D_R^* \left(\frac{C_{i+1}^{t+1} - C_i^{t+1} + C_{i+1}^t - C_i^t}{2\Delta z} \right) + U_R^* \left(\frac{C_{i+1}^{t+1} + C_i^{t+1} + C_{i+1}^t + C_i^t}{4} \right) \right] A_R \tag{27}$$

where ϕ_i and τ_i are the media porosity and tortuosity of the element i, A_i, is its cross sectional area {m^2}, and the super script * indicates that the velocity and diffusivities must be modified to account for effects of the porous media:

$$D_L^* = 2 \left(\frac{\phi_{i-1} D_{i-1}}{\tau_{i-1}} \right) \left(\frac{\phi_i D_i}{\tau_i} \right) \Bigg/ \left(\frac{\phi_{i-1} D_{i-1}}{\tau_{i-1}} + \frac{\phi_i D_i}{\tau_i} \right)$$

$$D_R^* = 2 \left(\frac{\phi_{i+1} D_{i+1}}{\tau_{i+1}} \right) \left(\frac{\phi_i D_i}{\tau_i} \right) \Bigg/ \left(\frac{\phi_{i+1} D_{i+1}}{\tau_{i+1}} + \frac{\phi_i D_i}{\tau_i} \right) \tag{28},$$

$$U_L^* = \left(\frac{2\phi_{i-1}\phi_i}{\phi_{i-1} + \phi_i} \right) U_L$$

$$U_R^* = \left(\frac{2\phi_i \phi_{i+1}}{\phi_i + \phi_{i+1}} \right) U_R \tag{29}.$$

Expanding and regrouping Equation (27):

$$C_{i-1}^{t+1}\left(-\frac{U_L^*A_L^*}{4\Delta z}-\frac{D_L^*A_L^*}{2\Delta z^2}\right)+C_i^{t+1}\left(\frac{1}{\Delta t}-\frac{U_L^*A_L^*}{4\Delta z}+\frac{D_L^*A_L^*}{2\Delta z^2}+\frac{U_R^*A_R^*}{4\Delta z}+\frac{D_R^*A_R^*}{2\Delta z^2}\right)+C_{i+1}^{t+1}\left(\frac{U_R^*A_R^*}{4\Delta z}-\frac{D_R^*A_R^*}{2\Delta z^2}\right)=$$

$$C_{i-1}^{t}\left(\frac{U_L^*A_L^*}{4\Delta z}+\frac{D_L^*A_L^*}{2\Delta z^2}\right)+C_i^{t}\left(\frac{1}{\Delta t}+\frac{U_L^*A_L^*}{4\Delta z}-\frac{D_L^*A_L^*}{2\Delta z^2}-\frac{U_R^*A_R^*}{4\Delta z}-\frac{D_R^*A_R^*}{2\Delta z^2}\right)+C_{i+1}^{t}\left(-\frac{U_R^*A_R^*}{4\Delta z}+\frac{D_R^*A_R^*}{2\Delta z^2}\right)$$

(30),

where:

$$A_L^*=\frac{A_L}{A_i\phi_i},A_L^*=\frac{A_R}{A_i\phi_i}$$

(31).

The boundary conditions at *z=0* and *z=L* (first and last element respectively) are:

$$A_1\frac{\Delta z}{2}\phi_1\frac{C_1^{t+1}-C_1^t}{\Delta t}=-\left[-D_R^*\left(\frac{C_2^{t+1}-C_1^{t+1}+C_2^t-C_1^t}{2\Delta z}\right)+U_R^*\left(\frac{C_2^{t+1}+C_1^{t+1}+C_2^t+C_1^t}{4}\right)\right]A_R$$

$$A_N\frac{\Delta z}{2}\phi_N\frac{C_N^{t+1}-C_N^t}{\Delta t}=\left[-D_L^*\left(\frac{C_N^{t+1}-C_{N-1}^{t+1}+C_N^t-C_{N-1}^t}{2\Delta z}\right)+U_L^*\left(\frac{C_N^{t+1}+C_{N-1}^{t+1}+C_N^t+C_{N-1}^t}{4}\right)\right]A_L$$

(32)

Grouping and rearranging:

$$C_1^{t+1}\left(\frac{1}{\Delta t}+\frac{U_R^*A_R^*}{2\Delta z}+\frac{D_R^*A_R^*}{\Delta z^2}\right)+C_2^{t+1}\left(\frac{U_R^*A_R^*}{2\Delta z}-\frac{D_R^*A_R^*}{\Delta z^2}\right)=C_1^t\left(\frac{1}{\Delta t}-\frac{U_R^*A_R^*}{2\Delta z}-\frac{D_R^*A_R^*}{\Delta z^2}\right)+C_2^t\left(-\frac{U_R^*A_R^*}{2\Delta z}+\frac{D_R^*A_R^*}{\Delta z^2}\right)$$

$$C_{N-1}^{t+1}\left(-\frac{U_L^*A_L^*}{2\Delta z}-\frac{D_L^*A_L^*}{\Delta z^2}\right)+C_N^{t+1}\left(\frac{1}{\Delta t}-\frac{U_L^*A_L^*}{2\Delta z}+\frac{D_L^*A_L^*}{\Delta z^2}\right)=C_{N-1}^{t}\left(\frac{U_L^*A_L^*}{2\Delta z}+\frac{D_L^*A_L^*}{\Delta z^2}\right)+C_N^{t}\left(\frac{1}{\Delta t}+\frac{U_L^*A_L^*}{2\Delta z}-\frac{D_L^*A_L^*}{\Delta z^2}\right) \tag{33}$$

Estimating diffusively driven velocity

Following the recommendation of the SIMPLE algorithm, a staggered grid shown in Figure 11 was used to determine the velocities in Equation (22).

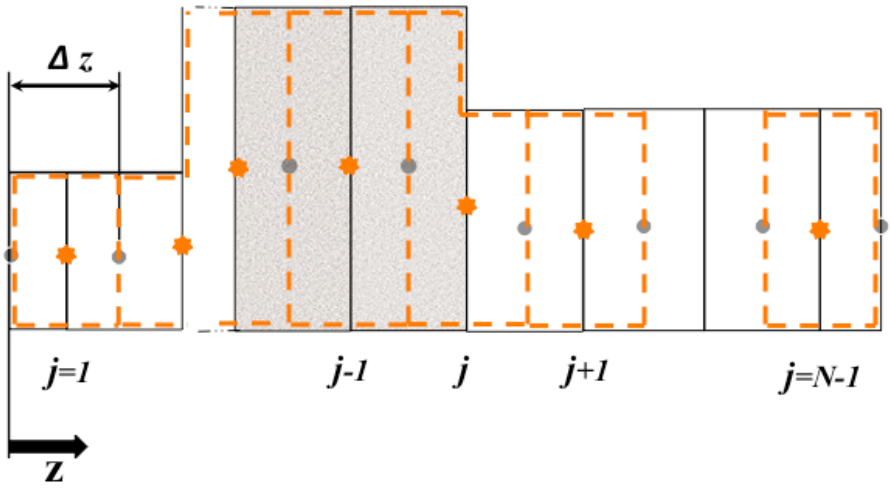

Figure 11 Schematic of staggered grid. Location of the staggered grid (orange) and principal grid (grey).

To differentiate between the discretization of the principal and staggered grids, lower case sub indices *j*, *l* and *r* will be used to indicate the element in the velocity grid under analysis, and its left and right boundaries, respectively. From conservation of momentum in a characteristic control volume with variable area and media, Equation (22) is simplified to:

$$\forall_{gas-j}\rho_{TOT-j}\frac{\partial V_j}{\partial t} = \rho_{TOT-l}V_l^2\phi_l A_l + p_l\phi_l A_l - \rho_{TOT-r}V_r^2\phi_r A_r - p_r\phi_r A_r + p_j\left(\phi_r A_r - \phi_l A_l\right) \tag{34}$$

where ρ_{TOT} is the mass density of the gas mixture {kg·m^{-3}}, ρ_j is the mixture pressure at the node *j* of the staggered grid, and all other symbols follow the nomenclature of the previous supplemental material. Note that Equation (34) neglects the shear forces at the wall gas interface, F_W (shown in Figure 12). Likewise, the reactions on the left and right of the solid matrix ($F_{matrix\text{-}l}$ and $F_{matrix\text{-}r}$ in Figure 12) are assumed to balance to each other. These two assumptions aim to increase the magnitude of the velocities and convection effects on the model here developed.

The velocities at the boundaries of every element in the staggered grid V_l and V_r are determined from a linear interpolation of elements *j-1* and *j*, and *j* and *j+1* respectively:

$$V_l = \frac{V_{j-1} + V_j}{2},\ V_r = \frac{V_j + V_{j+1}}{2} \tag{35}$$

The lower case sub indices from the staggered grid can be related to the principal grid. For example, the volume, densities, and areas of the staggered and principal grids (sub-indexes *j* and *i* respectively) in Figure 12 are related by:

$$\forall_{gas-j} = \frac{\left(\phi_i A_i + \phi_{i+1} A_{i+1}\right)\Delta z}{2}$$

$$\rho_{TOT-j} = \left(\frac{\rho_{TOT-i} + \rho_{TOT-(i+1)}}{2}\right), \quad \rho_{TOT-l} = \rho_{TOT-i}, \quad \rho_{TOT-r} = \rho_{TOT-(i+1)} \tag{36}$$

$$A_l = A_i, \quad A_r = A_{(i+1)}$$

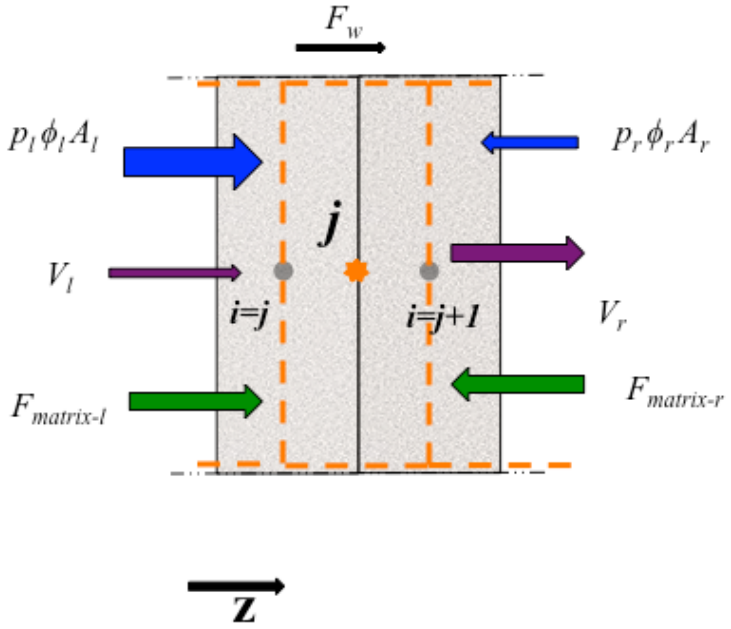

Figure 12 Momentum conservation in a characteristic control volume. Forces and fluid flows acting on a characteristic control volume: Wall-fluid friction force (F_W), pressure forces ($p_i A_i \phi_i$), solid matrix reactions ($F_{matrix-i}$), and mass averaged velocities (V_i).

Finally, since the nodes in the staggered grid are placed in the edges of the elements defined by the principal grid, the pressure at every node j can be estimated by a linear interpolation of p_i and p_{i+1} *i.e.* $p_j = (p_i + p_{i+1}) / 2$. Therefore, the pressure terms in Equation (34) can be rearranged to:

$$p_l\phi_l A_l - p_r\phi_r A_r + p_j\left(\phi_r A_r - \phi_l A_l\right) = \left(\frac{\phi_{i+1}A_{i+1} + \phi_i A_i}{2}\right)\left(p_i - p_{i+1}\right) \tag{37}$$

Combining this with Equations (35, 36), a fully explicit discretization on time of Equation (34) for *j=2* to *j=N-2* turns into:

$$\frac{\Delta z\left(\rho_{TOT-i} + \rho_{TOT-(i+1)}\right)\left(\phi_i A_i + A_{i+1}\phi_{i+1}\right)\left(V_j^{t+1} - V_j^t\right)}{4\Delta t} = \rho_{TOT-i}\phi_i A_i\left(\frac{V_{j-1}^t + V_j^t}{2}\right)^2 -$$

$$\rho_{TOT-(i+1)}\phi_{i+1}A_{i+1}\left(\frac{V_j^t + V_{j+1}^t}{2}\right)^2 + \left(\frac{\phi_{i+1}A_{i+1} + \phi_i A_i}{2}\right)\left(p_i - p_{i+1}\right) \tag{38},$$

which can be rearranged to:

$$V_j^{t+1} = V_j^t + \frac{4\Delta t}{\Delta z\left(\rho_{TOT-i} + \rho_{TOT-(i+1)}\right)\left(\phi_i A_i + A_{i+1}\phi_{i+1}\right)} \cdot$$
$$\left[\rho_{TOT-i}\phi_i A_i\left(\frac{V_{j-1}^t + V_j^t}{2}\right)^2 - \rho_{TOT-(i+1)}\phi_{i+1}A_{i+1}\left(\frac{V_j^t + V_{j+1}^t}{2}\right)^2 + \left(\frac{\phi_{i+1}A_{i+1} + \phi_i A_i}{2}\right)\left(p_i - p_{i+1}\right)\right] \tag{39}.$$

Following the above expression, the boundary conditions at *z=0*, *z=L+Δz* , *z=L-Δz*, and *z=L-Δz* are:

$$V_{j=0}^{t+1} = 0 \tag{40},$$

$$V_{j=1}^{t+1} = V_{j=1}^{t} + \frac{4\Delta t}{\Delta z\left(\rho_{TOT-1} + \rho_{TOT-2}\right)\left(\phi_1 A_1 + A_2\phi_2\right)} \cdot$$

$$\left[-\rho_{TOT-2}\phi_2 A_2\left(\frac{V_{j=1}^{t} + V_{j=2}^{t}}{2}\right)^2 + \left(\frac{\phi_2 A_2 + \phi_1 A_1}{2}\right)\left(p_1 - p_2\right)\right] \qquad (41),$$

$$V_{j=N-1}^{t+1} = V_{j=N-1}^{t} + \frac{4\Delta t}{\Delta z\left(\rho_{TOT-(N-1)} + \rho_{TOT-N}\right)\left(\phi_{N-1} A_{N-1} + A_N\phi_N\right)} \cdot$$

$$\left[\rho_{TOT-(N-1)}\phi_{N-1} A_{N-1}\left(\frac{V_{N-2}^{t} + V_{N-1}^{t}}{2}\right)^2 + \left(\frac{\phi_N A_N + \phi_{N-1} A_{N-1}}{2}\right)\left(p_{N-1} - p_N\right)\right] \qquad (42),$$

$$V_{j=N}^{t+1} = 0 \qquad (43).$$

It should be stressed that in Equations (39 to 43), the sub indices of the velocities indicated the location of this variable in the staggered grid. On the other hand, the sub indices of density, area, porosity, and pressure indicate the location in the principal grid. As a final note, it should be mentioned that the length of the experimental set-up model was slightly altered so diameter and media variations would occur between elements of the principal grid as shown in Figure 10.

Equations (28 to 33), describe species conservation when diffusion and advection effects are present. When the difference in diffusion rates between species is neglected, these equations can be simplified by making $D_{Xe} = D_{N2} = \mathrm{D_{XeN2}}$ and $U_L = U_R = 0$. The formulation of the equations for this simpler model can be obtained directly from Equations (30 to 33). As an example, for a general element *i*, Equation (30) is reduced to:

$$C_{i-1}^{t+1}\left(\frac{-D^*_{L\_XeN_2}A^*_L}{2\Delta z^2}\right)+C_i^{t+1}\left(\frac{1}{\Delta t}+\frac{D^*_{L\_XeN_2}A^*_L}{2\Delta z^2}+\frac{D^*_{R\_XeN_2}A^*_R}{2\Delta z^2}\right)+C_{i+1}^{t+1}\left(\frac{-D^*_{R\_XeN_2}A^*_R}{2\Delta z^2}\right)=$$

$$C_{i-1}^{t}\left(\frac{D^*_{L\_XeN_2}A^*_L}{2\Delta z^2}\right)+C_i^{t}\left(\frac{1}{\Delta t}-\frac{D^*_{L\_XeN_2}A^*_L}{2\Delta z^2}-\frac{D^*_{R\_XeN_2}A^*_R}{2\Delta z^2}\right)+C_{i+1}^{t}\left(\frac{D^*_{R\_XeN_2}A^*_R}{2\Delta z^2}\right)$$

(44).

b) Estimation of the effective diffusivity

Equation (25), and the empirical relation $\tau = 1 - k\ ln(\phi)$ [37], were used to determine an initial guess for the effective diffusivity within the porous media. As an initial guess, ϕ was taken to be *0.3*, and k=0.5 (hard sphere approximation). The diffusivity was varied incrementally between ± 5% of the initial guess until a minimum square error difference between the experimental data and the modeling results was minimized. The designated diffusivity to the system is the one with the minimum error [89].

3. RESULTS AND DISCUSSION.

Appendix B and *Appendix C* contain the programs developed in MATLAB and Fortran90 for implementation of the above models. *Appendix D* gives the results if a mesh reduction study as well as validation of the numerical approach against an analytical solution.

Figure 13 shows the comparison between argon experimental results listed in Table 3 and the implementation of Equation (21) in MATLAB when the effect of the molecular weight difference between gases is ignored. Following the procedure outlined in the previous section, an effective diffusion coefficient of 0.944×10^{-2} $cm^2 \cdot s^{-1}$ was determined for the argon-nitrogen experiments [89]. The correlation parameter between the model and experimental results was $R^2=0.98$, Figure 13. The good agreement between the optimized model and experimental results suggests that the weight difference between the argon and nitrogen molecules does not significantly affect the migration of the noble gas.

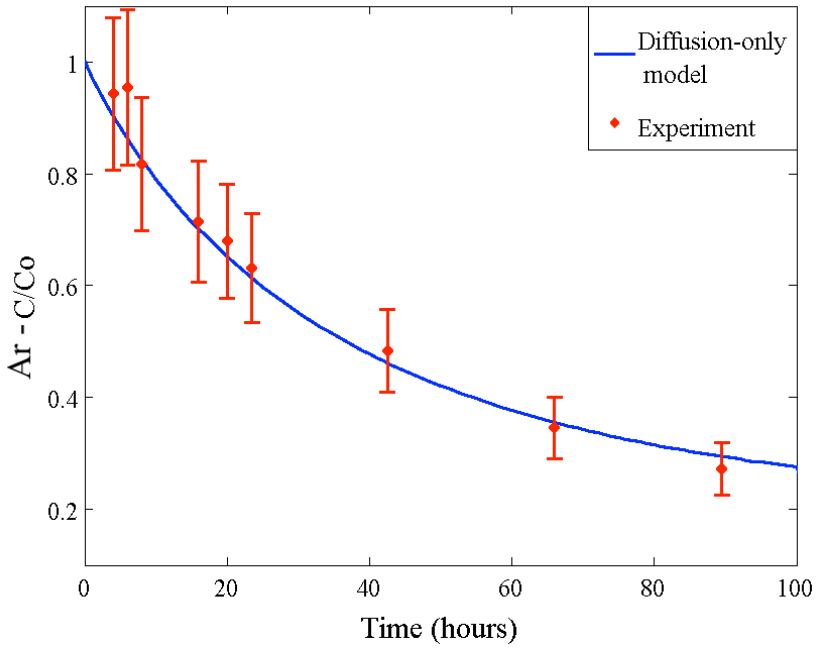

Figure 13 Estimated variation of argon concentration [89]. Comparison of the numerical model programmed in MATLAB for a diffusion only case, and the results of the diffusion experiments listed in Table 3. Experimental error estimated using Equation (14). The correlation parameter between the model and experimental results was $R^2=0.98$.

By contrast to the results in Figure 13, the diffusion-only model, clearly over predicts the concentration of xenon remaining in the sample cylinder. Figure 14 shows the comparison between the time variation of xenon concentration and the diffusion-only model when the free space diffusivity is calculated by Equation (25), and then varied in the porous medium section following the same procedure used in the argon-nitrogen case.

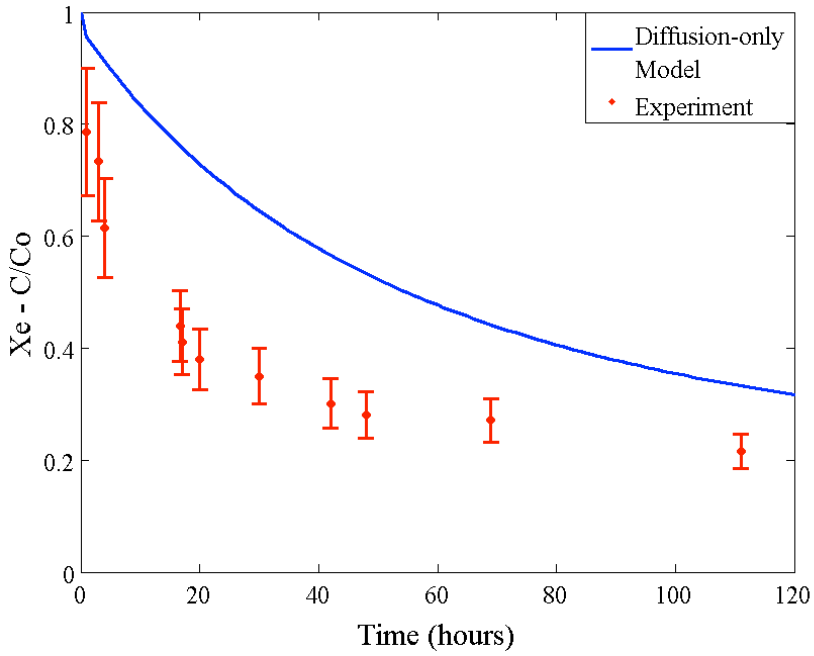

Figure 14 Comparison of xenon experimental data and diffusion only model. The initial guess of the Xe-N_2 binary diffusivity was estimated from a free-space diffusivity increased by a factor of five.

To reduce the difference between model and experiment using a diffusion only model, the free-space diffusivity was increased and then optimized in the porous medium section. After scaling the binary diffusivity, D_{XeN2}, estimated from Equation (25) by a factor of five, the root mean squared error of *C/Co* obtained is 0.0043, and the optimized diffusivity in the media determined is 1.02 x10^{-2} $cm^2 \cdot s^{-1}$. This improved the correlation

parameter between model and experiment, $R^2=0.89$. The still large difference between the diffusion-only model predictions and the values measured occurring in the first five hours of experiment suggest the presence of other transient and mass dependent transport mechanisms. Two options were explored to capture these effects using a one-dimensional transport model: consider the bulk advection that can rise from the different molecular migration rates of xenon and nitrogen after the isobaric process assumption is relaxed; consider the effect of gravity currents that follow the removal of the barrier that initially separates two fluids with large difference in their densities.

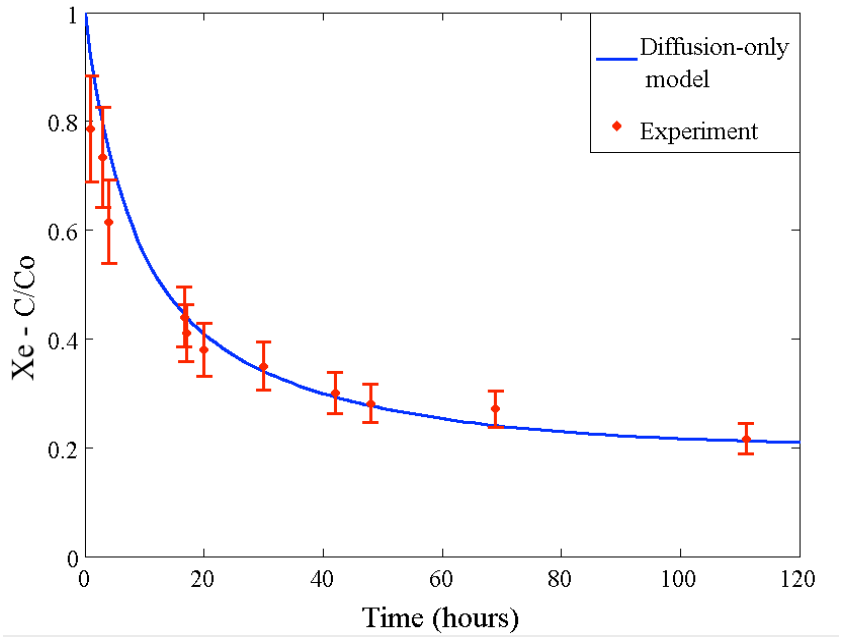

Figure 15 Comparison of xenon experimental data and optimized diffusion only model. The initial guess of the Xe-N_2 binary diffusivity was estimated from a free-space diffusivity increased by a factor of five. The correlation between model and experiment is $R^2=0.89$.

Relaxing the isobaric assumption of the diffusion-only model, and taking into account the pressure gradients that rise from the different migration rates of non equi-

molar gases, gives a better estimate of the xenon concentration on the first hours of experiment, Figure 16. The effective diffusivity estimated using this model is also 1.02×10^{-2} $cm^2 \cdot s^{-1}$ and the correlation coefficient is $R^2=0.95$. However, obtaining this better agreement still requires scaling up the diffusivity D_{XeN2} from Equation (25) by a factor of five and there is no physical justification for this.

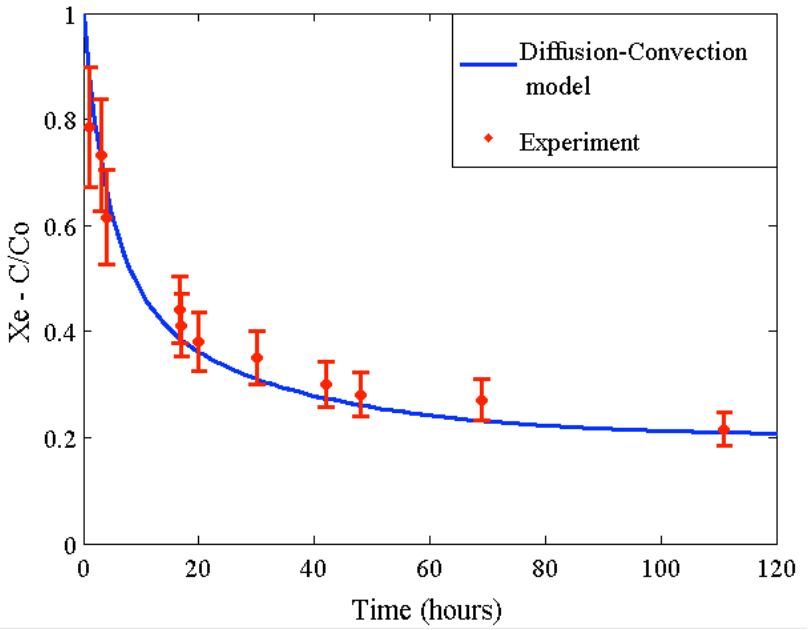

Figure 16 Comparison of xenon experimental data and the optimized Convection-Diffusion model. The initial guess of the Xe-N_2 binary diffusivity was estimated from a free-space diffusivity increased by a factor of five. The correlation between model and experiment is $R^2=0.95$.

Considering the effect of the gas mixture density variation (gravity currents), Equation (23) estimates initial pressure gradients of 0.25 $Pa \cdot cm^{-1}$ and 0.03 $Pa \cdot cm^{-1}$ at the xenon-nitrogen and argon-nitrogen interfaces, respectively. Pressure gradients of these magnitudes would raise initial bulk velocities of 4.8 and 0.7 $m \cdot s^{-1}$ at the gas interface (calculated using Darcy's law with a permeability $K = d^2/32$, where d=11.9 mm is the set-

up diameter at the initial interface). Dissipation of these relatively large velocities will start immediately after they are generated due to the viscous effects, fading of the gas interface as the species mix, and counter pressures that would rise in a closed volume. A more detailed evaluation of gravity currents will be considered in a later work.

Conclusions. Two numerical models were developed: a diffusion-only model and a diffusion-convection model for a binary system (argon-nitrogen and xenon-nitrogen). The argon concentration variation estimated by the diffusion-only model with an optimized diffusivity showed good agreement with experimental results. However, when this analysis is extended to xenon-nitrogen diffusion, the diffusion-only model is not as good in predicting the observed depletion rate of xenon in the gas cylinder. Even when the xenon-nitrogen free-space diffusivity is increased by a factor of five and optimized for the porous media section, the correlation between experiment and simulation ($R^2=0.89$) is still lower than for argon ($R^2=0.98$). The largest discrepancies occur during the first few hours where the model over predicts C/C_o by 6-13%. When the diffusion-convection model is used, a better approximation of these first data points was attained (the model differs form the experiments by 9.6% and 5.2% after 1 and 4 hours of diffusion respectively, and under estimate C/C_o by 0.9% after 3 hours of experiment). The correlation between the diffusion-convection simulation and experiment improves to $R^2=0.95$. Future work will consider the effect of gravity driven flow on the transport of xenon.

Using a nitrogen-noble gas binary system to investigate the effect of the difference on their molecular weights on their transport rate is a good first approximation to the transport of argon and xenon in the atmosphere. This is the case because of the similarity between the molecular weight and density of nitrogen (~28 $kg \cdot mol^{-1}$ and

$1.251x10^{-3}$ $g \cdot m^{-3}$ at STP conditions, respectively) and the molar average molecular weight and density of Earth's atmosphere at the Troposphere (~28.8 $kg \cdot mol^{-1}$ and $1.293x10^{-3}$ $g \cdot m^{-3}$ assuming a molar composition of 78.0% nitrogen, 20.9% oxygen, and 0.9% argon). More accurate predictions require knowledge of the underground atmosphere composition at the location of interest.

Chapter 3: Fractal analysis of the porous media tortuosity from its transport properties.

Predicting the transport of fluids in the subsurface requires accurate estimates for the transport coefficients. The Kozeny-Carman equation relates the medium's specific surface area, tortuosity and porosity to its saturated conductivity. For porous systems that exhibit fractal structure, scaling relationships have been used to show that the saturated conductivity is a function of both the pore volume, and pore surface fractal dimensions of a system. Previous work has shown that for a porous system, the tortuosity can be expressed as a function of the pore volume and spectral fractal dimensions of a medium. Gimenez *et al*. [102] proposed a methodology to determine this fractal dimension from saturated conductivity and porosity measurements. However, the fractal relations obtained were incorrect as they predicted negative connectivity parameters. In this chapter, I developed a new fractal model that correctly estimates positive connectivity parameters for the geological samples characterized in [102].

1. THEORETICAL BACKGROUND

Fluid transport in porous media affects the dynamics of systems that range in scale from microfluidic devices to the hydrologic cycle. The saturated conductivity of a medium is particularly important for understanding the movement and distribution of fluids within it. The saturated hydraulic conductivity of a system, K_{sat} {m·s^{-1}}, is defined by:

$$K_{sat} = k\frac{g}{\upsilon} \qquad (45),$$

where g {$m \cdot s^{-2}$} is the gravitational constant and υ is the fluid kinematic viscosity {$m^2 \cdot s^{-1}$}, and k is the permeability {m^2} of the system under analysis. On a porous medium, the Kozeny-Carman equation relates the permeability, k {m^2}, to the medium porosity, ϕ, specific surface area, S {m^{-1}}, and tortuosity, τ [103]:

$$k = \frac{C_o \phi}{\tau S^2} \tag{46}.$$

It is important to stress that in this document, the specific surface area is defined as the solid-fluid interface area (A) per unit of representative elementary volume, or REV volume (V_{REV}) [103, 104],:

$$S = \frac{A}{V_{REV}} \tag{47}.$$

From Equation (45, 46), the saturated conductivity of a porous medium can be estimated by:

$$K_{sat} = \frac{g k_o}{\upsilon}\left(\frac{\phi}{\tau S^2}\right) \tag{48}.$$

Deriving a simpler model for the saturated conductivity is complicated by the fact that fluid transport is also affected not just by the gross topology of the pore space by also by its interconnectedness. From the perspective of a fluid element, connectivity affects the effective length of a pore channel and the amount of momentum/kinetic energy

transferred to the media matrix [34, 69, 105, 106]. Both effects are taken into account by a tortuosity coefficient. In this regard, it is commonly assumed that the increase in tortuosity is related to a reduction in porosity by a power law [69, 105]:

$$\tau \sim \phi^{-\alpha} \qquad (49),$$

where α is the connectivity parameter. Note that by definition, the connectivity parameter, α, must be positive. A negative connectivity parameter would indicate that a medium with increasing porosity would have a smaller tortuosity. Combining Equation (48) and Equation (49), the saturated conductivity of a porous medium can be estimated by:

$$K_{sat} \sim \frac{\phi^{1+\alpha}}{S^2} \qquad (50).$$

Further simplification of Equation (50) requires knowing the interconnectivity parameter and the specific surface area, or a way to relate these variables to the medium porosity. Work over the last two decades has shown that many porous materials, both artificial and natural, exhibit fractal structure over a wide range of length scales *e.g.* [39, 107, 108]. Past work has often assumed that a single fractal dimension can be used to characterize the topology of a medium's pore space and models of capillary pressure and fluid conductivity have been related to this parameter [42, 43, 109]. Recent work, however, has shown that many porous systems can exhibit distinct fractal dimensions that are characteristic of their pore surfaces and pore volume as a whole [108]. Using ratios of scaling relationships, it was previously shown that this added complexity would affect

a medium's saturated conductivity [102]. More recently, it has been demonstrated how the multi-fractal character of medium would influence its equilibrium capillary pressure-moisture content relationship, as well as capillary condensation behavior [46].

Fractals

A fractal is a self-similar or statistical self-similar geometric set in a range of scales created by following a simple and recursive definition (generator) on a simple geometric set (initiator). For example, for a Siepinski gasket, the initiator is a square and generator applied recursively is dividing every square on nine parts and subtracting the one in the middle, Figure 17.

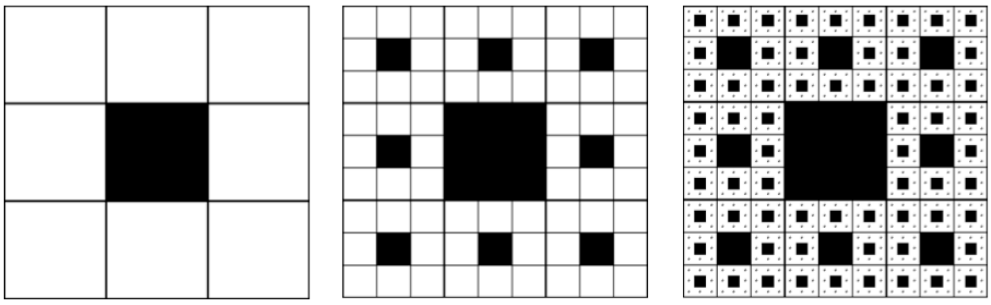

Figure 17 Generating a Sierpinski Gasket. From left to right: first generation pre-fractal (generator), second generation pre-fractal, and fourth generation pre-fractal. The Sierpinski gasket is the *n*-th generation pre-fractal when *n* tends to infinity.

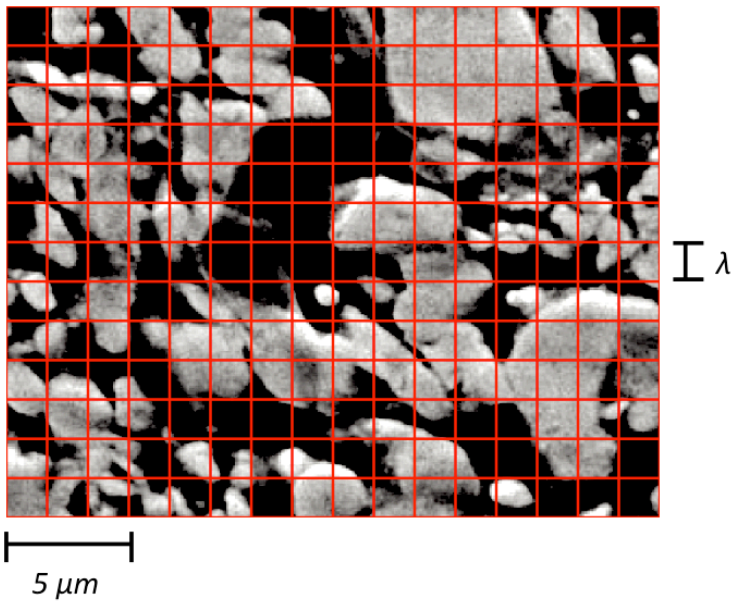

Figure 18 Box counting method on a porous media sample. Array of boxes with characteristic length λ superimposed on a 2-D image of a porous media to estimate the pore (black regions) surface fractal dimension. Image of tungsten powder 8-10 μm infiltrated with a 70Cu/30Ag.

Distinctive non-Euclidean and non-integer dimensions describe different characteristics of a fractal set. Several publications use geometrical arguments to relate the surface roughness, surface area, and path length of both natural and well-known fractal generators (such as the Sierpinski gasket or the Menger sponge) to their fractal dimensions of mass, length, surface, and volume. Arguably, the most popular technique to determine the dimensions of a fractal set in a soil characterization is by image analysis using the box counting method [34, 39, 48, 68, 102, 110, 111]. In this technique, an array of boxes of a characteristic length, λ in Figure 18, is superimposed to the two-dimension image under analysis. The number of boxes to fully cover a specific characteristic (pore area for example), N, and the box characteristic length, λ, are related by:

$$D_A = \lim_{\lambda \to \infty} \left(\frac{\log(N)}{\log(1/\lambda)} \right) \qquad (51),$$

where D_A is the pore area fractal dimension. A similar procedure is used to estimate the fractal dimension that describes the perimeter of the pore regions. A common practice to extend the fractal analysis of a two-dimension image to describe a three-dimension object is to simply increase the measured fractal dimension by one [112].

Developing a scaling relation for how saturation would vary with tortuosity has been difficult to do in terms of parameters that can be easily to measure (*i.e* pore volume and pore surface fractal dimensions). Instead, many authors use random walk or tortuosity fractal dimensions [34, 45, 48, 69, 113]. Previous work by Gimenez *et al*. [102] proposed the estimation of the connectivity parameter, α, by comparison of a porosity based conductivity model with saturated conductivity measurements, and resin-impregnated soil images from which pore surface and volume fractal dimension could be extracted. The methodology proposed by Gimenez *et al*. is remarkably clever as it relies on traditional and well-known laboratory techniques to determine α. However, the results obtained, which give negative connectivity parameters, question the fractal model that was used. Here I propose a new relationship for the saturated conductivity of a porous medium as a function of its porosity and surface and volume spectral fractal dimensions.

2. METHODOLOGY

If the pore space has a fractal structure, it is possible to follow Perrier *et al*. [43] who used the cumulative distribution function $N(volume^{1/dE} > \lambda) = F\ \lambda^{-D_V}$ to determine total pore volume, V, where λ is taken to the "radius" that corresponds to V, F is constant, and D_V is the pore fractal dimension and d_E is the Euclidean dimension of the space. The differential dN is then given by:

$$dN = -D_V F \lambda^{-D_V - 1} d\lambda \qquad (52).$$

Following Perrier *et al*. [43] and Tyler and Wheatcraft [114], V and A can be determined by integration of a differential volume $\{m^3\}$ and area $\{m^2\}$:

$$V = \int V_P dN \qquad (53),$$

$$A = \int A_P dN \qquad (54),$$

where V_P is the volume of a pore, and A_P is its pore-matrix interface area. Assuming that:

$$V_P = c\lambda^{d_E} \qquad (55),$$

then, replacing Equations (52, 55) into Equation (53) :

$$V = -cFD_V \int_{\lambda_{\max}}^{\lambda_{\min}} \lambda^{d_E - D_V - 1}\, d\lambda \qquad (56).$$

The limits of integration in the above expression go from λ_{max} to λ_{min} as fewer pores have a characteristic length λ_{max} than λ_{min}, *i.e.*, I am integrating from N_{min} to N_{max}. Solving Equation (56):

$$V = \frac{cFD_V}{d_E - D_V}\left(\lambda_{\max}^{d_E - D_V} - \lambda_{\min}^{d_E - D_V}\right) \qquad (57).$$

Since $\lambda_{min} << \lambda_{max}$, and $d_E - D_V > 0$:

$$\lambda_{\max}^{d_E - D_V} >> \lambda_{\min}^{d_E - D_V} \qquad (58).$$

Combining Equations (57, 58):

$$V \approx \beta_V \left(\frac{\lambda_{\max}}{\lambda_{\min}}\right)^{d_E - D_V} \qquad (59),$$

where β_V is a positive proportionality constant. From Equation (59), the porosity, ϕ, is:

$$\phi = \frac{V}{V_{REV}} \sim \left(\frac{\lambda_{\max}}{\lambda_{\min}}\right)^{d_E - D_V} \qquad (60).$$

Here, V_{REV} is the minimum volume which is statistically representative of the pore space [103].

For the fluid-matrix interface surface area, I use Mandelbrot's relation between a self-similar fractal area and the volume it encloses [112]:

$$A_P^{1/D_S} = F_S V_P^{1/d_E} = f^{1/D_S}\lambda \qquad (61),$$

where, $f^{1/Ds} = F_S c^{1/dE}$.

Then, from Equation (54), the total pore-matrix interface area is the integral of the areas of every pore within the system:

$$A = -cFfD_V \int_{\lambda_{max}}^{\lambda_{min}} \lambda^{D_S - D_V - 1}\, d\lambda \qquad (62).$$

Again, the integration limits on Equation (62) are from smaller to larger number of pores as in Equation (56). The solution of the above expression is:

$$A = \frac{cFfD_V}{D_V - D_S}\left(\lambda_{\min}^{D_S - D_V} - \lambda_{\max}^{D_S - D_V}\right) \qquad (63).$$

Since $\lambda_{min} << \lambda_{max}$, and $D_S < D_V$:

$$\lambda_{\min}^{D_S - D_V} >> \lambda_{\max}^{D_S - D_V} \qquad (64),$$

so Equation (63) can be expressed as:

$$A \approx \beta_S \left(\frac{\lambda_{\max}}{\lambda_{\min}} \right)^{D_V - D_S} \tag{65}.$$

$$S = \frac{A}{V_{REV}} \sim \left(\frac{\lambda_{\max}}{\lambda_{\min}} \right)^{D_V - D_S} \tag{66}.$$

Combining Equations (60 and 66), the relation between specific surface area and media porosity is:

$$S \sim \phi^{\frac{D_V - D_S}{d_E - D_V}} \tag{67}.$$

Replacing Equation (67) into Equation (50):

$$K_{sat} \sim \phi^{1+\alpha-2\left(\frac{D_V - D_S}{d_E - D_V}\right)} \tag{68}.$$

Assuming that the saturated conductivity scales with the porosity as $K_{sat} \sim \phi^N$ [102, 105, 115], where N is an empirical parameter, in a three three-dimensional fractal (d_E=3), the connectivity parameter, α is:

$$\alpha = N - 1 + 2\left(\frac{D_V - D_S}{3 - D_V} \right) \tag{69}.$$

Gimenez *et al*. [102], used a similar model to estimate the interconnectivity parameter α from a set of clay samples. However, the results obtained there lead to non-physically negative connectivity parameters. Here I use the data reported in [102]

(saturated conductivity, porosity, macro porosity, and surface and volume fractal dimensions) to test the validity of the model given in Equation (68). Before continuing, it must be noted that the data reported by Gimenez *et al*. in [102] for D_V and D_S assumed a two-dimensional fractal medium. Consequently, both fractal dimensions must be increased by 1 to scale a three-dimension system to represent a three-dimensional fractal [112].

3. RESULTS AND DISSCUSSION

Contrary to the model proposed by Gimenez *et al*. [102], Equation (69) estimates positive connectivity parameters when tested using the fractal dimensions, porosity and saturated conductivity measured in [102] and listed in Table 5. Here, the averaged value of N=1.30 ± 0.23, the volume and area fractal dimensions, and the macro-porosity, ϕ_m, values given in [102] were used to determine the interconnectivity factor, α for every undisturbed and packed soil sample. The results are shown in Table 6.

Sample ID	Porosity		Ksat	Dv		Dv	
	ϕ	ϕm		Low	High	Low	High
RED-1 $^{\alpha}$	0.5	0.16	46	1.62	1.61	1.30	1.23
RED-2 $^{\alpha}$	0.47	0.07	59.1	1.21	1.51	1.14	1.21
RED-3 $^{\alpha}$	0.56	0.14	35.4	1.59	1.63	1.30	1.22
SPC-1 $^{\alpha}$	0.53	0.10	67.3	1.49	1.52	1.17	1.21
SPC-2 $^{\alpha}$	0.54	0.09	69.8	1.54	1.52	1.28	1.23
SPC-3 $^{\alpha}$	0.53	0.13	72.2	1.40	1.47	1.25	1.21
CON-1 $^{\alpha}$	0.51	0.09	44.4	1.56	1.64	1.17	1.22
CON-2 $^{\alpha}$	0.5	0.07	30.2	1.46	1.67	1.1	1.22
SASF, large-1 $^{\beta}$	0.64	0.18	132.8	1.79	1.50	1.21	1.16
SASF, large-2 $^{\beta}$	0.64	0.21	127.1	1.70	1.53	1.21	1.12
SASF, small-1 $^{\beta}$	0.61	0.25	196.9	1.88	1.8	1.33	1.21
SASF, small-2 $^{\beta}$	0.61	0.25	185.0	1.84	1.81	1.37	1.35
ASD-range1/ fine 1 $^{\beta}$	0.45	0.17	115.2	1.81	1.79	1.31	1.35
ASD-range1/ fine 2 $^{\beta}$	0.43	0.22	115.2	1.72	1.76	1.41	1.33
ASD-range1/ coarse 1 $^{\beta}$	0.58	0.25	122.7	1.75	1.72	1.36	1.31
ASD-range1/ coarse 2 $^{\beta}$	0.58	0.17	85.9	1.77	1.8	1.36	1.34
ASD-range2/fine 1 $^{\beta}$	0.59	0.27	126.5	1.71	1.68	1.42	1.35
ASD-range2/coarse 1 $^{\beta}$	0.61	0.19	135.8	1.67	1.58	1.22	1.24
ASD-range2/coarse 2 $^{\beta}$	0.61	0.22	136.1	1.67	1.81	1.44	1.44

Table 5 Soil parameters from Gimenez *et al*. Porosity, hydraulic conductivity, volume and surface area fractal dimensions for undisturbed (α) and packed (β) samples of a Normania clay loam. Details on the sample ID nomenclature in [102].

	Connectivity parameter, α			
Sample ID	***Gimenez et al.***		***Equation (69)***	
	Low	***High***	***Low***	***High***
RED 1 [α]	-1.33	-0.36	1.98	2.25
RED 2 [α]	-0.94	-0.46	0.48	1.52
RED 3 [α]	-1.03	-0.83	1.71	2.52
SPC 1 [α]	-0.87	-0.89	1.55	1.59
SPC 2 [α]	-0.48	-0.74	1.43	1.51
SPC 3 [α]	-0.32	-0.83	0.80	1.28
CON 1 [α]	-0.12	-0.51	2.07	2.63
CON 2 [α]	-0.24	-0.5	1.63	3.03
SASF, large 1 [β]	0.23	-1.08	5.82	1.66
SASF, large 2 [β]	-0.25	-1.2	3.57	2.04
SASF, small1 [β]	3.66	0.43	9.47	6.20
SASF, small 2 [β]	3.03	1.98	6.17	5.14
ASD-range1/ fine 1 [β]	1.53	1.57	5.56	4.49
ASD-range1/ fine 2 [β]	1.25	1.01	2.51	3.88
ASD-range1/ coarse 1 [β]	1.15	0.46	3.42	3.23
ASD-range1/ coarse 2 [β]	1.39	1.69	3.87	4.90
ASD-range2/ fine 1 [β]	1.15	0.51	2.30	2.36
ASD-range2/ coarse 1 [β]	-0.37	-0.55	3.03	1.92
ASD-range2/ coarse 2 [β]	0.94	1.05	1.69	4.19

Table 6 Connectivity parameter comparisons. Estimated connectivity parameters factors for the undisturbed (α) and packed (β) samples of a Normania clay loam using the model from Gimenez *et al*. [102], and Equation(69),. Details on the sample ID nomenclature in [102].

Table 6 shows that more than half of the connectivity parameters estimated using the model proposed by Gimenez *et al*. proposed are negative, which is impossible as a negative connectivity parameter would mean a decrease on tortuosity for an increment in the medium porosity. By contrast, the model given by Equation (69) estimates connectivity parameters, α, that are within a physically allowable range. The large connectivity parameters on *samples SASF, small1*, *SASF, small2*, *ASD-range1/fine 1*, and *ASD-range1/fine 2*, suggest an extremely limited interconnection between pores.

Finally, the walking fractal dimension, D_W, was estimated from the values of tortuosity and connectivity factor, α, obtained from the model here developed and the one in [102]. Using the model developed by Coleman and Vassilicos [69]:

$$\tau \sim \phi^{\frac{D_W - 2}{D_f - d}} \qquad (70).$$

The results are shown in Table 7.

	Walking fractal dimension, D_W			
Sample ID	***Gimenez et al.***		***Equation (69)***	
	Low	***High***	***Low***	***High***
RED-1 $^{\alpha}$	1.49	1.86	2.75	2.88
RED-2 $^{\alpha}$	1.26	1.77	2.38	2.75
RED-3 $^{\alpha}$	1.58	1.69	2.70	2.93
SPC-1 $^{\alpha}$	1.56	1.57	2.79	2.76
SPC-2 $^{\alpha}$	1.78	1.64	2.66	2.72
SPC-3 $^{\alpha}$	1.81	1.56	2.48	2.68
CON-1 $^{\alpha}$	1.95	1.82	2.91	2.95
CON-2 $^{\alpha}$	1.87	1.84	2.88	3.00
SASF, large-1 $^{\beta}$	2.05	1.46	3.22	2.83
SASF, large-2 $^{\beta}$	1.93	1.44	3.07	2.96
SASF, small-1 $^{\beta}$	2.44	2.09	3.14	3.24
SASF, small-2 $^{\beta}$	2.48	2.38	2.99	2.98
ASD-range1/ fine 1 $^{\beta}$	2.29	2.33	3.06	2.94
ASD-range1/ fine 2 $^{\beta}$	2.35	2.24	2.70	2.93
ASD-range1/ coarse 1 $^{\beta}$	2.29	2.13	2.86	2.90
ASD-range1/ coarse2 $^{\beta}$	2.32	2.34	2.89	2.98
ASD-range2/ fine 1 $^{\beta}$	2.33	2.16	2.67	2.76
ASD-range2/ coarse 1 $^{\beta}$	1.88	1.77	3.00	2.81
ASD-range2/ coarse 2 $^{\beta}$	2.31	2.20	2.56	2.80

Table 7 Walking fractal dimension comparison. Estimated walking fractal dimensions for the undisturbed (α) and packed (β) samples of a Normania clay loam from Gimenez *et al*. [102] and Equation (70). Details on the sample ID nomenclature in [102].

Similar to the connectivity parameters given in Table 6, many of the walking fractal dimension than obtained using the model given by Gimenez *et al*. [102] fall outside of a physically allowable range, $2 \leq D_W \leq 3$. The model presented here gives walking fractal dimensions within this range for all but the *SASF, small-1* soil.

Conclusions. The methodology developed by Gimenez *et al*. to estimate the connectivity parameter of a porous medium based on measurements of saturated conductivity, macroporosity and pore surface and pore volume fractal dimensions is particularly attractive as the only requires standard measurements of well-developed laboratory techniques. However, their model gives connectivity parameters and walking fractal dimensions outside a physically allowable range. The model developed here, clearly avoids this flaw. Other type of transport experiments such as diffusion of gases could perform future validation of the model here established.

The model presented in this dissertation can be used to estimate the effect of a porous medium topology on the noble gas transport coefficients. Accurate approximation of the tortuosity factor would allow using the numerical models also developed in this dissertation to evaluate the noble gas migration through a porous medium without conducting diffusion experiments.

CONCLUSIONS

Diffusion plays a critical role in the movement of gases through a geological medium. Proper understanding of the parameters that affect this transport mechanism is essential for various applications such as predicting the movement of anthropogenic noble gas isotopes in the atmosphere after a below ground nuclear test has taken place. In this dissertation, I presented a novel methodology for using prompt gamma activation analysis to estimate noble gas diffusivities through a porous medium. I also present experimental evidence and a numerical model suggesting the rise of additional transport mechanisms when the difference in molecular weights of the species diffusing is large. In addition, I introduced a fractal model to correlate the tortuosity to the saturated conductivity, pore volume, porosity, and pore volume and pore surface fractal dimensions. The conclusions for each aim of this dissertation are:

Aim 1. I developed an experimental set-up and methodology for using prompt gamma activation analysis for measuring variations of noble gas concentrations by its diffusion within a porous media. I have shown that prompt gamma activation analysis is able to determine the variation in natural xenon and argon gas concentrations within a gas sample during diffusion experiments. However, the argon and xenon detection limits of the prompt gamma activation analysis facility at The University of Texas at Austin are not sufficient to trace the fractionation of stable xenon isotopes expected because of their different molecular weights. Detection of variations in the isotopic composition of a natural xenon sample after diffusing through a porous medium may be possible if a gas sample is extracted from the noble gas source, irradiated with a larger neutron flux

(introducing it to the reactor for example), and then analyzed with neutron activation analysis. I recommend that future work on this aim will look at conducting transport experiments with radioactive xenon and a multichannel scaling (MCS) option to track the intensity of a specific gamma ration as a function of time. Using noble gas samples with high activity may allow obtaining experimental evidence of isotope fractionation in a xenon-nitrogen system

Aim 2. I have developed a methodology to determine the binary diffusion coefficient of quasi equi-molar gases, *e.g.* argon and nitrogen, within a porous medium using prompt gamma activation analysis: 1) I performed a series of diffusion experiments where the tracer gas concentration was analyzed at its source before and after different diffusing times; 2) I compared the variations in the tracer gas concentration with a numerical model where the effective diffusivity is first estimated using empirical correlations. I then systematically varied the effective diffusivity until the sum of squared errors between the numerical predictions and measured values is minimized. The correct effective diffusivity then corresponds to the minimum. Following the methodology here outlined, an effective diffusivity of 0.057 ± 0.089 cm^2s^{-1} was estimated with a strong correlation between the numerical model and experiments ($R^2 = 0.98$).

Different than when using argon, a one-dimensional numerical diffusion model largely underestimated the rate of depletion of xenon during the first hours of xenon-nitrogen diffusion experiments. Even after proportionally varying the binary diffusivity of xenon, the transient behavior of the xenon depletion rates could not be estimated by a one-dimensional pure-diffusion model at short times. The short times at which this faster depletion occurs suggests this might not be not a porous media-fluid interaction effect, as the xenon has not reached this region according to the model I developed. Most likely,

phenomena such as three-dimension diffusively driven convection, or gravity effects are driving the observed phenomena. The effect of density (gravity currents) in both, a one- and two-dimension approximation should be explored in in future work.

Aim 3. I developed a new fractal model to estimate the tortuosity of a porous media from its saturated conductivity, porosity, pore volume and pore surface fractal dimensions. This model, opposite to the one proposed by Gimenez *et al*. predicts physically reasonable transport properties, *i.e*. tortuosity factors larger than one and walking fractal dimensions larger than two but less than three. Another important characteristic of this model is that it estimates the transport properties of the porous media from parameters that are traditionally measured (saturated conductivity and porosity), and the fractal characteristic of the geological media. Other correlations available in the literature to estimate media tortuosities rely on knowing before hand a tortuosity or random walk fractal dimension determined from numerical models such as random walk or Monte Carlo. Future work on this aim will look to extend the validation of the model here developed using experimental data to estimate the tortuosity of a geological porous medium and comparing the results with experimental transport coefficients.

Appendices

APPENDIX A: DIFFUSION EXPERIMENT PROCEDURE

The procedure followed for the diffusion experiments can be grouped in four major steps: Sample cylinder preparation, porous media column ventilation, pressure regulation, concentration analysis, and gas diffusion. The units used here correspond to those read in the instrumentation and are not necessarily SI units.

Sample cylinder preparation

1. Perform or request a radiation survey to the sample cylinder to the Health Physicist
2. Connect the sample cylinder to the gas exchange manifold
3. Connect the noble gas source (argon or xenon) to the gas exchange manifold. Check the valve to the noble gas source cylinder is closed
4. Close all ball valves (shut-off valves) to gas cylinder and noble gas source and open the valve to the vacuum pump
5. Turn ON vacuum pump to clean all tubing until pressure transducer reads 3.0 Torr
6. Close all electronic valves and turn OFF vacuum pump
7. Open all the valves (including pressure regulators and shut-off valve) between pressure transducer and sample cylinder
8. Open the valve to the vacuum pump
9. Turn ON vacuum pump and vacuum the cylinder up to 5.0 - 10.0 Torr

10. Close valve to vacuum pump, turn it OFF, and let the pressure come to equilibrium. Write down equilibrium pressure. If not smaller than 10.0 Torr, repeat Steps 8 to 10
11. Check that valve between vacuum pump and pressure transducer is closed and pressure regulator of noble gas source is open
12. Open shut-off valve to noble gas source (ball or gate valve) and start increasing the delivery pressure by closing pressure regulator gradually up to 150 kPa (20 psi or 1.4 bar)
13. Open valve to noble gas source and fill the sample cylinder up to reach an minimum equilibrium pressure of 500 Torr
14. Close valve to noble gas source and let the pressure come to equilibrium. Write down equilibrium pressure. If not smaller than 500 Torr, repeat Steps 13 and 14
15. Check valve to noble gas source is close and repeat Steps 8 to 10 and 13 to 14, this time filling the cylinder up to 790 Torr (105 kPa (abs)). Write down the value
16. The partial pressure of any contaminant in the cylinder is < 0.03%
17. Close the all valves in the gas exchange manifold
18. Close shut-off valves of sample cylinder and noble gas source tightly
19. Detach sample cylinder and noble gas source from gas exchange manifold
20. Open valve to vacuum pump and turn it ON to clean the tubing in the manifold up to pressure transducer reads 3 Torr
21. Turn OFF the vacuum pump and close its valve
22. Put all tools and noble gas source back on their respective place

Porous media column ventilation

1. Perform or request a radiation survey to the sample cylinder to the Health Physicist if the column was previously irradiated
2. Open ball valves at both ends of experimental set-up (filling and purging ends)
3. Connect each barbed fittings from the porous media column to the HIGH pressure port of the differential transducers. One to each pressure transducer. Be sure the valves are open
4. Connect the filling adapter (full-flow to instrumentation quick connectors) to the stainless steel end of the column (filling end)
5. Connect the flow-meter (already connected to the nitrogen cylinder) to the filling adapter
6. Close flow-meter valve, open shut-off valve of nitrogen cylinder, and adjust its pressure regulator to 150 kPa (20 psi or 1.4 bar) minimum
7. Open flow-meter valve and regulate flow to 1.5 liters per minute. Check that purge valve is open and nitrogen is flowing through the system
8. Flow nitrogen through the system for 60 minutes
9. Decrease the nitrogen flowrate to 0.5 liters per minute and keep venting the column for 30 minutes
10. Close the purge valve (brass valve) while keep flowing nitrogen into the system
11. Increase the gauge pressure of the system up to 4.5±0.5 in H_2O (reading on the LabVIEW program from either pressure transducer)
12. Close the flow-meter valve and also stainless steel filling valve
13. Detach the flow-meter from the system

14. Wait to the pressure in both pressure transducers equilibrate and write down value
15. Close both valves to pressure transducers
16. Change the connection of the barbed fittings at the filling end of the porous media column (stainless steel) to the LOW pressure port in the differential pressure transducer. DO NOT open any valve

Pressure regulation

1. Bring the sample cylinder and porous media column to the same room and leave them together for at least 12 hours to reach thermal equilibrium with environment
2. Connect the metering valve assembly to the sample cylinder
3. Connect the barbed end of the metering valve assembly to the differential pressure transducer at the filling end of the porous media column (stainless steel)
4. Check that the one pressure transducer is connected to the metering valve assembly (HIGH pressure port) and porous media column (LOW pressure port). The second pressure transducer must me connected only to the purging end of the porous media column (HIGH pressure port)
5. Close the meeting valve completely and open it half-turn
6. Open all valves between sample cylinder and the pressure transducer to which it is connected
7. Open all valves between porous media column and both pressure transducers
8. Allow reading from pressure at the porous media column to equilibrate. Write down the value

9. Regulate the opening of the metering valve to allow the noble gas flow out as the pressure difference between the sample cylinder and porous media column gets to 4.0 in H_2O (reading in the LabVIEW program).
10. Close the metering valve and allow the reading to stabilize
11. Carefully and in cycles re-open and close the metering valve lowering the pressure difference between cylinder and porous media column up to 2.5 in H_2O (larger in the sample cylinder) to compensate for the lower pressure within the full-flow quick connectors volume after cylinder and column are connected (see note at the end of this appendix)
12. Once the desired pressure difference is reached, close all the valves in both, cylinder and porous media column.
13. Close the valves to pressure transducers and DON'T open the metering valve
14. Detach the cylinder from the metering valve assembly

Concentration analysis

1. Take the sample cylinder to the prompt gamma activation facility at the reactor bay
2. Carefully follow the working procedure detailed at the radiation working permit
3. Place the sample cylinder in the neutron beam path at the location previously determine that ensures proper alignment between sample and neutron beam (using a neutron camera)
4. Check there is nothing obstructing the path of the neutron beam between the collimator and the sample
5. Check the beam stopper between the neutron camera and sample cylinder is on place

6. With the reactor operating at 950 kW open the beam shutter and start irradiation of sample.
7. Count the prompt photons emitted using Genie2000 for the analysis time necessary (live-time)
8. Once time has elapsed, save data, close the beam shutter and allow activated sample to decay for 24 hours before handling it

Diffusion experiment

1. Connect sample cylinder to porous media column
2. Check that all valves in the assembly are closed
3. Slowly, open the valves (two) between the sample cylinder and the porous media column. Open FIRST the closest one to the sample cylinder
4. Allow the noble gas diffusing in the porous media column for the selected time
5. Monitor the pressure readings from the two pressure transducers during the whole experiment
6. Once the diffusion time has elapsed, closed the valves between sample cylinder and porous media column slowly. Close FIRST the valve closest to the sample cylinder
7. Detach the sample cylinder from the porous media column and proceed to analyze its noble gas concentration

Note: Variations of this procedure were explored to assure the faster depletion of xenon was not caused by non-desired pressure gradients between sample cylinder and porous media column. These pressures gradients may rise from variations on the room pressure

between the moments when pressure regulation and diffusion experiments take place. The two variations explored were:

Variation 1: During the pressure regulation process, get a pressure at the porous media column 2.5 in H_2O larger than the pressure at the sample cylinder. During the diffusion experiment, open the valve closed to the porous media column FIRST. The change in noble gas concentration after 17 hours of diffusion was similar to the one following the nominal procedure.

Variation 2: Following the attachment of the sample cylinder and porous media column, the two valves between them were open for 5 seconds and immediately closed. In this case, the noble gas concentration at the sample cylinder was analyzed three times without detaching the cylinder form the column: 1) Before opening the valves for 5 seconds, 2) After opening the valves for 5 seconds, and 3) After the diffusion time has elapsed (1 hour and 42 hours). The changes in noble gas concentration between the second and last analyses were similar to the values obtained following the nominal procedure.

APPENDIX B: DIFFUSION ONLY MATLAB PROGRAM

```
%=========================================
%FD CODE FOR BINARY DIFFUSION
%=========================================

%Assumptions: 1D, constant properties and uniform within each section,
%constant pressure, and no sources/sinks of concentration

%DIFFUSION COEFFICIENT [129Xe, 131Xe]
D=5*0.11832; %[cm^2/s]  0.11832
D=D/10000; %[m^2/s]

%DENSITY OF SAMPLE GAS
rho=5.894; %1.784; %[kg/m^3] 5.894

%MOLECULAR WEIGHT OF GAS
M=131.293/1000; %[kg/mol] 131.293

%FIRST SECTION (CYLINDER)
V_cyl= 0.001016 ; %[m^3]
d1=3*0.0254/4;%[m]
Acyl=pi*d1^2/4;%[m^2]

pressure=3.5; %pressure of cylinder in [inH2O]
pressure=406.782+pressure;
T=280; %Temperature of environment at BP3[K]
R=8.31446; %Ideal gas constant [J/molK]
pressure=pressure*0.0254/0.00010197; %[Pa]
Conc_cyl=pressure/(R*T); %Molar conc of sample in cylinder

%MEDIA CHARACTERISTIC (STARTING POINT)
porosity=0.445;
tort=1-0.5*log(porosity);
factorD=porosity/tort;
%++++++++++++
%READING THE EXPERIMENTAL VALUES
%++++++++++++
```

The HORIZONTAL vectors where conc and time will be input are named "EXPE"and "TIME" respectively

```
EXP=EXPE';
sizePGAA=numel(EXP);
time=TIME'; %The vector time is given in hours

%++++++++++++
%START THE FOR LOOP TO FIND ERRORc
%++++++++++++

for iii=1:5

   %============================
   %GEOMETRY OF EXPERIMENTAL SET-UP
   %============================

   % SECTIONS

   N=5; %number of sections of different diameters(incluiding the cylinder)
   d=[3; 0.5; 4; 4; 4]; %diameter of each section in inches
   d=0.0254*d; %diameters of sections in meters
   length=[.2794; .2; .1016; 1.0; .1016]; %length of each section [m](vector)
   Afactor=[1 1 1 factorD 1]; %Factor to modify the diffusivity
   A=(3.1416/4)*(d.^2);
   A2=diag(A*Afactor);
   AA=A2'; %Horizontal Area vector

   % ELEMENTS

   Dx=0.01; %Length of each element [m]
   n=round(length/Dx); %number of elements per section (vector)
   long=n*Dx; %modified length of each section
   Vol=A.*Dx; %volume of an element in a specific section
   VV=Vol'; %Horizontal vector
   num=sum(n); % total number of elements;

   %Let's build the area and volume HORIZONTAL vectors for ALL THE ELEMENTS
of each
   %section

   Area=zeros(1,num); %Vector with the area of every element for all sections
   V=zeros(1,num); %Vector with the volume of every element for all sections
```

```
%In the first section:
for i=1:n(1,1);
   Area(1,i)=AA(1,1);
   V(1,i)=VV(1,1);
end
%In the second section:
for i=n(1,1)+1:n(1,1)+n(2,1);
   Area(1,i)=AA(1,2);
   V(1,i)=VV(1,2);
end
%In the third section:
for i=n(1,1)+n(2,1)+1:n(1,1)+n(2,1)+n(3,1);
   Area(1,i)=AA(1,3);
   V(1,i)=VV(1,3);
end
%In the fourth section:
for i=n(1,1)+n(2,1)+n(3,1)+1:n(1,1)+n(2,1)+n(3,1)+n(4,1);
   Area(1,i)=AA(1,4);
   V(1,i)=VV(1,4)*porosity;
end
%In the fifth section:
for i=n(1,1)+n(2,1)+n(3,1)+n(4,1)+1:n(1,1)+n(2,1)+n(3,1)+n(4,1)+n(5,1);
   Area(1,i)=AA(1,5);
   V(1,i)=VV(1,5);
end

%=======================
%DURATION OF EXPERIMENT
%=======================
t_tot=1*3600; %[s] Total duration of experiment [s]
nt=45000; %number of time intervals
Dt=t_tot/nt; %Duration of intervals [s]

%---------------
%THE INITIAL CONDITION
%---------------
C=zeros(nt,num); %On the concentration matrix, each row corresponds to the
%concentration at a specific instant
for i=1:n(1,1)
   C(1,i)=Conc_cyl; %concentration of cylinder [mol/m^3]
end
%-----------------
```

```
%CROSS SECTION AREAS OF MASS TRANSFER
%-----------------

%Although each element has 2 areas (left and right) we will call as the
%area of the elemnt J to the one on the RIGHT side of that element

for i=1:num
   if i==num %On  the very last element (assuming there are more than 2
      %elements in the last section)
      Area(1,i)=Area(1,i);

   elseif Area(1,i+1)<Area(1,i); %when we have a reduction of diameter,
      Area(1,i)=Area(1,i+1);    %the mass transfer area is the one of
      %the next element

   else%Otherwise, the mass transfer area is the
      %of the element we are looking at
      Area(1,i)=Area(1,i);
   end
end
%==================
%SOLUTION OF SYSTEM OF EQUATIONS
%==================
A1 = zeros(1,num);
A2 = zeros(1,num);
A3 = zeros(1,num);
A4 = zeros(1,num);
for i=2:nt;
   Veloc=zeros(1,num);
   A1=(1-D*Dt*Area./(Dx*V));
   A2=D*Dt*Area.*(V.^-1)/(Dx);
   %At the left end
   C(i,1)=C(i-1,1)*A1(1)+A2(1)*C(i-1,2);

   % At the right end
   A3(1,num) = (D*Dt/(Dx*V(1,num)))*(Area(1,num-1));
   A4(1,num) = D*Dt*Area(1,num-1)/(V(1,num)*Dx);
   C(i,num)=C(i-1,num-1)*A3(num)+(1-A4(num))*C(i-1,num);

   % Everywhere in the middle
   A3(1,2:num-1) = (D*Dt*(V(2:num-1).^-1)/Dx).*(Area(1,1:num-2));
   A4(1,2:num-1) = D*Dt*Area(1,1:num-2).*(V(1,2:num-1).^-1)/Dx;
```

```
      C(i,2:num-1)= C(i-1,1:num-2).*A3(2:num-1)+(A1(2:num-1)-A4(2:num-1)).*C(i-
1,2:num-1)+A2(2:num-1).*C(i-1,3:num);

   end

   %NOTE, a more accurate solution should analyze section by section and use boundary
conditions of continuity of concentration and conc. gradient

   %+++++
   %VALUES OF THE MODEL AT THE TIME OF INTEREST
   %+++++
   TOTC=zeros(sizePGAA,1); %Vertical vector of total bottle conc defined as a zero
vector

   %Let's first calculate the values of the solution at the times of interest
   %tt
   Cbottle=zeros(sizePGAA,n(1,1));

   for tt=1:sizePGAA;
      x=time(1,tt)*3600; %The time in seconds
      t1=floor(x/Dt); %The two instants right before and after the instant we are interested
      t2=t1+1;
      Dt1=x-t1*Dt; %the time gap between the values calculated and the one we care
about
      Dt2=t2*Dt-x;
      for jj=1:n(1,1)
         Cbottle(tt,jj)=(C(t2-1,jj)-C(t1-1,jj))*(0-Dt2)/(Dt2+Dt1)+C(t2-1,jj);
         TOTC(tt,1)=TOTC(tt,1)+Cbottle(tt,jj)/Conc_cyl;
      end
      MODEL(iii,tt)=TOTC(tt,1)/(n(1,1));%The horizontal vector of the total conc in the
cylinder
   end;
   TOTSQR=0;

   %++++
   % THE ERROR
   %++++
   for tt=1:sizePGAA;
      error(tt,iii)=abs(MODEL(1,tt)-EXP(1,tt));
      errorSQR(1,iii)=error(tt,iii)^2;
      TOTSQR=TOTSQR+errorSQR(1,iii);
   end
```

```
    SQRROOTerror(1,iii)=TOTSQR^0.5;
    factorD=factorD+0.05*(porosity/tort);

    %=====
    %PLOTS
    %=====

    xo=[0;0;0;0;0]; %Locations where the solutions will be plotted [hours]
    Location=round(xo./Dx);
    T=0:Dt:Dt*(nt-1);
    factorD=D*((porosity/tort)+0.02*index);
    T=T/3600;
    for i=1:4;
       if Location(i,1)==0;
          loc=1;
       else
          loc=Location(i,1);
       end
       for j=1:nt;
          Ct(j,i)=C(j,loc)*(1/Conc_cyl);
       end
    end;
    plot(T,Ct),xlabel('t [hours]'),ylabel('C/Co'), grid on, hold on;

end;
```

APPENDIX C: DIFFUSION - CONVECTION FORTRAN 90 PROGRAM

```
PROGRAM main
!This program aims to solve the equation using a CRANK-NICHOLSON algorith:
!dC/dt = alpha * d(CV)/dz + d(D dC/dz)/dz

!!IMPORTANT!!
!============
!In this new version of the code, the velocities are NOT estimated from Darcy's Law.
!The velocities are estimated from Momentum conservation

!===ASSUMPTIONS===
!1D, constant properties and uniform within each section,
!no sinks/sources, and pressures from known concentrations

!!Conc array, the first 2 columns are GAS1, the last 2 are GAS2. and it goes form
!!OLD in the left to NEW on the right.  Each row is a time step
!!BC array, again, it has 4 columns, each row is one time step

USE mod_constants  !makes the data form the module constants vissible
USE HDF5
USE interface_variables

IMPLICIT NONE

CHARACTER(LEN=13) :: fname_out =   "outputfile.h5"
CHARACTER(LEN=13) :: fname_rstrt = "rstartfile.h5"
CHARACTER(LEN=13) :: FnameREAD   != "InitialCon.h5"
CHARACTER(LEN=5) :: groupname
CHARACTER(LEN=9)  :: dsetname  !Data set name for output file
CHARACTER(LEN=9), PARAMETER :: dset_rstrt= "rstrtConc"
CHARACTER(LEN=10) :: countstring
REAL*8, ALLOCATABLE, DIMENSION(:,:) :: CONC
REAL*8, ALLOCATABLE, DIMENSION(:,:) :: CONCrstrt
REAL*8, ALLOCATABLE, DIMENSION(:) :: CYL_CONC  !vector with the conc of
gas 1 in cyl ONLY
REAL*8, ALLOCATABLE, DIMENSION(:,:)  :: Veloc
REAL*8, ALLOCATABLE, DIMENSION(:,:)  :: Veloc_old
REAL*8, DIMENSION(2,4)  :: BC
REAL*8 :: t_r   !Relaxation time
REAL*8 :: dt_conv   !Relaxation time
```

```
REAL*8 :: stab_criteria  !sum of gas concentrations within cylinder
REAL*8 :: stab_check !To check the conc. within the cylinder is still OK
REAL*8 :: ff  !factor used to average the pressure gradient
INTEGER :: nn ! number of data I will collect  (won't collect data every time step)
INTEGER :: mm ! number of data I will collect  (won't collect data every time step)
INTEGER :: unstability
INTEGER :: i  !loop index for Conv ONLY
INTEGER :: ii !loop index for Conv and Diff
INTEGER :: j  !counter
INTEGER :: jj !lopp index for the results array Cgas1Cgas2
INTEGER :: k !counter
INTEGER :: kk !counter
INTEGER :: status   !status of allocation at the end of this program
INTEGER :: error !Error flag for the HDF5 subroutines
INTEGER :: counter
INTEGER :: input
INTEGER :: nt_conv  !number of time steps for a convection-diffusion scenario

CALL setConstants  !subroutine to estimate the initial values all the outcomes are in the
"con" variable type
CALL CREATEFILE(fname_rstrt)!Create the restart file
CALL CREATEFILE(fname_out)!Create the output file

!!===Allocating the memory===

ALLOCATE ( Veloc(con%num,2), STAT=status)
IF (status /= 0) THEN
WRITE(*,*) 'Check allocation of Veloc'
END IF

ALLOCATE ( Veloc_old(con%num,2), STAT=status)
IF (status /= 0) THEN
WRITE(*,*) 'Check allocation of Veloc_old'
END IF

ALLOCATE ( CONC(con%num,4), STAT=status)
IF (status /= 0) THEN
  WRITE(*,*) 'Check allocation of CONC'
END IF

ALLOCATE ( CONCrstrt(con%num,2), STAT=status)
IF (status /= 0) THEN
```

```
  WRITE(*,*) 'Check allocation of CONCstrt'
END IF

ALLOCATE ( CYL_CONC(con%n_vector(1)) )
IF (status /= 0) THEN
  WRITE(*,*) 'Check allocation of CYL_CONC'
END IF

!====INITIAL CONDITIONS====
!=========================
jj = 1!FLOOR(con%num/15.0D0)

WRITE (*,*) 'Do you wanna input the IC manually? (YES = 1   NO = 0)'
READ (*,*)   input

IF (input==1) THEN
 FnameREAD = "initialCon.h5"
 CALL RDFILE(FnameREAD, dset_rstrt, CONCrstrt, con%num)
 CONC(:,1) = CONCrstrt(:,1)
 CONC(:,3) = CONCrstrt(:,2)
 WRITE (*,*) 'The initial concentration for GAS1 is =  ',CONC(:,1)
 WRITE (*,*) 'The initial conc for GAS2 is =  ',CONC(:,3)
ELSE
 WRITE (*,*) 'The initial concentration have been calculated internally'
 CALL setConcs(con%num, con%Co, con%n_vector, CONC)
 WRITE (*,*) 'The initial concentration for GAS1 is =  ',CONC(:,1)
 WRITE (*,*) 'The initial conc for GAS2 is =  ',CONC(:,3)
END IF

BC =RESHAPE((/con%Co, 0.0D0, 0.0D0, 0.0D0, 0.0D0, con%Co, 0.0D0,
0.0D0/),(/2,4/))
!The initial BCs.  From left to right: BC1LEFT_old, BC1RIGHT_old, BC1LEFT_new,
BC1RIGHT_new, BC2LEFT_old, BC2RIGHT_old, ...
stab_criteria = SUM(CONC(:,1)) +10

CONC(:,2) = CONC(:,1)
CONC(:,4) = CONC(:,3)
dt_conv = con%dt/con%nt_conv !The diffusion time step will be divided in
con%nt_conv smaller steps

!!SOLVING THE SYSTEM OF EQUATIONS EVERY TIME STEP
!!=============================================
```

```
WRITE (*,*) 'time step =', con%dt
WRITE (*,*) 'mesh size =',  con%dx
WRITE (*,*) 'number of time steps =', con%nt
WRITE (*,*)'number of elements on the array Cgas1Cgas2=', con%nn
WRITE (*,*) 'Time between datapoint in array Cgas1gas2 (SECONDS) =',
con%dt*con%nt/con%nn
WRITE (*,*) 'Diffusivity gas 2 =', con%D2
WRITE (*,*) 'Convection time step              =', dt_conv

j=1  !start the counter to save data
counter = 1
unstability = 0;
Veloc_old = 0;

DO i=1,con%nt !The system subroutine will be solved nt times
  j=j+1 !This indicator will tell us when to save data
  nn = 0  !indicator of the number of steps on the diffusion/convection loop   !!NEW!!
   IF (unstability ==1 ) EXIT !Finish the WHOLE loop if not stable

  ! Stability check !
  !-----------------!
    CYL_CONC = CONC(1:con%n_vector(1),1)
    stab_check = SUM (CYL_CONC)

   IF (stab_check > stab_criteria+10) THEN
      WRITE(*,*) 'ITERATION #',i
      WRITE(*,*) 'CODE IS UNSTABLE!!!!'
      unstability = 1;
   END IF
   IF (stab_check > stab_criteria) EXIT !Finish the DO loops if not stable

 !===DIFFUSION AND CONVECTION====
 !==============================
 DO ii =1,con%nt_conv   !Diffusion convection loop
   nn = nn+1

   CALL Velocity_NSexplicit (con%num, CONC, Veloc_old, Veloc,dt_conv)
   CALL CN_Diff_Conv(con%num, dt_conv, CONC, BC, Veloc)
   !CALL fluxes(CONC,Veloc)

 ! Updating CONC, and BCs !
 !------------------------!
```

```
    Veloc_old = Veloc
    CONC(:,1) = CONC(:,2)
    CONC(:,3) = CONC(:,4)
    BC(:,1) = BC(:,2)
    BC(:,3) = BC(:,4)
  END DO   !end of the Diffusion convection loop  !!NEW!!

  !=== WRITING DATA ON h5 FILES AND SCREEN ===
  !==========================================
   IF (j ==NINT(REAL(con%nt/con%nn)))THEN  ! j = collection frequency(s) / Dt(s)

     WRITE (*,*)'number of steps',j

     !Finding the name of the dataset and writing data!
     !-----------------------------------------------!
     counter = INT(i*con%dt)   !This is the counter I need to include for each dataset
     WRITE (*,*) 'COUNTER =   ',counter
     WRITE (countstring,'(I5)'), counter !I am converting the counter into  a string
     countstring = adjustl(countstring)
     groupname = 'Cgas1'
     dsetname = 't='//trim(countstring)//'s'
     WRITE(*,*) ' DATASET NAME',dsetname
     CALL WRTFILE(fname_out, dsetname, CONC(:,1), CONC(:,3), con%num) !Writing
the concentrations on the outputfile
     WRITE(*,*)'NUMBER OF DATASETS WE HAVE SO FAR =   ', jj
     WRITE (*,*)'CONC GAS1  =   ',CONC(:,1)
     WRITE (*,*)'CONC GAS2  =   ',CONC(:,3)
     WRITE (*,*) 'VELOCITY  =   ', Veloc
     j=0  ! We reset j
     jj=jj+1 !we get ready for the next time we will save a dataset
   END IF
END DO  !End of time step loop

CALL WRTFILE(fname_rstrt,dset_rstrt, CONC(:,1), CONC(:,3), con%num) !Writing
the last concentration on the restart file
   FnameREAD = fname_rstrt
CALL RDFILE(fname_rstrt, dset_rstrt, CONCrstrt, con%num)

WRITE(*,*)'the new initial conc1 =', CONCrstrt(:,1)
WRITE(*,*)'CODE NON-STABLE @ i= ', i
```

```
DEALLOCATE (con%alpha, con%alpha_vec, con%KK, con%DD1, con%DD2, Veloc,
STAT=status)
DEALLOCATE (con%DD, con%DD_vec, CYL_CONC, CONCrstrt, CONC,
STAT=status)!

END PROGRAM
```

```
MODULE mod_constants

SAVE
TYPE userConstants

  REAL*8  :: D1  !diffusivity gas 1 {m^2/s}
  REAL*8  :: D2  !diffusivity gas 2 {m^2/s}
  REAL*8  :: Co   !Initial concnetration of gasses 1 and 2 {mol/m^3}

  REAL*8, DIMENSION(11) :: diam_vector
  REAL*8, DIMENSION(11) :: length_vector
  REAL*8  :: dt = 1.0D-4   !time step{s}
  REAL*8  :: dx = 1.0D-2!size of element {m}
  INTEGER :: nt          !number of time steps
  INTEGER, DIMENSION(11) :: n_vector !vector w/ number of elements on each
section
  INTEGER :: num         !total number of elements
  INTEGER :: nn   !number of data I will collect (not collecting every time step)
  INTEGER :: nt_conv  = 10 !number of time steps that will be within a diffusion time
step
  REAL*8  :: factorD   !medium characteistics
  REAL*8  :: perm = 3.125D-8 !10.0D-11 !media permeability {m^2}
  REAL*8, ALLOCATABLE, DIMENSION (:) :: alpha
  REAL*8, ALLOCATABLE, DIMENSION (:) :: alpha_vec !This is the vector used for
varying areas
  REAL*8, ALLOCATABLE, DIMENSION (:) :: A_vec !This is the ELEMENT area
vector
  REAL*8, ALLOCATABLE, DIMENSION (:) :: AT_vec !This is the TRANSPORT
area vector
  REAL*8, ALLOCATABLE, DIMENSION (:) :: KK
  REAL*8, ALLOCATABLE, DIMENSION (:) :: DD1 ! Diffusivity vector of gas 1
  REAL*8, ALLOCATABLE, DIMENSION (:) :: DD2 ! Diffusivity vector if gas 2
  REAL*8, ALLOCATABLE, DIMENSION (:,:) :: DD !Diffusivity array. left columns
for GAS1, second column for GAS2
  REAL*8, ALLOCATABLE, DIMENSION (:,:) :: DD_self !Diffusivity array. left
columns for GAS1, second column for GAS2

  REAL*8, ALLOCATABLE, DIMENSION (:,:) :: DD_vec !Array used for varying
areas
  REAL*8 :: R = 8.31446621D0  ! ideal gas constant {J/molK}
  REAL*8 :: temp = 290D0     !temperature {K}
  REAL*8 :: M1 = 40.0D0     !Molecular weight of gas in cyinder (xenon or argon)
```

```
  REAL*8 :: M2 = 28.0D0     !Molecular weight of gas in tube (nitrogen)

END TYPE
type(userConstants) :: con

CONTAINS
 SUBROUTINE setConstants()
  IMPLICIT NONE
  SAVE
  REAL*8,PARAMETER  :: pressure = 85.5D1 !pressure in cylinder {torr}
  REAL*8,PARAMETER  :: visc = 17.81D-6   ! gas viscocity {Pa*s} or {kg*m/s}
  REAL*8,PARAMETER  :: porosity = 4.45D-1  !medium chracteristics
  REAL*8  :: tort
  REAL*8,PARAMETER  :: tot_time = 3600.0D0 !experiment characteristicsduration
{s}
  REAL*8, PARAMETER :: collection_freq =1.0D1!1.0D1 !time in SECONDS between
collections
  REAL*8  :: tot_length
  INTEGER,DIMENSION(11) :: acc_n_vec !accuulative number of elements on each
secion
  INTEGER :: i     !loop index
  INTEGER :: status  !The status of allocation. If zero, we succeded
  INTEGER :: count !To check teh allocation of all the variables

  con%Co  = pressure*101325.D0/(con%R*con%temp*760.D0)
  con%D1  = 18.1D-6!18.06D-6  !binry diffusivity gas 1 {m^2/s}
  con%D2  = 18.1D-6!18.06D-6 !25.06D-6!25.4902D-6!18.06D-6 !binary diffusivity gas
2 {m^2/s}

  tort = 1.0D0-0.5D0*LOG(porosity)
  con%factorD = porosity/tort
  WRITE(*,*)'FACTOR DIFFUSION = ', con%factorD

  con%diam_vector   = (/6.6D-2, 5.7D-2, 3.70D-2, 2.70D-2, 1.5D-2, 1.5D-2, 3.0D-2,
1.5D-2, 10.16D-2, 10.16D-2, 10.16D-2/) !diameter vector {m},  The first four sections
are filled with xenon

  con%length_vector = (/0.263D0, 0.015D0, 0.020D0, 0.028D0, 0.05D0, 0.178D0,
0.015D0, 0.01D0, 0.1D0, 1.0D0, 0.1D0/) !length vector {m}
  con%nt          =NINT( tot_time/con%dt)         !number of time steps for a specific Dt
  con%nn          =NINT(tot_time/collection_freq)  !number of times I will save data
(number of datasets)
```

```
 con%num = 0

!The first section:
 con%n_vector(1) = NINT( ((con%length_vector(1)-con%dx/2.0D0))/con%dx )+1
!vector w/ number of steps on each section
 con%num = con%num + con%n_vector(1)
 acc_n_vec(1) = con%num

!Sections 2 to 10:
 DO i = 2,10
   con%n_vector(i)   = NINT(con%length_vector(i)/con%dx) !vector w/ number of steps
on each section
   con%num = con%num + con%n_vector(i)
   acc_n_vec(i) = con%num
 END DO

!Section eleven:
 con%n_vector(11) = NINT( ((con%length_vector(11)-con%dx/2.0D0))/con%dx )+1
!vector w/ number of steps on each section
 con%num = con%num + con%n_vector(11)
 acc_n_vec(11) = con%num

 count = con%num
 !Allocating the memory for all the variables in constants
 WRITE(*,*) 'Allocating the number of elements in set up =', con%num
 ALLOCATE ( con%alpha(count), STAT=status)
  IF (status /= 0) THEN
  WRITE(*,*) 'Check allocation of alpha'
  END IF
 ALLOCATE ( con%alpha_vec(count), STAT=status)
  IF (status /= 0) THEN
  WRITE(*,*) 'Check allocation of alpha_vec'
  END IF
 ALLOCATE ( con%AT_vec(count), STAT=status)
  IF (status /= 0) THEN
  WRITE(*,*) 'Check allocation of AA_vec'
  END IF
 ALLOCATE ( con%A_vec(count), STAT=status)
  IF (status /= 0) THEN
  WRITE(*,*) 'Check allocation of A_vec'
  END IF
 ALLOCATE ( con%KK(con%num), STAT=status)
```

```
  IF (status /= 0) THEN
  WRITE(*,*) 'Check allocation of KK'
  END IF
ALLOCATE ( con%DD1(con%num), STAT=status)
  IF (status /= 0) THEN
  WRITE(*,*) 'Check allocation of DD1'
  END IF
ALLOCATE ( con%DD2(con%num), STAT=status)
  IF (status /= 0) THEN
  WRITE(*,*) 'Check allocation of DD2'
  END IF
ALLOCATE ( con%DD(con%num,2), STAT=status)
  IF (status /= 0) THEN
  WRITE(*,*) 'Check allocation of DD'
  END IF
ALLOCATE ( con%DD_self(con%num,2), STAT=status)
  IF (status /= 0) THEN
  WRITE(*,*) 'Check allocation of DD_self'
  END IF
ALLOCATE ( con%DD_vec(con%num,2), STAT=status)
  IF (status /= 0) THEN
  WRITE(*,*) 'Check allocation of DD_vec'
  END IF
!===Making vectors KK, DD1, and DD2===!
con%KK=0

DO i = 1,acc_n_vec(1)
  con%KK(i) = (con%diam_vector(1)**2)/32.0D0
  con%DD1(i) = con%D1!*con%factorD
  con%DD2(i) = con%D2!*con%factorD
  con%A_vec(i) = (3.1415927D0*con%diam_vector(1)**2)/4.0D0
  con%AT_vec(i)=con%A_vec(i)
END DO

DO i = acc_n_vec(1)+1,acc_n_vec(2)
  con%KK(i) = (con%diam_vector(2)**2)/32.0D0
  con%DD1(i) = con%D1!*con%factorD
  con%DD2(i) = con%D2!*con%factorD
  con%A_vec(i) = (3.1415927D0*con%diam_vector(2)**2)/4.0D0
  con%AT_vec(i)=con%A_vec(i)
END DO
```

```
 DO i =  acc_n_vec(2)+1,acc_n_vec(3)
   con%KK(i) = (con%diam_vector(3)**2)/32.0D0
   con%DD1(i) = con%D1!*con%factorD
   con%DD2(i) = con%D2!*con%factorD
   con%A_vec(i) = (3.1415927D0*con%diam_vector(3)**2)/4.0D0
   con%AT_vec(i)=con%A_vec(i)
 END DO

 DO i =  acc_n_vec(3)+1,acc_n_vec(4)
   con%KK(i) = (con%diam_vector(4)**2)/32.0D0
   con%DD1(i) = con%D1!*con%factorD
   con%DD2(i) = con%D2!*con%factorD
   con%A_vec(i) = (3.1415927D0*con%diam_vector(4)**2)/4.0D0
   con%AT_vec(i)=con%A_vec(i)
 END DO


DO i =  acc_n_vec(4)+1,acc_n_vec(5)
con%KK(i) = (con%diam_vector(5)**2)/32.0D0
con%DD1(i) = con%D1!*con%factorD
con%DD2(i) = con%D2!*con%factorD
con%A_vec(i) = (3.1415927D0*con%diam_vector(5)**2)/4.0D0
con%AT_vec(i)=con%A_vec(i)
END DO


DO i =  acc_n_vec(5)+1,acc_n_vec(6)
con%KK(i) = (con%diam_vector(6)**2)/32.0D0
con%DD1(i) = con%D1!*con%factorD
con%DD2(i) = con%D2!*con%factorD
con%A_vec(i) = (3.1415927D0*con%diam_vector(6)**2)/4.0D0
con%AT_vec(i)=con%A_vec(i)
END DO



 DO i =  acc_n_vec(6)+1,acc_n_vec(7)
   con%KK(i) = (con%diam_vector(7)**2)/32.0D0
   con%DD1(i) = con%D1!*con%factorD
   con%DD2(i) = con%D2!*con%factorD
   con%A_vec(i) = (3.1415927D0*con%diam_vector(7)**2)/4.0D0
   con%AT_vec(i)=con%A_vec(i)
```

```
 END DO


 DO i =  acc_n_vec(7)+1,acc_n_vec(8)
  con%KK(i) = (con%diam_vector(8)**2)/32.0D0
  con%DD1(i) = con%D1!*con%factorD
  con%DD2(i) = con%D2!*con%factorD
  con%A_vec(i) = (3.1415927D0*con%diam_vector(8)**2)/4.0D0
  con%AT_vec(i)=con%A_vec(i)
 END DO

 DO i =  acc_n_vec(8)+1,acc_n_vec(9)
  con%KK(i)  = (con%diam_vector(9)**2)/32.0D0
  con%DD1(i) = con%D1!*con%factorD
  con%DD2(i) = con%D2!*con%factorD
  con%A_vec(i) = (3.1415927D0*con%diam_vector(9)**2)/4.0D0
  con%AT_vec(i)=con%A_vec(i)
 END DO

!Only on the TENTH (out of ELEVEN) section has a different permeability and
diffusivity vectors
 DO i =  acc_n_vec(9)+1,acc_n_vec(10)
  con%KK(i) = con%perm
  con%DD1(i) = con%D1*con%factorD
  con%DD2(i) = con%D2*con%factorD
  con%A_vec(i) = (porosity*3.1415927D0*con%diam_vector(10)**2)/4.0D0
  con%AT_vec(i)=(3.1415927D0*con%diam_vector(10)**2)/4.0D0
 END DO

 DO i =  acc_n_vec(10)+1,acc_n_vec(11)
  con%KK(i)  = (con%diam_vector(11)**2)/32.0D0
  con%DD1(i) = con%D1!*con%factorD
  con%DD2(i) = con%D2!*con%factorD
  con%A_vec(i) = (3.1415927D0*con%diam_vector(11)**2)/4.0D0
  con%AT_vec(i)=con%A_vec(i)
 END DO

 con%alpha = con%KK / visc
 con%DD(:,1) = con%DD1
 con%DD(:,2) = con%DD2

 DO i=1,con%num-1
```

```
   con%DD_vec(i,1) = (2*con%DD(i,1)*con%DD(i+1,1) )/(
con%DD(i,1)+con%DD(i+1,1) )
   con%DD_vec(i,2) = (2*con%DD(i,2)*con%DD(i+1,2) )/(
con%DD(i,2)+con%DD(i+1,2) )
   con%alpha_vec(i) = (2*con%alpha(i)*con%alpha(i+1) )/(
con%alpha(i)+con%alpha(i+1) )
   con%AT_vec(i) = MIN(con%AT_vec(i), con%AT_vec(i+1))
   con%DD_self (i,1) = 5.415D-6    !sef diffusivity of xenon
   con%DD_self (i,2) = 15.925D-6  !self diffusivity of nitrogen
  END DO

  con%DD_vec(con%num,1) = con%DD(con%num,1)
  con%DD_vec(con%num,2) = con%DD(con%num,2)
  con%alpha_vec(con%num) = con%alpha(con%num)
  con%DD_self (con%num,1) = 5.415D-6    !sef diffusivity of xenon
  con%DD_self (con%num,2) = 15.925D-6  !self diffusivity of nitrogen

  WRITE(*,*) ' n_vector   = ', con%n_vector
  WRITE(*,*)'area vector =   ', con%A_vec

 WRITE(*,*)'DIFFUSION VECTOR =   ', con%DD_vec

 END SUBROUTINE setConstants

END MODULE
```

```
SUBROUTINE setConcs(num, Co, n_vector, CONC)

  IMPLICIT NONE
   INTEGER, INTENT(IN) :: num
   REAL*8, DIMENSION(num,4), INTENT(OUT) :: CONC  !This is an array of 4
columns, from left to right: OLD_C1, NEW_C1, OLD_C2, NEW_C2
   REAL*8, INTENT(IN)  :: Co   !Initial concnetration of gasses 1 and 2 {mol/m^3}
   INTEGER, DIMENSION(5), INTENT(IN) :: n_vector

    CONC = 0.0D0
    CONC(:n_vector(1)+n_vector(2)+n_vector(3)+n_vector(4)+n_vector(5),1)=Co
    CONC(n_vector(1)+n_vector(2)+n_vector(3)+n_vector(4)+n_vector(5)+1:,3)=Co

END SUBROUTINE setConcs
```

```
SUBROUTINE CREATEFILE (filename)
!This subroutine will create a file named "filename" with two !groups:  ConcGas1 and
ConcGas2 with two initial datasets: mesh !and parameters module load hdf5
USE mod_constants
USE HDF5 ! This module contains all hdf5 info needed
    IMPLICIT NONE

   CHARACTER(LEN=13), INTENT(IN):: filename !This can only be "rstartfile.h5" or
"outputfile.h5"
   CHARACTER(LEN=4) :: dsetname1 = "Prm1"
   CHARACTER(LEN=4) :: dsetname2 = "Prm2"
   CHARACTER(LEN=5) :: grpname1 = "CGas1"  !Group gas 1
   CHARACTER(LEN=5) :: grpname2 = "CGas2"  !Group gas 2
   INTEGER(HID_T) :: file_id       ! File identifier
   INTEGER(HID_T) :: group1_id     ! Group 1 identifier
   INTEGER(HID_T) :: group2_id     ! Group 2 identifier
   INTEGER(HID_T) :: dset_id       ! Dataset identifier
   INTEGER(HID_T) :: dspace_id     ! Dataspace identifier
   INTEGER(HSIZE_T), DIMENSION(2) :: dset_dims
   INTEGER(HSIZE_T), DIMENSION(2) :: d_dims     !Data dimensions
   INTEGER  :: dsetrank = 2              ! Dataset rank
   REAL*8, DIMENSION(6,1) :: parameters ! Data buffers this is where the data is
straged in the program?

   INTEGER     ::   error ! Error flag
! The parameters are: time step(seconds) // # of time steps// # of elements on array
Cgas1Cgsa2 // Time between datapoints recorded (sec) // Diffusivity gas 2 // mesh size
(m)

   parameters(1,1) = con%dt
   parameters(2,1) = con%nt
   parameters(3,1) = con%nn
   parameters(4,1) = con%dt*con%nt/con%nn
   parameters(5,1) = con%D2
   parameters(6,1) = con%dx

   CALL h5open_f(error)  ! This always have to go to give access to predetermned
datatypes
   CALL h5fcreate_f(trim(filename), H5F_ACC_TRUNC_F, file_id, error) !new file w/
default properties returns a file_id

  !The parameters that will be saved on  the first dataset are:
```

```
   dset_dims =(/6,1/)
   !=========
   !Create group 1 and save data set of parameters, then close data set and group
   !=========
   CALL h5gcreate_f(file_id, grpname1, group1_id, error)  !create group ConcGas1
   CALL h5screate_simple_f(dsetrank, dset_dims, dspace_id, error)  !simple dataspace
(N-dimensional array of points) returns a dspace_id
   CALL h5dcreate_f(group1_id, dsetname1,  H5T_IEEE_F64LE, dspace_id, dset_id,
error) ! Create the dataset "Parameters" in ConcGas1
   d_dims=(/6,1/)
   !d_dims(2)=1
   CALL H5DWRITE_F(dset_id,  H5T_IEEE_F64LE, parameters, d_dims, error)
!Writing the matrix CONC in dset_id

   CALL h5dclose_f(dset_id, error)  !End access to dataset
   CALL h5sclose_f(dspace_id, error) !End access to dataspace
   CALL h5gclose_f(group1_id, error)  !Close group ConcGas1
   !=========
   !Create group 2 and save data set of parameters, then close data set and group
   !=========
   CALL h5gcreate_f(file_id, grpname2, group2_id, error)  !Create group ConcGas2
   CALL h5screate_simple_f(dsetrank, dset_dims, dspace_id, error)  !simple dataspace
(N-dimensional array of points) returns a dspace_id
   CALL h5dcreate_f(group2_id, dsetname2, H5T_IEEE_F64LE, dspace_id, dset_id,
error)   ! Create the dataset "Parameters' in ConcGas2
   d_dims=(/5,1/)
   !d_dims(2)=1
   CALL h5DWRITE_F(dset_id,  H5T_IEEE_F64LE, parameters, d_dims, error)
!Writing the matrix CONC in dset_id

   CALL h5dclose_f(dset_id, error)  !End access to dataset
   CALL h5sclose_f(dspace_id, error) !End access to dataspace
   CALL h5gclose_f(group2_id, error)  !Close group ConcGas2
   !==========
   !Close file
   !==========
   CALL h5fclose_f(file_id, error)  !closes file
   CALL h5close_f(error)   !closes FORTRAN access

END SUBROUTINE CREATEFILE
```

```
SUBROUTINE RDFILE (FnameREAD, dsetname, CONCrstrt, num)
!This subroutine will write the data of CONC on  a .h5 file
   USE HDF5
   USE mod_constants
   IMPLICIT NONE

   CHARACTER(LEN=13), INTENT(IN) :: FnameREAD != "rstartfile.h5"
   CHARACTER(LEN=9), INTENT(IN) :: dsetname !Name of data set to open and read
   CHARACTER(LEN=5):: grpname1 = "CGas1"  !Group gas 1
   CHARACTER(LEN=5):: grpname2 = "CGas2"  !Group gas 2
   INTEGER(HID_T) :: file_id       ! File identifier
   INTEGER(HID_T) :: group1_id     ! Group 1 identifier
   INTEGER(HID_T) :: group2_id     ! Group 2 identifier
   INTEGER(HID_T) :: dset_id       ! Dataset identifier
   INTEGER(HSIZE_T), DIMENSION(2) :: d_dims    !Data dimensions

   REAL*8, DIMENSION(num,2), INTENT(OUT) :: CONCrstrt ! Data buffers to be
used by the program?
   INTEGER, INTENT(IN) :: num
   INTEGER     ::   error ! Error flag
    d_dims = (/con%num,1/)

   CALL h5open_f(error)
   CALL h5fopen_f(trim(FnameREAD), H5F_ACC_RDWR_F, file_id, error) !OPEN
file
   !=========
   !READ from  group 1
   !=========
   CALL h5gopen_f(file_id, grpname1, group1_id, error)  !open group ConcGas1
   CALL h5dopen_f(group1_id, TRIM(dsetname), dset_id, error) ! open dataset

   CALL H5DREAD_f(dset_id,  H5T_IEEE_F64LE, CONCrstrt(:,1), d_dims, error)
!Reading the dataset

   CALL h5dclose_f(dset_id, error)  !End access to dataset
   CALL h5gclose_f(group1_id, error)  !Close group ConcGas1
   !=========
   !READ from group 2
   !=========
   CALL h5gopen_f(file_id, grpname2, group2_id, error)  !Create group ConcGas2
   CALL h5dopen_f(group2_id, TRIM(dsetname), dset_id, error)   ! Open dataset
```

```
   CALL H5DREAD_F(dset_id,  H5T_IEEE_F64LE, CONCrstrt(:,2), d_dims, error)
!Reading dataset

   CALL h5dclose_f(dset_id, error)  !End access to dataset
   CALL h5gclose_f(group2_id, error)  !Close group ConcGas2
   !===========
   !Close file
   !===========
   CALL h5fclose_f(file_id, error)  !closes file
   CALL h5close_f(error)   !closes FORTRAN access

END SUBROUTINE RDFILE
```

```
SUBROUTINE Velocity_NSexplicit (num, CONC, Veloc_old, Veloc_NS, dt)

!!In this subroutine the Velocity is estimated from a NS 1-D relation.  This is a FULLY
EXPLICIT discretization.  This subroutine assumes there is no friction losses in the
fittings/tue walls (I expect this subroutine to overpredict the velocities generated).

USE mod_constants

IMPLICIT NONE
REAL*8, DIMENSION (num,4), INTENT(IN) :: CONC
REAL*8, DIMENSION (num,2), INTENT(IN) :: Veloc_old
REAL*8, DIMENSION (num,2), INTENT(OUT) :: Veloc_NS
REAL*8, DIMENSION (num,2)  :: Veloc_NS1
REAL*8, DIMENSION (num) :: P_vec !pressure vector form known concentrations
REAL*8, DIMENSION (num) :: P_grad !pressure gradient vector
REAL*8, DIMENSION (num):: CONC_tot  !Concentration vector
REAL*8, DIMENSION (num) :: rho !gas mixture density vector
REAL*8, DIMENSION (num) :: rho_R !gas mixture density-R
REAL*8, DIMENSION (num) :: vol_R !Volume-R
REAL*8, DIMENSION (num,2) :: Diff
REAL*8, DIMENSION(num) :: x1 !molar fraction vector of GAS1
REAL*8, DIMENSION(num) :: x2 !molar fraction vectoe of GAS2
REAL*8, DIMENSION(num) :: M !molecular weight of the gas mixture (M = x1M1 +
x2M2)
REAL*8, INTENT(IN) ::dt !time step
INTEGER, INTENT(IN) :: num
INTEGER :: i  !counter
INTEGER :: j  !array sub index

CALL Diffusivity(num, CONC, Diff)

CONC_tot = CONC(:,1) + CONC(:,3)  !Total concentration vector at time t (estimated
from a diffusion ONLY process)

x1 = CONC(:,1) / CONC_tot(:)
x2 = CONC(:,3) / CONC_tot(:)
M(:num) = x1(:num)*con%M1 + x2(:num)*con%M2

P_vec = (con%R *con%temp *CONC_tot)  !pressure vector from known concentrations

P_grad (1:num-1) = (P_vec(2:num)-P_vec(1:num-1))/con%dx
P_grad (num) = 0.0D0
```

```
rho = 0.001D0*(CONC(:,1)*con%M1 + CONC(:,3)*con%M2)  !The factor of 0.001 is to
convert this to kg/m3

rho_R(1:num-1)= (rho(1:num-1) + rho(2:num) )/2.0D0
vol_R(1:num-1)= (con%A_vec(1:num-1) + con%A_vec(2:num))*con%dx /2.0D0 !Note
this is also OK for the first element since it is dx/2

rho_R(num)= rho(num) !This value should't be needed since U_n = 0
vol_R(num)= 1.1D20  !this value shouldn't be needed since U_n = 0


DO j=1,2
  Veloc_NS1(1,j) = Veloc_old(1,j) +
(4.0D0*dt/((rho(1)+rho(2))*(con%A_vec(1)+con%A_vec(2))*con%dx))*((con%A_vec(
1)+&
   &con%A_vec(2))*(P_vec(1)- P_vec(2))/2.0D0 -
rho(2)*con%A_vec(2)*((Veloc_old(1,j)+Veloc_old(2,j))**2)/4.0D0)

  DO i=2,num-2
   Veloc_NS1(i,j) = Veloc_old(i,j)+
(4.0D0*dt/((rho(i)+rho(i+1))*(con%A_vec(i)+con%A_vec(i+1))*con%dx))*((con%A_v
ec(i)+&
   &con%A_vec(i+1))*(P_vec(i)-P_vec(i+1))/2.0D0 +
rho(i)*con%A_vec(i)*((Veloc_old(i,j)+Veloc_old(i-1,j))**2)/4.0D0 -&
   &rho(i+1)*con%A_vec(i+1)*((Veloc_old(i,j)+Veloc_old(i+1,j))**2)/4.0D0)
  END DO

  Veloc_NS1(num-1,j) = Veloc_old(num-1,j) + (4.0D0*dt/((rho(num-
1)+rho(num))*(con%A_vec(num-1)+&
   con%A_vec(num))*con%dx))*((con%A_vec(num-1)+
con%A_vec(num))*(P_vec(num-1)-P_vec(num))/2.0D0 + &
   &rho(num-1)*con%A_vec(num-1)*((Veloc_old(num-1,j)+Veloc_old(num-
2,j))**2)/4.0D0)

  Veloc_NS1(num,j) = 0.0D0
  ! CORRECTION dp/p TER
M !
  !----------------------!
  Veloc_NS (1:num-1,j) = Veloc_NS1(:num-1,j) + con%DD_vec(:num-
1,j)*P_grad(:num-1)*2.0D0/(P_vec(1:num-1)+P_vec(2:num))
  Veloc_NS (num,j) = 0
```

```
END DO
END SUBROUTINE Velocity_NSexplicit
```

```
SUBROUTINE Diffusivity (num, CONC, Diff_vec)

!!In this subroutine the pressure gradient is estimated @ THE BOUNDARIES from
concentrations after a diffusion step

USE mod_constants

IMPLICIT NONE
REAL*8, DIMENSION (num,4), INTENT(IN) :: CONC
REAL*8, DIMENSION (num,2), INTENT(OUT) :: Diff_vec
REAL*8, DIMENSION (num,2) :: DD
INTEGER, INTENT(IN) :: num
INTEGER :: i  !counter
REAL*8, dimension(num) :: x1 !molar fraction vector of GAS1
REAL*8, DIMENSION(num) :: x2 !molar fraction vectoe of GAS2
REAL*8, DIMENSION(num) :: C_tot  !total molar cocnetration

!!== MOLAR FRACTION VECTORS ===!
!-----------------------------!
C_tot = CONC(:,1) +CONC(:,3)
x1 = CONC(:,1) / C_tot(:)
x2 = CONC(:,3) / C_tot(:)

DD(:,1) = con%DD(:,1)*con%M2 / (con%M1*x1 +con%M2*x2)
DD(:,2) = con%DD(:,2)*con%M1 / (con%M1*x1 +con%M2*x2)

Diff_vec(1:con%num-1,1) = (2*DD(1:con%num-1,1)*DD(1:con%num,1) )/(
DD(1:con%num-1,1)+DD(1:con%num,1) )
Diff_vec(1:con%num-1,2) = (2*DD(1:con%num-1,2)*DD(1:con%num,2) )/(
DD(1:con%num-1,2)+DD(1:con%num,2) )

Diff_vec(con%num,1) = DD(con%num,1)
Diff_vec(con%num,2) = DD(con%num,2)

END SUBROUTINE Diffusivity
```

```
SUBROUTINE CN_Diff_Conv(num, dt_conv, CONC, BC, Veloc)

!This subroutine will estimate the GAS1 and GAS2 concentrations at time step "t+1"
!based on the concentrations at time "t" using a Crank-Nicholson approach

USE mod_constants
IMPLICIT NONE

!GAS1 and GAS2 conc matrix.  The 1st column is the known GAS1 conc, the 3th column
!is the guessed GAS1 conc.  The 2nd and 4th columns are the known and guessed conc
! of GAS 2 respectively
INTEGER, INTENT(IN) :: num
REAL*8, DIMENSION(num,4),INTENT(INOUT) :: CONC
REAL*8, DIMENSION(num,2), INTENT(IN)  :: Veloc
REAL*8, DIMENSION(2,4), INTENT(INOUT)  :: BC
REAL*8, ALLOCATABLE, DIMENSION(:,:) :: aL_vec
REAL*8, ALLOCATABLE, DIMENSION(:,:) :: bL_vec
REAL*8, ALLOCATABLE, DIMENSION(:,:) :: cL_vec
REAL*8, ALLOCATABLE, DIMENSION(:,:) :: aR_vec
REAL*8, ALLOCATABLE, DIMENSION(:,:) :: bR_vec
REAL*8, ALLOCATABLE, DIMENSION(:,:) :: cR_vec
REAL*8, ALLOCATABLE, DIMENSION(:,:) :: aL
REAL*8, ALLOCATABLE, DIMENSION(:,:) :: bL
REAL*8, ALLOCATABLE, DIMENSION(:,:) :: cL
REAL*8, DIMENSION(num) :: RHS1
REAL*8, DIMENSION(num) :: RHS2
REAL*8, DIMENSION(num) :: LHS1
REAL*8, DIMENSION(num) :: LHS2
REAL*8, DIMENSION(num+2,2) ::Cold_ext
REAL*8, INTENT(IN) :: dt_conv
REAL*8 :: max_error
REAL*8 :: min_error
REAL*8, DIMENSION(num):: error

INTEGER :: status
INTEGER :: INFO  !Info from DGSTV subroutine


ALLOCATE ( aL_vec(con%num,2), STAT=status)
IF (status /= 0) THEN
  WRITE(*,*) 'Check allocation of aL_vec'
END IF
```

```
ALLOCATE ( bL_vec(con%num,2), STAT=status)
IF (status /= 0) THEN
  WRITE(*,*) 'Check allocation of bL_vec'
END IF
ALLOCATE ( cL_vec(con%num,2), STAT=status)
IF (status /= 0) THEN
  WRITE(*,*) 'Check allocation of cL_vec'
END IF
ALLOCATE ( aR_vec(con%num,2), STAT=status)
IF (status /= 0) THEN
  WRITE(*,*) 'Check allocation of aR_vec'
END IF
ALLOCATE ( bR_vec(con%num,2), STAT=status)
IF (status /= 0) THEN
  WRITE(*,*) 'Check allocation of bR'
END IF
ALLOCATE ( cR_vec(con%num,2), STAT=status)
IF (status /= 0) THEN
  WRITE(*,*) 'Check allocation of cR'
END IF
!!NOTE THAT THE FOLLOWING ALOCATIONS ARE FOR A DIFFERENT
VARIABLES!!
ALLOCATE ( aL(con%num,2), STAT=status)
IF (status /= 0) THEN
 WRITE(*,*) 'Check allocation of aL'
END IF
ALLOCATE ( bL(con%num,2), STAT=status)
IF (status /= 0) THEN
 WRITE(*,*) 'Check allocation of bL'
END IF
ALLOCATE ( cL(con%num,2), STAT=status)
IF (status /= 0) THEN
 WRITE(*,*) 'Check allocation of cL'
END IF


!WRITE(*,*) 'VELOCITY VECTOR IN CN_DIFF_CONV SUBROUTINE    =', Veloc
CALL coeff_CN (con%num, dt_conv, CONC, aL_vec, bL_vec, cL_vec, aR_vec,
bR_vec, cR_vec, Veloc)!=Estimation of coefficient matrix

aL = aL_vec
bL = bL_vec
```

```
cL = cL_vec
  ! we are looking to assemble a matrix of the form
! | b1L  a1L   0     0    0  |  |C1new|   |  b1R  a1R   0     0      0     0 |  |C1old|
! | c2L  b2L  a2L   0    0  |  |C2new|   |  c2R  b2R  a2R   0      0     0 |  |C2old|
! |  0   c3L  b3L  a3L   0  |  |C3new| = |    0  c3R  b3R  a3R    0     0 |  |C3old|
! |  0    0   c4L  b4L  a4L |  |C4new|   |    0   0   c4R  b4R   a4R    0 |  |C4old|
! |  0    0    0   c5L  b5L |  |C5new|   |    0   0    0   c5R   b5R  a5R|  |C5old|

   !Where the left side has the unknown concentrations and the right one the known ones
   !Remember that the boundary conditions have been included in b1L, b1R, c1R, b5L,
   ! b5R and a5R making th LHS a tridiagonal matrix

  !!==THE RHS==

   CALL expandVector (con%num, CONC(:,1), CONC(:,3), BC(:,1), BC(:,3), Cold_ext)
   RHS1 = aR_vec(:,1)*Cold_ext(3:con%num+2,1) +
bR_vec(:,1)*Cold_ext(2:con%num+1,1) +cR_vec(:,1)*Cold_ext(1:con%num,1)
   RHS2 = aR_vec(:,2)*Cold_ext(3:con%num+2,2) +
bR_vec(:,2)*Cold_ext(2:con%num+1,2) +cR_vec(:,2)*Cold_ext(1:con%num,2)

   !RHS1 = aR_vec(:num-1,1)*CONC(2:num,1) + bR_vec(:,1)*CONC(1:num,1)
+cR_vec(2:,1)*CONC(1:num-1,1)
   !RHS2 = aR_vec(:num-1,2)*CONC(2:num,3) + bR_vec(:,2)*CONC(1:num,3)
+cR_vec(2:,2)*CONC(1:num-1,3)

  !!===THE LHS==
    LHS1=RHS1
    LHS2=RHS2

   CALL DGTSV (con%num, 1, cL_vec(2:,1), bL_vec(:,1), aL_vec(:con%num-1,1),
LHS1, con%num, INFO)
    IF (INFO /= 0) THEN
     WRITE (*,*) 'INFO check DGTSV inputs for GAS1 @ Conv_Diff unless =0', INFO
    END IF

   aL_vec = aL
   bL_vec = bL
   cL_vec = cL
   CONC(:,2) = LHS1  !The new concentration vector is updated

!CALL error_test (LHS1, RHS1, aL_vec(:,1), bL_vec(:,1), cL_vec(:,1), max_error,
min_error, error)
```

```
  CALL DGTSV (con%num, 1, cL_vec(2:,2), bL_vec(:,2), aL_vec(:con%num-1,2),
LHS2, con%num, INFO)
  IF (INFO /= 0)THEN
  WRITE (*,*) 'INFO check DGTSV inputs for GAS2 @Conv_Diff unless =0', INFO
  END IF
  aL_vec = aL
  bL_vec = bL
  cL_vec = cL

  CONC(:,4) = LHS2  !The new concentration vector is updated

  !CALL error_test (LHS2, RHS2, aL_vec(:,2), bL_vec(:,2), cL_vec(:,2), max_error,
min_error, error)

DEALLOCATE (aL_vec, bL_vec, cL_vec, aR_vec, bR_vec, cR_vec, aL, bL, cL)

END SUBROUTINE CN_Diff_Conv
```

```
SUBROUTINE coeff_CN (num, dt_conv, CONC, aL_vec, bL_vec, cL_vec, aR_vec,
bR_vec, cR_vec, Veloc)

USE mod_constants

IMPLICIT NONE

REAL*8, DIMENSION(num,4), INTENT(IN) :: CONC
REAL*8, DIMENSION(num,2), INTENT(IN)  :: Veloc
REAL*8, DIMENSION(num,2), INTENT(OUT) :: aL_vec
REAL*8, DIMENSION(num,2), INTENT(OUT) :: bL_vec
REAL*8, DIMENSION(num,2), INTENT(OUT) :: cL_vec
REAL*8, DIMENSION(num,2), INTENT(OUT) :: aR_vec
REAL*8, DIMENSION(num,2), INTENT(OUT) :: bR_vec
REAL*8, DIMENSION(num,2), INTENT(OUT) :: cR_vec
REAL*8, DIMENSION (num,2) :: Diff

REAL*8, INTENT(IN) :: dt_conv

INTEGER, INTENT(IN) :: num
INTEGER :: i  !Loop index
INTEGER :: j  !loop index

CALL Diffusivity (num, CONC, Diff)!!THIS IS CALLING THE SELF DIFFUSIVITY
NOW!!!
DO j=1,2
 cL_vec(2:num-1,j)=(-con%AT_vec(1:num-2)*Veloc(1:num-2,j)/(con%A_vec(2:num-
1)*4.0D0*con%dx))- &
   & (con%AT_vec(1:num-2)*Diff(1:num-2,j)/(2.0D0*con%A_vec(2:num-
1)*con%dx**2))

  bL_vec(2:num-1,j)=1.0/dt_conv-con%AT_vec(1:num-2)*Veloc(1:num-
2,j)/(con%A_vec(2:num-1)*4.0D0*con%dx)+&
   &(con%AT_vec(1:num-2)*Diff(1:num-2,j)/(2.0D0*con%A_vec(2:num-
1)*con%dx**2))+&
   &(con%AT_vec(2:num-1)*Veloc(2:num-1,j)/(con%A_vec(2:num-
1)*4.0D0*con%dx)) + &
   &(con%AT_vec(2:num-1)*Diff(2:num-1,j)/(2.0D0*con%A_vec(2:num-
1)*con%dx**2))

  aL_vec(2:num-1,j)=(con%AT_vec(2:num-1)*Veloc(2:num-1,j)/(con%A_vec(2:num-
1)*4.0D0*con%dx))-&
```

```
   &( con%AT_vec(2:num-1)*Diff(2:num-1,j)/(2.0D0*con%A_vec(2:num-
1)*con%dx**2) )

 cR_vec(2:num-1,j)=(con%AT_vec(1:num-2)*Veloc(1:num-2,j)/(con%A_vec(2:num-
1)*4.0D0*con%dx))+&
   &( con%AT_vec(1:num-2)*Diff(1:num-2,j)/(2.0D0*con%A_vec(2:num-
1)*con%dx**2) )

 bR_vec(2:num-1,j)=1.0/dt_conv+con%AT_vec(1:num-2)*Veloc(1:num-
2,j)/(con%A_vec(2:num-1)*4.0D0*con%dx)-&
   &( con%AT_vec(1:num-2)*Diff(1:num-2,j)/(2.0D0*con%A_vec(2:num-
1)*con%dx**2))- &
   &(con%AT_vec(2:num-1)*Veloc(2:num-1,j)/(con%A_vec(2:num-
1)*4.0D0*con%dx))-&
   &( con%AT_vec(2:num-1)*Diff(2:num-1,j)/(2.0D0*con%A_vec(2:num-
1)*con%dx**2) )

 aR_vec(2:num-1,j)=-(con%AT_vec(2:num-1)*Veloc(2:num-1,j)/(con%A_vec(2:num-
1)*4.0D0*con%dx))+&
   &( con%AT_vec(2:num-1)*Diff(2:num-1,j)/(2.0D0*con%A_vec(2:num-
1)*con%dx**2) )

END DO

!==================
!BOUNDARY CONDITIONS
!==================

DO j =1,2


bL_vec(1,j) = 1.0/dt_conv +
(con%AT_vec(1)*Veloc(1,j)/(con%A_vec(1)*2.0D0*con%dx)) + &
&( con%AT_vec(1)*Diff(1,j)/(con%A_vec(1)*con%dx**2) )

aL_vec(1,j) = (con%AT_vec(1)*Veloc(1,j)/(con%A_vec(1)*2.0D0*con%dx)) - &
&( con%AT_vec(1)*Diff(1,j)/(con%A_vec(1)*con%dx**2) )

bR_vec(1,j) = 1.0/dt_conv -
(con%AT_vec(1)*Veloc(1,j)/(con%A_vec(1)*2.0D0*con%dx)) - &
&( con%AT_vec(1)*Diff(1,j)/(con%A_vec(1)*con%dx**2) )
```

```
aR_vec(1,j) = -(con%AT_vec(1)*Veloc(1,j)/(con%A_vec(1)*2.0D0*con%dx)) + &
&( con%AT_vec(1)*Diff(1,j)/(con%A_vec(1)*con%dx**2) )

cL_vec(1,j) = 0.0D0

cR_vec(1,j) = 0.0D0

cL_vec(num,j) = -(con%AT_vec(num-1)*Veloc(num-
1,j)/(con%A_vec(num)*2.0D0*con%dx))-&
   &( con%AT_vec(num-1)*Diff(num-1,j)/(con%A_vec(num)*con%dx**2))

bL_vec(num,j)=1.0/dt_conv-con%AT_vec(num-1)*Veloc(num-
1,j)/(con%A_vec(num)*2.0D0*con%dx)+&
   &( con%AT_vec(num-1)*Diff(num-1,j)/(con%A_vec(num)*con%dx**2))

cR_vec(num,j) =  (con%AT_vec(num-1)*Veloc(num-
1,j)/(con%A_vec(num)*2.0D0*con%dx))+&
   &( con%AT_vec(num-1)*Diff(num-1,j)/(con%A_vec(num)*con%dx**2))

bR_vec(num,j)=1.0/dt_conv + con%AT_vec(num-1)*Veloc(num-
1,j)/(con%A_vec(num)*2.0D0*con%dx)-&
   &( con%AT_vec(num-1)*Diff(num-1,j)/(con%A_vec(num)*con%dx**2))

aL_vec(num,j) = 0.0D0

aR_vec(num,j) = 0.0D0

END DO

END SUBROUTINE coeff_CN
```

```
SUBROUTINE expandVector (num, C1, C2, BC1, BC2, Cold_ext )

!This subroutine expands the vector C1 and C2 using BC1 and BC2

IMPLICIT NONE

REAL*8, DIMENSION(num), INTENT(IN) :: C1
REAL*8, DIMENSION(2), INTENT(IN) :: BC1
REAL*8, DIMENSION(num), INTENT(IN) :: C2
REAL*8, DIMENSION(2), INTENT(IN) :: BC2
REAL*8, DIMENSION(num+2,2), INTENT(INOUT):: Cold_ext
INTEGER :: i !loop counter
INTEGER, INTENT(IN) :: num

 Cold_ext(1,1) = BC1(1)
 Cold_ext(1,2) = BC2(1)
 Cold_ext(num+2,1) = BC1(2)
 Cold_ext(num+2,2) = BC2(2)

Cold_ext(2:num+1,1) = C1!(i)
Cold_ext(2:num+1,2) = C2!(i)

END SUBROUTINE expandVector
```

```
SUBROUTINE WRTFILE (filename, dsetname1, CONC1, CONC2, num)
!This subroutine will write the data of CONC on  a .h5 file
   USE HDF5
   USE mod_constants
   IMPLICIT NONE

   CHARACTER(LEN=13), INTENT(IN):: filename !This can only be "rstartfile.h5" or
"outputfile.h5"
   CHARACTER(LEN=9), INTENT(IN) :: dsetname1
   CHARACTER(LEN=5):: grpname1 = "CGas1"  !Group gas 1
   CHARACTER(LEN=5):: grpname2 = "CGas2"  !Group gas 2
   INTEGER(HID_T) :: file_id       ! File identifier
   INTEGER(HID_T) :: group1_id     ! Group 1 identifier
   INTEGER(HID_T) :: group2_id     ! Group 2 identifier
   INTEGER(HID_T) :: dset_id       ! Dataset identifier
   INTEGER(HID_T) :: dspace_id     ! Dataspace identifier

   INTEGER(HSIZE_T), DIMENSION(2) :: dset_dims  ! Dataset dimensions they will
later define as (/5/): Dx, Dt, D1, D2, freq_sv,tot
   INTEGER(HSIZE_T), DIMENSION(2) :: d_dims     !Data dimensions
   INTEGER  :: dsetrank = 2              ! Dataset rank

   REAL*8, DIMENSION(num,1), INTENT(IN) :: CONC1 ! Conc of gas 1 from
program
   REAL*8, DIMENSION(num,1), INTENT(IN) :: CONC2 ! Conc of gas 2 from
program

   INTEGER     ::   error ! Error flag
   INTEGER, INTENT(IN) :: num

   CALL h5open_f(error)
   CALL h5fopen_f(trim(filename), H5F_ACC_RDWR_F, file_id, error) !OPEN file

   dset_dims =(/con%num,1/)
   !=========
   !WIRTE in  group 1
   !=========
   CALL h5gopen_f(file_id, grpname1, group1_id, error)  !open group ConcGas1
   CALL h5screate_simple_f(dsetrank, dset_dims, dspace_id, error)  !simple dataspace
(N-dimensional array of points)
   CALL h5dcreate_f(group1_id, TRIM(dsetname1),  H5T_IEEE_F64LE, dspace_id,
dset_id, error) ! Create dataset
```

```
   d_dims=(/con%num,1/)

   CALL H5DWRITE_F(dset_id,  H5T_IEEE_F64LE, CONC1, d_dims, error) !Writing
the matrix CONC in dset_id

   CALL h5dclose_f(dset_id, error)  !End access to dataset
   CALL h5sclose_f(dspace_id, error) !End access to dataspace
   CALL h5gclose_f(group1_id, error)  !Close group ConcGas1
   !=========
   !WRITE in group 2
   !=========
   CALL h5gopen_f(file_id, grpname2, group2_id, error)  !Create group ConcGas2
   CALL h5screate_simple_f(dsetrank, dset_dims, dspace_id, error)  !simple dataspace
(N-dimensional array of points)
   CALL h5dcreate_f(group2_id, dsetname1, H5T_IEEE_F64LE, dspace_id, dset_id,
error)   ! Create dataset
   d_dims=(/con%num,1/)

   CALL H5DWRITE_F(dset_id,  H5T_IEEE_F64LE, CONC2, d_dims, error) !Writing
the matrix CONC in dset_id

   CALL h5dclose_f(dset_id, error)  !End access to dataset
   CALL h5sclose_f(dspace_id, error) !End access to dataspace
   CALL h5gclose_f(group2_id, error)  !Close group ConcGas2
   !==========
   !Close file
   !==========
   CALL h5fclose_f(file_id, error)  !closes file
   CALL h5close_f(error)   !closes FORTRAN access

END SUBROUTINE WRTFILE
```

```
PROGRAM := ConvDiffHDFVAR
FC := gfortran
#Flags for debugging
FCFLAGS := -O3 -I$(TACC_HDF5_INC)
#FCFLAGS := -g -I$(TACC_HDF5_INC)
#Libraries
LDLIBS := -Wl,-rpath,$(TACC_HDF5_LIB) -L$(TACC_HDF5_LIB) -lhdf5 -
lhdf5_fortran -lz
#LDFLAGS = ...
#Executable program
RM := rm -f
# Rules

$(PROGRAM):  main.f90 mod_constants.o interface_variables.o sub_setConcs.o
sub_Velocity.o sub_Velocity_NSexplicit.o  sub_pressure_grad_known.o
sub_Diffusivity.o sub_setCgas1Cgas2.o sub_CN_Diff_Conv.o sub_error_test.o
sub_expandVector.o sub_fluxes.o dgtsv.o sub_xerbla.o sub_coeff_CN.o sub_createfile.o
sub_wrtfile.o sub_rdfile.o
	$(FC) $(FCFLAGS) $^ -o $@ $(LDLIBS)

#main.o: main.f90
#	$(FC) $(FCFLAGS) -c $<

mod_constants.o: mod_constants.f90
	$(FC) $(FCFLAGS) -c $<

interface_variables.o: interface_variables.f90
	$(FC) $(FCFLAGS) -c $(LDLIBS) $<

sub_CN_Diff_Conv.o: sub_CN_Diff_Conv.f90 sub_coeff_CN.o sub_expandVector.o
dgtsv.o sub_xerbla.o
	$(FC) $(FCFLAGS) -c $<

sub_fluxes.o:sub_fluxes.f90 sub_Diffusivity.o
	$(FC) $(FCFLAGS) -c $<

sub_coeff_CN.o:sub_coeff_CN.f90 sub_Diffusivity.o
	$(FC) $(FCFLAGS) -c $<

sub_Diffusivity.o: sub_Diffusivity.f90
	$(FC) $(FCFLAGS) -c $<
```

```
dgtsv.o:dgtsv.f sub_xerbla.f90
	$(FC) $(FCFLAGS) -c $<

sub_setConcs.o: sub_setConcs.f90
	$(FC) $(FCFLAGS) -c $<

sub_setCgas1Cgas2.o: sub_setCgas1Cgas2.f90
	$(FC) $(FCFLAGS) -c $<

sub_xerbla.o: sub_xerbla.f90
	$(FC) $(FCFLAGS) -c $<

sub_expandVector.o: sub_expandVector.f90
	$(FC) $(FCFLAGS) -c $<

sub_error_test.o: sub_error_test.f90
	$(FC) $(FCFLAGS) -c $<

sub_Velocity.o: sub_Velocity.f90 sub_Diffusivity.o
	$(FC) $(FCFLAGS) -c $<

sub_Velocity_NSexplicit.o: sub_Velocity_NSexplicit.f90 sub_Diffusivity.o
	$(FC) $(FCFLAGS) -c $<

sub_pressure_grad_known.o: sub_pressure_grad_known.f90
	$(FC) $(FCFLAGS) -c $<

sub_createfile.o: sub_createfile.f90
	$(FC) $(FCFLAGS) -c $(LDLIBS) $<

sub_wrtfile.o: sub_wrtfile.f90
	$(FC) $(FCFLAGS) -c $(LDLIBS) $<

sub_rdfile.o: sub_rdfile.f90
	$(FC) $(FCFLAGS) -c $(LDLIBS) $<

#Utilitytargets

.PHONY := clobber clean
clobber: clean
	$(RM) $(PROGRAM) *.ncd *.h5
clean:
```

```
$(RM) *.o *~ *.bak *.mod
```

The HDF5 soubroutines and more information about it are available at:

http://www.hdfgroup.org/HDF5/

The subroutine to solve the linear system of equations (DGTSV) can be download from:

http://www.netlib.org/lapack/explore-html/d1/db3/dgtsv_8f_source.html

APPENDIX D: MESH INDEPENDENCE ANALYSIS AND VALIDATION OF MODELS

Mesh reduction analysis

A mesh reduction analysis was performed on both, the MATLAB and Fortran90 models. This study was conducted comparing the average cylinder concentration ratio *C/Co* for different discretized element Δz *{m}* after one hour of diffusion. For each Δz, the time discretization was also varied to ensure time independence. The results are listed in Table 8. The "Variation" listed here corresponds to the difference between any listed case and the one at the top in Table 8 (Δz = 0.005 m. and Δt= 0.04 s).

Element length {m}	***Δt {seconds}***	***C/Co {%}***	***Variation* {%}***
Δz = 0.005	0.04	90.67	
Δz = 0.005	0.08	90.67	9.73e-5
Δz = 0.01	0.80	90.86	0.21
Δz = 0.05	0.80	92.69	2.22

Table 8 Mesh reduction analysis of the Diffusion Only model

A similar procedure determined a variation of 2.38% between Δz = 0.05 m. and Δz=0.01 m. for the Diffusion-Convection model after 30 minutes of experiment.

Comparison of models among them

Figure 19 shows the comparison of the cylinder concentration variation estimated by the Diffusion only model (implemented in MATLAB) and the Diffusion-Convection model (implemented in Fortran90). To compare these two models, the velocities in the Convection-Diffusion model was forced to be zero. Likewise, the diffusivities of the two gases involved were set equal for both gases, and constant.

The largest difference between the results in Figure 19 occurs at t=10 hours. The estimated dimensionless argon concentrations, C/Co, in the sample cylinder are 0.826 and 0.832 for the Diffusion-Convection and Diffusion only models, respectively. Then, the maximum relative difference between these models is 0.72% of the MATLAB model. This results shows both models are comparable and can be used indistinctively.

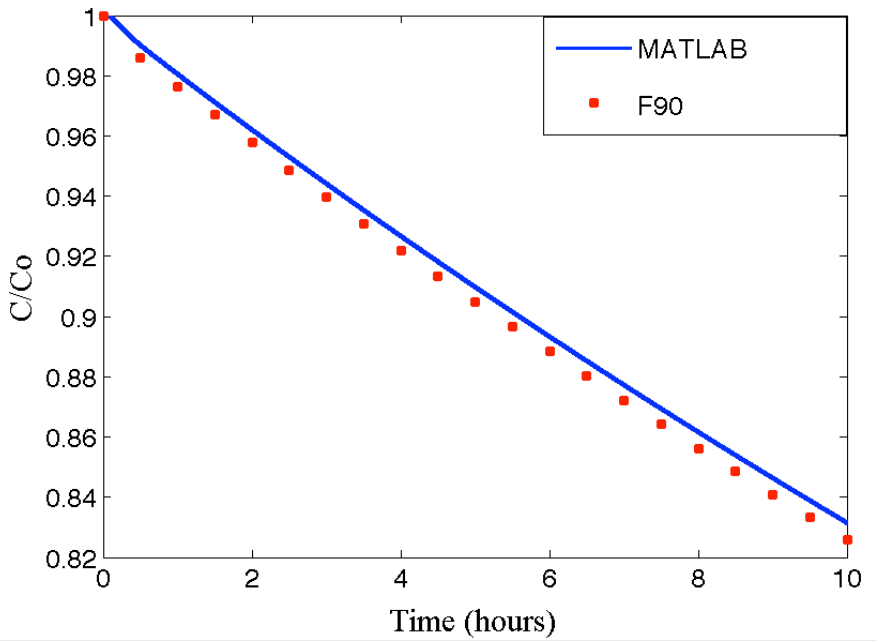

Figure 19 Comparison of the Diffusion-only and Diffusion-Convection models. The comparison was made on a set-up with 5 sections with varying areas.

Validation of FORTRAN 90 model

To validate the models developed in this dissertation I compared the Diffusion-Convection and Diffusion-Only models to the analytical solution for a gas diffusion form a finite volume, *Vin* {m^3}, along a semi-infinite porous media :

$$\frac{C}{Co}(z,t) = \exp\left(\frac{\alpha A^2 D_e t}{V_{in}^2} + \frac{z\alpha AL}{LV_{in}}\right) erfc\left(\frac{A\sqrt{\alpha D_e t}}{V_{in}} + \frac{z\sqrt{\alpha}}{2\sqrt{D_e t}}\right) \qquad (71),$$

where *Co* is the concentration {mol·m-^{3}} of the source with a volume V_{in} and cross sectional area *A* {m^2} through which the gas diffuses into the porous media. D_e is the effective diffusivity of the gas {$m^2 \cdot s^{-1}$},

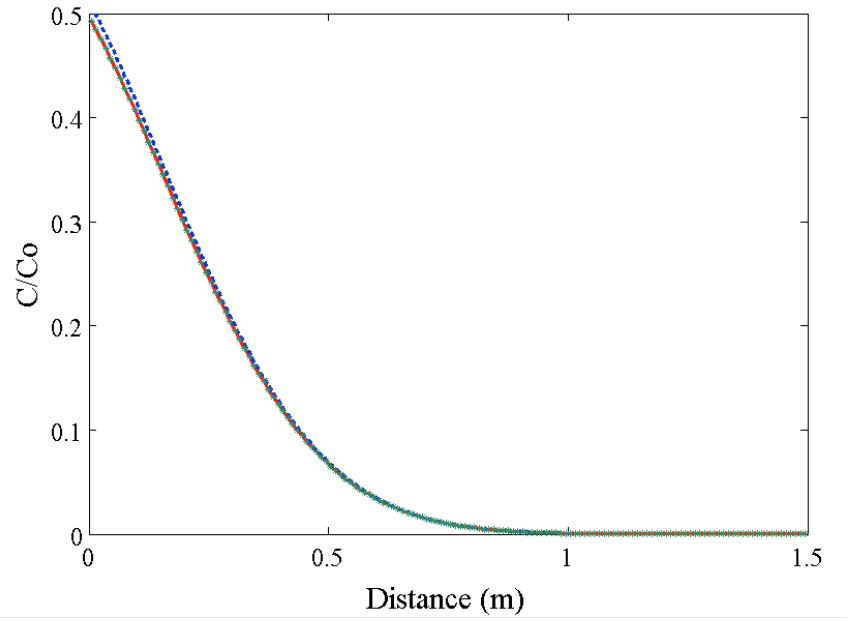

Figure 20 Comparison of analytical solution (blue), Diffusion-Only model (green) and Diffusion-Convection model (red developed in this dissertation.

The largest difference of the Diffusion only and Diffusion-Convection models and the analytical solution occur where z equals zero. The relative differences (with respect of the analytical solution) are 2.86% for the Convection-Diffusion model and 2.91% for the Diffusion-Only model. Although both values seem to be non-negligible, the absolute differences are lower than 2% and are taken as acceptable for this first approximation.

References

[1] P. Moldrup, T. Olesn, P. Schjonning, T. Yamaguchi, and D. E. Rolston, "Predicting the Gas Diffusion Coefficient in Undisturbed Soil from Soil Water Characteristics," *Soil Science Society Journal,* vol. 64, pp. 94-100, 2000.

[2] W. Abu-El-Sha'r and L. M. Abriola, "Experimentala ssessment of gas transport mechanisms in natural porous media: Parameter evaluation," *Water Resources Research,* vol. 33, pp. 505-516, 1997.

[3] A. Becker, G. Wotawa, A. Ringbom, and P. Saey, "Backtracking of Noble Gas Measurements Taken in the Aftermath of the Announced October 2006 Event in North Korea by Means of PTS Methods in Nuclear Source Estimation and Reconstruction," *Pure and Applied Geophysics,* vol. 167, pp. 581-599, 2010.

[4] T. Bowyer, K. Abel, C. Hubbard, A. McKinnon, M. Panisko, R. Perkins, P. Reeder, R. Thompson, and R. Warner, "Automated separation and measurement of radioxenon for the Comprehensive Test Ban Treaty," *Journal of Radioanalytical and Nuclear Chemistry,* vol. 235, pp. 77-82, 1998.

[5] M. Kalinowski, A. Axelsson, M. Bean, X. Blanchard, T. Bowyer, G. Brachet, S. Hebel, J. McIntyre, J. Peters, C. Pistner, M. Raith, A. Ringbom, P. Saey, C. Schlosser, T. Stocki, T. Taffary, and R. Kurt Ungar, "Discrimination of Nuclear Explosions against Civilian Sources Based on Atmospheric Xenon Isotopic Activity Ratios," *Pure and Applied Geophysics,* vol. 167, pp. 517-539, 2010.

[6] M. Auer, T. Kumberg, H. Sartorius, B. Wernsperger, and C. Schlosser, "Ten Years of Development of Equipment for Measurement of Atmospheric Radioactive Xenon for the Verification of the CTBT," *Pure and Applied Geophysics,* vol. 167, pp. 471-486, 2010.

[7] M. Zähringer, A. Becker, M. Nikkinen, P. Saey, and G. Wotawa, "CTBT radioxenon monitoring for verification: today's challenges," *Journal of Radioanalytical and Nuclear Chemistry,* vol. 282, pp. 737-742, 2009.

[8] Preparatory Commission CTBTO, "The CTBT Verification Regime: Monitoring the Earth for Nuclear Explosions," in http://www.ctbto.org, CTBTO, Ed., ed. Vienna International Center, 2011, p. 6.

[9] P. E. W. S. R. Dresel. (2004). *Evaluation of xenon gas detection as a means for identifying buried transuranic waste at the Radioactive Waste Management Complex, Idaho National Environmental and Engineering Laboratory*. Available: http://www.pnl.gov/main/publications/external/technical%5Freports/PNNL-14617.pdf

[10] CTBTO. (2008). *CTBTO Preparatry Commission*. Available: http://www.ctbto.org/

[11] T. W. Bowyer, C. Schlosser, K. H. Abel, M. Auer, J. C. Hayes, T. R. Heimbigner, J. I. McIntyre, M. E. Panisko, P. L. Reeder, H. Satorius, J. Schulze, and W. Weiss, "Detection and analysis of xenon isotopes for the comprehensive nuclear-test-ban treaty international monitoring system," *Journal of Environmental Radioactivity,* vol. 59, pp. 139-151, 2002.

[12] A. Stohl, P. Seibert, G. Wotawa, D. Arnold, J. F. Burkhart, S. Eckhardt, C. Tapia, A. Vargas, and T. J. Yasunari, "Xenon-133 and caesium-137 releases into the atmosphere from the Fukushima Dai-ichi nuclear power plant: determination of the source term, atmospheric dispersion, and deposition," *Atmos. Chem. Phys.,* vol. 12, p. 31, 2012/03/01 2012.

[13] M. B. Kalinowski and M. P. Tuma, "Global radioxenon emission inventory based on nuclear power reactor reports," *Journal of Environmental Radioactivity,* vol. 100, pp. 58-70, 2009.

[14] A. G. Fay and S. R. Biegalski, "Contributions to the 37Ar background by research reactor operations," *Journal of Radioanalytical and Nuclear Chemistry,* vol. 296, pp. 273-277, 2013/04/01 2013.

[15] C. Egnatuk, J. Lowrey, S. Biegalski, T. Bowyer, D. Haas, J. Orrell, V. Woods, and M. Keillor, "Production of 37Ar in The University of Texas TRIGA reactor facility," *Journal of Radioanalytical and Nuclear Chemistry,* vol. 291, pp. 257-260, 2012/01/01 2012.

[16] D. A. Hass, J. L. Orrell, T. W. Bowyer, J. I. McIntyre, H. S. Miley, C. E. Aalseth, and J. C. Hayes, "The Science Case for 37Ar as a Monitor for Underground Nuclear Explosions," Pacific Northwest National Laboratory, Richland, WA2010.

[17] C. E. Aalseth, A. R. Day, D. A. Haas, E. W. Hoppe, B. J. Hyronimus, M. E. Keillor, E. K. Mace, J. L. Orrell, A. Seifert, and V. T. Woods, "Measurement of 37Ar to support technology for On-Site Inspection under the Comprehensive Nuclear-Test-BanTreaty," *Nuclear Instruments and Methods in Physics Research Section A: Accelerators, Spectrometers, Detectors and Associated Equipment,* vol. 652, pp. 58-61, 2011.

[18] C. I. Center. (2013, 04/30/2013). *CTBTO detects radioactivity consistent with 12 February announced North Korean nuclear test*. Available: http://ctbto.org/press-centre/press-releases/2013/ctbto-detects-radioactivity-consistent-with-12-february-announced-north-korean-nuclear-test/

[19] J. D. Lowrey, S. R. Biegalski, A. G. Osborne, and M. R. Deinert, "Subsurface mass transport affects the radioxenon signatures that are used to identify

clandestine nuclear tests," *Geophysical Research Letters,* vol. 40, pp. 111-115, 2013.

[20] J. D. Lowrey, S. R. Biegalski, and M. R. Deinert, "UTEX modeling of radioxenon isotopic fractionation resulting from subsurface transport," *Journal of Radioanalytical and Nuclear Chemistry* vol. Submitted: March 2012, 2012.

[21] R. B. Bird, W. E. Stewart, and E. N. Lightfoot, *Transport Phenomena*, Second ed. New York: John Willey & Sons, Inc., 2007.

[22] W. M. Deen, *Analysis of Transport Phenomena*. New York: Oxford University Press, Inc., 1998.

[23] E. A. Mason and A. P. Malinauskas, *Gas Transport in Porous Media: The Dusty-Gas Model*. New York: Elsevier, 1983.

[24] C. K. Ho and S. W. Webb, *Gas Trasnport in Porous Media*. London: Springer, 2006.

[25] D. C. Thorstenson and D. W. Pollock, "Gas transport in unsaturated porous media: The adequacy of Fick's law," *Rev. Geophys.,* vol. 27, pp. 61-78, 1989.

[26] S. W. Webb, "Gas-phase diffusion in porous media - Evaluation of an advective-dispersive formulation and the dusty-gas model for binary mixtures," *Journal of Porous Media,* vol. 1, pp. 187-199, Mar 1998.

[27] M. Nuevo, iacute, J. a, J. J. Morales, and D. M. Heyes, "Mass dependence of isotope self-diffusion by molecular dynamics," *Physical Review E,* vol. 51, p. 2026, 1995.

[28] T. W. Trull and M. D. Kurz, "Isotopic fractionation accompanying helium diffusion in basaltic glass," *Journal of Molecular Structure,* vol. 485–486, pp. 555-567, 1999.

[29] F. M. Richter, E. B. Watson, R. Mendybaev, N. Dauphas, B. Georg, J. Watkins, and J. Valley, "Isotopic fractionation of the major elements of molten basalt by chemical and thermal diffusion," *Geochimica et Cosmochimica Acta,* vol. 73, pp. 4250-4263, 2009.

[30] I. C. Bourg and G. Sposito, "Isotopic fractionation of noble gases by diffusion in liquid water: Molecular dynamics simulations and hydrologic applications," *Geochimica et Cosmochimica Acta,* vol. 72, pp. 2237-2247, 2008.

[31] A. Verney-Carron, N. Vigier, and R. Millot, "Experimental determination of the role of diffusion on Li isotope fractionation during basaltic glass weathering," *Geochimica et Cosmochimica Acta,* vol. 75, pp. 3452-3468, 2011.

[32] D. Bouchard, P. HoÃàhener, and D. Hunkeler, "Carbon Isotope Fractionation During Volatilization of Petroleum Hydrocarbons and Diffusion Across a Porous

Medium: A Column Experiment," *Environmental Science & Technology,* vol. 42, pp. 7801-7806, 2008.

[33] G. Liu, B. Li, K. Hu, and M. T. Van Genuchten, "Simulating the gas diffusion coefficient in macropore network images: Influence of soil pore morphology," *Soil Science Society of America Journal,* vol. 70, pp. 1252-1261, 2006.

[34] A. N. Anderson, J. W. Crawford, and A. B. McBratney, "On Diffusion in Fractal Soil Structures," *Soil Sci. Soc. Am. J.,* vol. 64, pp. 19-24, 2000/1 2000.

[35] L. Shen and Z. Chen, "Critical review of the impact of tortuosity on diffusion," *Chemical Engineering Science,* vol. 62, pp. 3748-3755, 2007.

[36] G. S. Armatas, D. E. Petrakis, and P. J. Pomonis, "Estimation of diffusion parameters in functionalized silicas with modulated porosity: Part II: Pore network modeling," *Journal of Chromatography A,* vol. 1074, pp. 61-69, 2005.

[37] M. Matyka, A. Khalili, and Z. Koza, "Tortuosity-porosity relation in porous media flow," *Physical Review E,* vol. 78, Aug 2008.

[38] D. Mu, Z.-S. Liu, C. Huang, and N. Djilali, "Prediction of the effective diffusion coefficient in random porous media using the finite element method," *Journal of Porous Materials,* vol. 14, pp. 49-54, 2007.

[39] A. N. Anderson, A. B. McBratney, and J. W. Crawford, "Applications of Fractals to Soil Studies," in *Advances in Agronomy*. vol. Volume 63, L. S. Donald, Ed., ed: Academic Press, 1997, pp. 1-76.

[40] B. Yu and J. Li, "Some Fractal Characters of Porous Media," *Fractals,* vol. 9, p. 365, 2001.

[41] L. Gang, L. Baoguo, H. Kelin, and M. T. van Genuchten, "Simulating the Gas Diffusion Coefficient in Macropore Network Images: Influence of Soil Pore Morphology," *Soil Science Society of America Journal,* vol. 70, pp. 1252-1261, 2006.

[42] S. W. Tyler and S. W. Wheatcraft, "Fractal processes in soil water retention," *Water Resour. Res.,* vol. 26, pp. 1047-1054, 1990.

[43] E. Perrier, M. Rieu, G. Sposito, and G. de Marsily, "Models of the water retention curve for soils with a fractal pore size distribution," *Water Resour. Res.,* vol. 32, pp. 3025-3031, 1996.

[44] N. Henderson, J. C. Brêttas, and W. F. Sacco, "A three-parameter Kozeny–Carman generalized equation for fractal porous media," *Chemical Engineering Science,* vol. 65, pp. 4432-4442, 2010.

[45] B. Yu and P. Cheng, "A fractal permeability model for bi-dispersed porous media," *International Journal of Heat and Mass Transfer,* vol. 45, pp. 2983-2993, 2002.

[46] M. R. Deinert and J. Y. Parlange, "Effect of pore structure on capillary condensation in a porous medium," *Physical Review E,* vol. 79, p. 021202, 2009.

[47] R. F. Probstein, *Physicochemical Hydrodynamics*, Second ed. Hoboken, New Jersey: John Wiley & Sons, Inc., 2003.

[48] S. W. Wheatcraft and S. W. Tyler, "An explanation of scale-dependent dispersivity in heterogeneous aquifers using concepts of fractal geometry," *Water Resour. Res.,* vol. 24, pp. 566-578, 1988.

[49] R. Wu, Q. Liao, X. Zhu, and H. Wang, "A fractal model for determining oxygen effective diffusivity of gas diffusion layer under the dry and wet conditions," *International Journal of Heat and Mass Transfer,* vol. 54, pp. 4341-4348, 2011.

[50] M. GarcÌa-GutiÈrrez, M. Mingarro, T. Missana, P. L. MartÌn, L. A. Sedano, and J. L. Cormenzana, "Diffusion experiments with compacted powder/pellets clay mixtures," *Applied Clay Science,* vol. 26, pp. 57-64, 2004.

[51] S. E. Allaire, J. A. Lafond, A. R. Cabral, and S. F. Lange, "Measurement of gas diffusion through soils: comparison of laboratory methods," *Journal of Environmental Monitoring,* vol. 10, pp. 1326-1336, 2008.

[52] W. i. Abu-El-Sha'r and L. M. Abriola, "Experimental assessment of gas transport mechanisms in natural porous media: Parameter evaluation," *Water Resour. Res.,* vol. 33, pp. 505-516, 1997.

[53] K. C. J. Van Rees, E. A. Sudicky, P. Suresh C. Rao, and K. R. Reddy, "Evaluation of laboratory techniques for measuring diffusion coefficients in sediments," *Environmental Science and Technology,* vol. 25, pp. 1605-1611, 1991.

[54] M. Takeda, H. Nakajima, M. Zhang, and T. Hiratsuka, "Laboratory longitudinal diffusion tests: 1. Dimensionless formulations and validity of simplified solutions," *Journal of Contaminant Hydrology,* vol. 97, pp. 117-134, 2008.

[55] K. Vaatainen, J. Timonen, and A. Hautojarvi, "Development of a gas method for migration studies in fractured and porous media," in *Proceedings of the 16th International Symposium on the Scientific Basis for Nuclear Waste Management, November 30, 1992 - December 4, 1992*, Boston, MA, USA, 1993, pp. 851-856.

[56] J. A. Currie, "Gaseous diffusion in porous media Part 1. - A non-steady state method," *British Journal of Applied Physics,* vol. 11, p. 314, 1960.

[57] U. Beyerle, W. Aeschbach-Hertig, D. M. Imboden, H. Baur, T. Graf, and R. Kipfer, "A Mass Spectrometric System for the Analysis of Noble Gases and

Tritium from Water Samples," *Environmental Science & Technology,* vol. 34, pp. 2042-2050, 2000/05/01 2000.

[58] D. F. Mark, F. M. Stuart, and M. de Podesta, "New high-precision measurements of the isotopic composition of atmospheric argon," *Geochimica et Cosmochimica Acta,* vol. 75, pp. 7494-7501, 2011.

[59] Agilent Technologies, "Inductively Coupled Plasma Mass Spectrometry " in *Course Number H8974A*, ed: Agilent Technologies, 2001.

[60] R. W. Mair, G. P. Wong, D. Hoffmann, uuml, M. D. rlimann, S. Patz, L. M. Schwartz, and R. L. Walsworth, "Probing Porous Media with Gas Diffusion NMR," *Physical Review Letters,* vol. 83, p. 3324, 1999.

[61] R. W. Mair, M. S. Rosen, R. Wang, D. G. Cory, and R. L. Walsworth, "Diffusion NMR methods applied to xenon gas for materials study," *Magnetic Resonance in Chemistry,* vol. 40, pp. S29-S39, Dec 2002.

[62] L. M. Pereira, R. D. Souza, H. R. B. Orlande, and R. M. Cotta, "A comparison of concentration measurement techniques for the estimation of the apparent mass diffusion coefficient," *Brazilian Journal of Chemical Engineering,* vol. 18, pp. 253-265, 2001.

[63] Z. Revay, "Prompt gamma activation analysis of samples in thick containers," *Journal of Radioanalytical and Nuclear Chemistry,* vol. 276, pp. 825-830, 2008.

[64] C. Rios Perez, J. Lowrey, S. Biegalski, and M. Deinert, "Xenon diffusion studies with prompt gamma activation analysis," *Journal of Radioanalytical and Nuclear Chemistry,* vol. 291, pp. 261-265, 2012.

[65] G. Knoll, *Radiation Detection and Measurement*, Fourth ed. Hoboken: Jhon Wiley & Sons, Inc., 2010.

[66] K. S. Krane, *Introductory Nuclear Physics*. New York: John Wiley & Sons, 1988.

[67] G. L. Molnar, Ed., *Handbook of Prompt Gamma Activation Analysis with Neutron Beams*. Kluwer Academic Publishers, 2004, p.^pp. Pages.

[68] D. Giménez, E. Perfect, W. J. Rawls, and Y. Pachepsky, "Fractal models for predicting soil hydraulic properties: a review," *Engineering Geology,* vol. 48, pp. 161-183, 1997.

[69] S. W. Coleman and J. C. Vassilicos, "Tortuosity of unsaturated porous fractal materials," *Physical Review E,* vol. 78, p. 016308, 2008.

[70] K. C. J. V. Rees, E. A. Sudicky, P. S. C. Rao, and R. Reddy, "Evaluation of laboratory techniques for measuring diffusion coefficients in sediments," *Environmental Science and Technology,* vol. 25, pp. 1605-1611, 1991.

[71] R. Islas-Juarez, F. Samanego-V, E. Luna, C. Perez-Rosales, and J. Cruz, "Experimental study of effective diffusion in porous media," in *2004 SPE International Petroleum Conference in Mexico, November 7, 2004 - November 9, 2004*, Puebla, Mexico, 2004, pp. 781-787.

[72] J. H. Rohling, J. Shen, C. Wang, J. Zhou, and C. E. Gu, "Determination of binary diffusion coefficients of gases using photothermal deflection technique," *Applied Physics B: Lasers & Optics,* vol. 87, pp. 355-362, 2007.

[73] N. Pekula, K. Heller, P. A. Chuang, A. Turhan, M. M. Mench, J. S. Brenizer, and K. Unlu, "Study of water distribution and transport in a polymer electrolyte fuel cell using neutron imaging," *Nuclear Instruments in Physics Research A,* vol. 542, pp. 134-141, 2005.

[74] M. R. Deinert, J. Y. Parlange, T. Steenhuis, J. Throop, K. Ünlü, and K. B. Cady, "Measurement of fluid contents and wetting front profiles by real-time neutron radiography," *Journal of Hydrology,* vol. 290, pp. 192-201, 2004.

[75] S. Takai, T. Mandai, Y. Kawabata, and T. Esaka, "Diffusion coefficient measurements of La2/3-xLi3xTiO3 using neutron radiography," *Solid State Ionics,* vol. 176, pp. 2227-2233, 2005.

[76] J. A. Mercer, E. M. A. Hussein, and E. J. Walker, "A non-intrusive neutron device for in situ detection of petroleum contamination in soil," *Nuclear Instruments in Physics Research B,* vol. 263, 2007.

[77] R. G. Downing and G. P. Lamaze, "Near-surface profiling of semiconductor materials using neutron depth profiling," *Semiconductor Science and Technology,* vol. 10, p. 1423, 1995.

[78] C. Rios Martinez, "Prompt gamma activation analysis using the Texas cold neutron source," Ph. D., Mechanical Engineering, University of Texas at Austin, Austin, 1995.

[79] K. Pandey, "Characterization of the Prompt Gamma Activation Analysis System at The Univeristy of Texas at Austin," Master of Science in Engineering Thesis, Mechanical Engineering, The University of Texas at Austin, Austin, 2002.

[80] N. Tsoulfanidis and S. Landsberger, *Measurement and Detection of Radiation*, Third ed. Sound Parkway: CRC Press, 2011.

[81] I. A. E. Agency, "Database of Prompt Gamma Rays from Slow Neutron Capture for Elemental Analysis," ed. Austria: IAEA, 2007.

[82] H.-J. Cho, Y.-S. Chung, and Y.-J. Kim, "Study on prompt gamma-ray spectrometer using Compton suppression system," *Nuclear Instruments and Methods in Physics Research Section B: Beam Interactions with Materials and Atoms,* vol. 229, pp. 499-507, 2005.

[83] P. P. Ember, T. Belgya, and G. L. Moln·r, "Improvement of the capabilities of PGAA by coincidence techniques," *Applied Radiation and Isotopes,* vol. 56, pp. 535-541, 2002.

[84] W. A. Metwally, C. W. Mayo, X. Han, and R. P. Gardner, "Coincidence counting for PGNAA applications: Is it the optimum method?," *Journal of Radioanalytical and Nuclear Chemistry,* vol. 265, pp. 309-314, 2005.

[85] L. A. Currie, "Limits for qualitative detection and quantitative determination. Application to radiochemistry," *Analytical Chemistry,* vol. 40, pp. 586-593, 1968/03/01 1968.

[86] L. A. Currie, "Nomenclature in Evaluation of Analytical Methods Including Detection and Quantification Capabilities," *Pure & Applied Chemistry,* vol. 67, p. 25, 1995.

[87] S. R. Biegalski, T. C. Green, E. Alvarez, and S. Aghara, "Background characterization of The University of Texas PGAA Facility," *Journal of Radioanalytical and Nuclear Chemistry,* vol. 271, pp. 413-417, 2007.

[88] C. Rios Perez, S. R. Biegalski, and M. R. Deinert, "Measuring the diffusion of Noble gasses through a porous medium using prompt gamma activation analysis," *Journal of Radioanalytical & Nuclear Chemistry,* 2012.

[89] C. A. Rios Perez, S. R. Biegalski, and M. R. Deinert, "Methodology for using prompt gamma activation analysis to measure the binary diffusion coefficient of a gas in a porous medium," *Nuclear Instruments and Methods in Physics Research Section B: Beam Interactions with Materials and Atoms,* vol. 293, pp. 21-25, 2012.

[90] R. K. Harrison and S. Landsberger, "Determination of boron over a large dynamic range by prompt-gamma activation analysis," *Nuclear Instruments and Methods in Physics Research Section B: Beam Interactions with Materials and Atoms,* vol. 267, pp. 513-518, 2009.

[91] Z. Rèvay, R. K. Harrison, E. Alvarez, S. R. Biegalski, and S. Landsberger, "Construction and characterization of the redesigned PGAA facility at The University of Texas at Austin," *Nuclear Instruments and Methods in Physics Research Section A: Accelerators, Spectrometers, Detectors and Associated Equipment,* vol. 577, pp. 611-618, 2007.

[92] R. S. Figliola and D. E. Beasley, *Theory and Design for Mechanical Measurements*, 3rd ed. New York: John Wiley & Sons, Inc., 2000.

[93] A. Z. Moss, "Diffusive gas transport through capillaries: A solution to the intermediate case based upon the kinetic theory of gases," *Journal of Applied Physics,* vol. 59, p. 2673, 1986.

[94] C. Huber, U. Beyerle, M. Leuenberger, J. Schwander, R. Kipfer, R. Spahni, J. P. Severinghaus, and K. Weiler, "Evidence for molecular size dependent gas fractionation in firn air derived from noble gases, oxygen, and nitrogen measurements," *Earth & Planetary Science Letters,* vol. 243, pp. 61-73, 2006.

[95] R. B. Evans III, G. M. Watson, and E. A. Mason, "Gaseous Diffusion in Porous Media at Uniform Pressure," *The Journal of Chemical Physics,* vol. 35, pp. 2076-2083, 1961.

[96] K. P. McCarty and E. A. Mason, "Kirkendall Effect in Gaseous Diffusion," *Physics of Fluids,* vol. 3, pp. 908-922, 1960.

[97] E. A. Mason, A. P. Malinauskas, and R. B. Evans Iii, "Flow and diffusion of gases in porous media," *Journal of Chemical Physics,* vol. 46, pp. 3199-3216, 1967.

[98] R. C. Goodknight, W. A. Klikoff, and I. Fatt, "NON-STEADY-STATE FLUID FLOW AND DIFFUSION IN POROUS MEDIA CONTAINING DEAD-END PORE VOLUME1," *The Journal of Physical Chemistry,* vol. 64, pp. 1162-1168, 1960/09/01 1960.

[99] M. A. HESSE, H. A. TCHELEPI, B. J. CANTWEL, and F. M. ORR, "Gravity currents in horizontal porous layers: transition from early to late self-similarity," *Journal of Fluid Mechanics,* vol. 577, pp. 363-383, 2007.

[100] R. B. Bird, W. E. Stewart, and E. N. Lightfoot, *Transport Phenomena*. New York, New York: John Wiley & Sons, 1960.

[101] J. Bear, *The dynamics of fluids in porous media*. Mineola, NY: Dover Publications, 1988.

[102] D. Giménez, R. R. Allmaras, D. R. Huggins, and E. A. Nater, "Prediction of the Saturated Hydraulic Conductivity-Porosity Dependence Using Fractals," *Soil Sci. Soc. Am. J.,* vol. 61, pp. 1285-1292, 1997 1997.

[103] J. Bear, *Dynamics of fluids in porous media*. New York: American Elsevier Publishing COmpany, Inc., 1988.

[104] A. Costa, "Permeability-porosity relationship: A reexamination of the Kozeny-Carman equation based on a fractal pore-space geometry assumption," *Geophysical Research Letters,* vol. 33, p. L02318, 2006.

[105] L. R. Ahuja, J. W. Naney, R. E. Green, and D. R. Nielsen, "Macroporosity to Characterize Spatial Variability of Hydraulic Conductivity and Effects of Land Management1," *Soil Sci. Soc. Am. J.,* vol. 48, pp. 699-702, 1984 1984.

[106] W. Kast and C. R. Hohenthanner, "Mass transfer within the gas-phase of porous media," *International Journal of Heat and Mass Transfer,* vol. 43, pp. 807-823, 2000.

[107] P. Pfeifer and D. Avnir, "Chemistry in noninteger dimensions between two and three. I. Fractal theory of heterogeneous surfaces," *The Journal of Chemical Physics,* vol. 79, pp. 3558-3565, 1983.

[108] A. Dathe and M. Thullner, "The relationship between fractal properties of solid matrix and pore space in porous media," *Geoderma,* vol. 129, pp. 279-290, 2005.

[109] Y. F. Xu, D. a. Sun, and Y. Yao, "Surface fractal dimension of bentonite and its application to determination of swelling properties," *Chaos, Solitons & Fractals,* vol. 19, pp. 347-356, 2004.

[110] J. J. Gagnepain and C. Roques-Carmes, "Fractal approach to two-dimensional and three-dimensional surface roughness," *Wear,* vol. 109, pp. 119-126, 1986.

[111] D. Giménez, R. R. Allmaras, E. A. Nater, and D. R. Huggins, "Fractal dimensions for volume and surface of interaggregate pores — scale effects," *Geoderma,* vol. 77, pp. 19-38, 1997.

[112] B. B. Mandelbrot, "Length-Area-Volume Relations," in *The fractal geometry of nature*, ed San Francisco: W.H. Freeman, 1983, pp. 109-115.

[113] I. Majid, D. B. Avraham, S. Havlin, and H. E. Stanley, "Exact-enumeration approach to random walks on percolation clusters in two dimensions," *Physical Review B,* vol. 30, pp. 1626-1628, 1984.

[114] S. W. Tyler and S. W. Wheatcraft, "Fractal Scaling of Soil Particle-Size Distributions: Analysis and Limitations," *Soil Sci. Soc. Am. J.,* vol. 56, pp. 362-369, 1992 1992.

[115] A. J. Katz and A. H. Thompson, "Fractal Sandstone Pores: Implications for Conductivity and Pore Formation," *Physical Review Letters,* vol. 54, pp. 1325-1328, 1985.